Investigation into the role of primer, pre-treatments and coating microstructure in preventing cut edge corrosion of organically coated steels.

Khan, Khalil

Swansea University
Prifysgol Abertawe

Investigation into the role of primer, pretreatments and coating microstructure in preventing cut edge corrosion of organically coated steels

Khalil Khan
B.Eng (Hons)

Thesis submitted to the Swansea University for a Doctorate of Philosophy

August 2012

Materials Research Centre
College of Engineering
Swansea University

ProQuest LLC.
789 East Eisenhower Parkway
P.O. Box 1346
Ann Arbor, MI 48106 – 1346

DECLARATION

Declaration: This work has not previously been accepted in substance for any degree and is not being concurrently submitted in candidature for any degree.

Signed: Date: 20-02-2013

Statement: This thesis is the result of my own investigations, except where otherwise stated. Other sources are acknowledged by footnotes giving explicit references.

Signed: Date: 20-02-2013

Statement: I hereby give consent for my thesis, if accepted, to be available for photocopying and interlibrary loan and for the title and summary to be made available to outside organisations.

Signed: Date: 20-02-2013

Thesis summary

Investigations were carried out to assess the role of primer, pretreatments and coating microstructure in preventing cutedge corrosion of chrome free organically coated steels.

Zinc runoff was monitored from a range of organically coated steels with a large cutedge length exposed over 18 months at Swansea University roof top site. The zinc in the runoff leaches from the zinc-aluminium alloy coating of the substrate. The paint systems' corrosion performance was assessed by monitoring the levels of zinc in the runoff. Consequently the levels of zinc reflected the effectiveness of the applied paint system against corrosion. Runoff was high in initial months with zinc levels reducing with time due to the build up of corrosion products that hindered the progress of corrosion.

An accelerated laboratory test using a distilled water electrolyte was developed that predict long-term external weathering runoff from panels of a range of organically coated steels.

The corrosion mechanisms of a variety of organically coated Galvalloy steel have been examined using the scanning vibrating electrode technique (SVET) in 0.1%NaCl. The corrosion behaviour of a coating is related to the zinc-aluminium alloy coating structure and combination of pretreatment and primer. The SVET has been used to assess total zinc loss and the corrosion rate for a comparative measure of organically coating system performance. A correlation has been developed from SVET 24hour experiment data to accelerated weathering data and external weather data that can aid more accurately predicting the in service life of the product.

Also considered were the effects of electrolyte conductivity on the morphology of corrosion on pure zinc. A mathematical model has been developed to predict corrosion pit population.

Altered microstructure of solidifying zinc aluminium alloy melt via ultrasonication was investigated. Ultrasound irradiation significantly altered the final microstructure. The influence of morphed microstructure upon the corrosion behaviour was explored using the SVET in 0.1%NaCl. The ultrasound manipulated microstructure had generally a positive effect on the corrosion behaviour.

Acknowledgements

Alhamdulillah (الحمد لله) Gratitude to God.

It would not have been possible to write this doctoral thesis without the help and support of the kind people around me, to only some of whom it is possible to give particular mention here.

I would like to acknowledge the financial support from EPSRC and Tata Steel during this research.

I am immensely thankful to my supervisor, Dr. James Sullivan, whose friendship as well as his academic experience, have been invaluable to me. Incalculable thanks to Dr Dave Worsley for his leadership, amusement and enthusiasm. Thanks to Dr Geraint Williams and Prof. Neil McMurray for their wealth of knowledge and willingness to help. I thank Dr. Corinne Howse for her role in this research. Thanks also (in no particular order) to Dr. John Elvins, Dr. Ian Mabbett, Dr. Trystan Watson, Dr. Matthew Carnie, Dr. Andrew Robinson, Dr. Cristopher Wierman, Dr. Justin Searle, Mrs. Beverly Williams, Miss Rhian Nurse

To all in the Corrosion group, keep up the good work. As long as there are metals there will be corrosion.

My parents Abdul Rehman and Surriya who have given me their unequivocal support throughout, as always, for which my mere expression of appreciation does not suffice. It is thanks to my father that I first became interested in science and engineering, and it is to him that this thesis is dedicated.

I want to acknowledge the support my wife Rukhsanah gave during the period of this research. Understanding without protest my very long work hours, weekends and holidays lost to research. You are kind, patient and my shining light and I thank you.

My sons Hassan and Mohsin will always be my inspiration and my motivation.

Khalil Khan

Table of contents

Chapter 1

Introduction

1.0 Introduction

Tata Steel Europe is one of the largest European steel producers that supply a variety of innovative products for a broad range of applications such as aerospace industry, automotive, construction, energy and power generation, rail security and defence industries.

The UK business is split into many entities and the ones of interest to this study are Tata Strip Products (TSP), and Tata Steel Colors (TSC). The primary functions of these units are as follows;

a) TSP production of hot metal; hot and cold rolled steel coil and metallic coated steels from Llanwern and Port Talbot blast furnaces.

b) TSC produces a range of Organically Coated Steel (OCS) products; using TSP coils to fulfil the demand on construction, domestic appliances and other consumer products.

This work consists of different types of corrosion, corrosion control and corrosion testing. The focus of the study is to investigate the performance of existing Tata Steel products from both TSP and TSC lines i.e. Galvatite (99.85% Zn – 0.15% Al), Galfan or Galvalloy (95.2% Zn – 4.8% Al), Galvalume or Zalutite (55% Al – 43.5% Zn and 1.5% Si), MagiZinc (96.8% Zn – 1.6% Mg and 1.6% Al) and those that have been coated with organic based coating system (OCS) with and without inhibitors.

The aim this work is to investigate the failure of the product under a corrosive environment, to understand fully the corrosion mechanism that assists in selection of the appropriate product for given prevalent conditions. The latest innovative products and their performance have been evaluated using standard accelerated corrosion tests. Comparisons of new products with existing products are conducted by ranking them according to their respective corrosion performance via accelerated tests. The experimental data are used to determine life expectancy accurately. The mechanisms of corrosion are certified by scanning electrochemical techniques and accelerated laboratory tests that have been developed to assess coating performance and overall usage.

1.1 Definition of Corrosion

To the great majority corrosion means rust. Rust is reserved for the corrosion of iron while corrosion is the destructive phenomenon which affects most metals [1]. Corrosion is defined as the destruction or deterioration of a metal or an alloy by an electrochemical reaction with its environment [2].

With the exception of noble metals (Au, Ag and Pt) that are naturally found and are considered to be non-reactive, all other metals are chemically extracted from their ores. Thermodynamically there is a drive for the metal to revert back to its oxide state i.e. back to naturally occurring stable ore. The atmosphere contains sufficient oxygen and humidity to initiate the oxidation reactions for most metals.

1.2 Corrosion Mechanism

Corrosion is an electrochemical reaction, where the metal loses its electrons to the environment and forms a metal ion, as given in equation (1.1).

Anodic reaction: $$M_{(s)} \rightarrow M^{n+}_{(aq)} + ne^- \quad (1.1)$$

The transformation of metal M atom to metal M^{n+} ion by losing n number of electrons, e, is referred to oxidation and the reaction is named anodic. An oxidation or anodic reaction is indicated by an increase in valence charge or production of number of electrons. A decrease in valence charge or consumption of electrons signifies to a reduction or a cathodic reaction, e.g. hydrogen production in equation (1.2),

Cathodic reaction: $$2H^+_{(aq)} + 2e^- \rightarrow H_{2\,(g)} \quad (1.2)$$

or more commonly under aerobic conditions where oxygen is readily available at near neutral pH, reduction of dissolved oxygen occurs via equation (1.3).

Cathodic reaction: $$O_{2\,(g)} + 2H_2O_{(aq)} + 4e^- \rightarrow 4OH^-_{(aq)} \quad (1.3)$$

Iron (Fe), or steel as an engineering material that has a natural drive to revert back to its oxide state (stable). The element, Fe, does not need a highly corrosive environment or any extreme conditions to form the more stable form iron oxide, this process occurs in normal atmosphere where there is moisture and oxygen. In case of steel in humid air there is a drive to form an oxide but the reaction rate in normal atmosphere is slow. This drive can be explained by considering Gibbs free energy, ΔG. The change in free energy is a direct measure of the work capacity or maximum electric energy available for a system [2]. In any chemical reaction the driving force is to lower the overall free energy. Oxidation is one such reaction. Negative ΔG results in spontaneous reaction, ΔG equal to zero represents equilibrium and positive ΔG a reaction is not possible.

1.2.1 Kinetics of Corrosion

A corroding metallic surface consists of anodic and cathodic sites. These sites act as a system of two or more couples (polyelectrode) function simultaneously on a single electrode surface not in a mutual thermodynamic equilibrium[1,2]. The additivity principle also defines that total current flowing into an external circuit is the summation of the currents present due to individual couples that exist on a corroding surface, given equation (1.4) [3]. Therefore under conditions of free corrosion, sum of anodic currents are equal to the sum of cathodic currents that represent the overall corrosion current.

$$\sum i_{anodic} = -\sum i_{cathodic} = i_{corr} \tag{1.4}$$

Where i_{anodic} is the partial current density due to the anode, $i_{cathodic}$ is the partial current density due to the cathode and i_{corr} is the corrosion rate expressed in terms of current. All electrochemical currents are potential dependent therefore the corroding metallic substrate will adopt a unique potential which is known as E_{corr}, the corrosion potential.

A mathematical relationship for the current density, I, and potential, E, exists defined empirically by Tafel and is given by equation (1.5) and (1.6).

$$i_{anodic} \propto \exp(E) \tag{1.5}$$

$$i_{cathodic} \propto \exp(-E) \tag{1.6}$$

A graphical representation of the relation is be plotted, as potential E, against the logarithm to the base of 10 of the current, i, ($\log_{10}$ i). A graph E versus $\log_{10}$ i can be plotted producing a straight line known as a Tafel plot. Combination of Tafel plots for the individual electrode processes produces Evans diagram. Figure 1.1 is an example of an Evans diagram for a simple corrosion process for a metal in contact with an aerated electrolyte. The corroding metal via the anodic reaction ion formation occurs, ions enter the solution, the metal is left with an excess of electrons in this area that flow to the cathode area. In progress of corrosion, the anode becomes less negative and there is a local potential shift (polarised) upwards by an amount η_a, the anodic polarisation. Conversely, the cathode becomes more negative and its potential shifts downwards by an amount η_c, the cathodic polarisation. These positive and negative polarisation shifts of the anode and cathode are depicted in Figure 1.1. Where the Tafel slopes intersect the anodic and cathodic current densities are equal i.e. their sum is zero, and as stated in equation 3 this point defines the free corrosion current density, i_{corr}. Subsequently the free corrosion potential, E_{corr}, for the system can be derived from the Evans diagram.

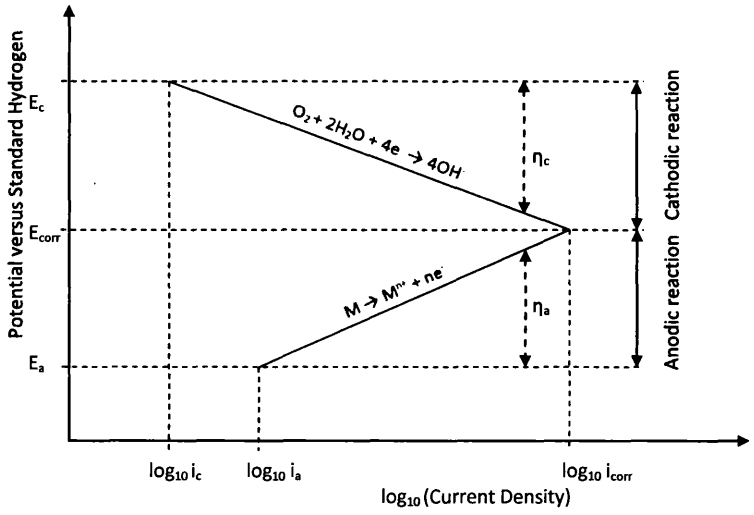

Figure 1.1 Theoretical Evans diagram for a metal in an aerated solution. Where E_a = anodic potential, E_c = cathodic potential, i_a = anodic current density and i_c = cathodic current density, E_{corr} and i_{corr} are the free corrosion potential and current density respectively.

1.3 Classification of Corrosion

Corrosion can be classified in many different ways; one method divides corrosion into two classes, *low temperature* and *high temperature corrosion*. Corrosion may further be classified as *wet* corrosion and *dry* corrosion. Wet corrosion usually involves aqueous solutions where electrolytes are present. A common example is corrosion of steel by water. Dry corrosion occurs in absence of a liquid phase, vapours and gases are usually the corrodents. Dry corrosion is often associated with high temperatures, an example is attack on steel by furnace gases[2].

Corrosion can be further divided into a number of forms of corrosion. In this section only those forms are considered that were applicable to this research study. Some of the forms of corrosion are considered to be unique, but all of them are interrelated. Various characteristics and forms of corrosion are discussed in brief in the following subsections.

1.3.1 Uniform Attack

This is the most common form of corrosion, it is normally characterised by chemical or electrochemical reaction that proceeds uniformly of the entirely exposed surface or over a large area. The metal becomes thinner and eventually fails as direct result of corrosion. Uniform attack or general overall corrosion can be prevented or reduced by proper material selection for the environment to serve in or an application of one of the following coating, inhibitors or cathodic protection.

1.3.2 Galvanic or Bi-metallic Corrosion

Galvanic corrosion typically occurs when two dissimilar metals are brought into electrical contact with each other. A potential difference usually exists between the two dissimilar metals when immersed in a corrosive or conductive solution. The corrosion reaction depends on the reactivity of the metals relative to each other. The potential difference produces electron flow between the dissimilar metals. Corrosion of the less corrosion resistant metal is usually increased and attack of the more resistant material decreased as compared to the behaviour of these metals when they are not in contact. The less resistant metal becomes the anode and the more resistant metal behaves like a cathode. Usually the cathodic metal corrodes very little or not at all in this type of couple.

In a basic wet corrosion cell a potential difference exists between the anode and the cathode; that could be measured by simply inserting a voltmeter into the circuit. This principal is applied to the dissimilar metals in electrical contact via corrosive or conductive solution (electrolyte) and the potential difference is measured. It is impossible to measure the potential of a single metal electrode in an electrolyte, since all measurements are a comparison of one potential with another. By introducing a standard electrode against which all other measurements can be made i.e. hydrogen is used as a standard reference, where it is given an electrode potential of exactly zero volts. The electrode potentials of another element (metal) is then compared with that for hydrogen and is called the standard electrode potential for that element (metal), a table is compiled for different metals, table 1.1.

Table 1.1 – The Galvanic Series (reduced).

Platinum	↑ More noble (positive ΔG)
Gold	
Zirconium	
Graphite	
Titanium	
Silver	
Copper	
Hydrogen	
Lead	
Tin	
Stainless Steel	
Cast Iron	
Mild Steel	
Aluminium	
Zinc	
Magnesium	↓ Less noble (negative ΔG)

1.3.3 Crevice Corrosion

A general definition of crevice corrosion is the attack which occurs because part of the metal surface is in a shielded or restricted corrosive environment, compared to the rest of the significantly larger metal surface which is exposed to a greater volume of environment. The overall reaction involves the dissolution of metal (see equation 1.1) and the reduction of oxygen to hydroxide ions (see equation 1.3). At first the oxidation and reduction reactions occur uniformly over the entire surface, including the interior of the crevice. Following the depletion of oxygen from within the crevice, there is a local increase in metal ion concentration, which is balanced by the migration of negatively charged ions into the crevice. The cathodic reaction is sustained in areas away from the crevice where O2 access is with ease and the anodic reaction is focused within the crevice. Conditions of crevice interior can become such that dissolution rates of most metals and alloys is accelerated.

1.3.4 Pitting Corrosion

Pitting is a form of extremely localised attack that results in holes in the metal. Generally a pit may be described as a cavity or hole with the surface diameter about the same or less than the depth. Pitting causes failure due to perforation with only a small percent weight loss of the entire surface. It is often difficult to detect pitting due to its small size and often is covered with corrosion products. Localised pitting attack which selectively attacks a small area of metal surface where this is a scratch or mechanical break in the protective film; composition heterogeneity such as inclusions or segregate or precipitates. A corrosion pit is

a unique type of anodic reaction, it is an autocatalytic process. That is, the corrosion process within the pit produces conditions which are both stimulating and necessary for sustaining the continued activity of the pit or even accelerate the process.

1.3.5 Intergranular and Transgranular Corrosion

A metal corrodes by a uniform attack starting at grain boundaries which are more reactive than the matrix. Intergranular corrosion occurs under certain conditions, when grain interfaces are reactive, as these boundaries are often preferred sites for precipitation and segregation process observed in many alloys. Intergranular corrosion initiates by these defects caused by impurities which are at times deliberately encouraged as part of a sacrificial protection layer over the main matrix i.e. Zinc- Aluminium- Magnesium coating over steel. The same kind of subsurface fissures can be produced by transgranular corrosion. In this, a small volume of metal is corroded in preferential paths that proceed across or through the grains. This occurs only under certain conditions with certain alloys and possibly promotes pitting and crevice corrosion.

1.3.6 Erosion Corrosion

Erosion corrosion is considered to be the acceleration or increase in the rate of deterioration of a metal that results when the metal is attacked because of the relative motion between an electrolyte (corrosive fluid) and the metal surface. Metal is removed from the surface as dissolved ions or its form solid corrosion product that are mechanically swept from the metal surface. Factors that govern the erosion corrosion process are velocity of electrolyte flow, turbulence of flow, impingement and temperature. Erosion corrosion can be applicable to corrosion attack of organically coated sheet steel as these are often applied with cut-edge exposed to impact of falling rain. The corrosion instigated by the erosion corrosion phenomenon can lead to crevice and pitting.

1.3.7 Stress Corrosion Cracking

Stress corrosion cracking refers to the failure mode by formation of crack that is initiated by corrosion. In the case of stress corrosion cracking the bulk of metal or alloy is almost not attacked over most of its surface, while fine cracks progress through it. Fine cracks form at grain boundary where the usual crystal structure is broken or that impurities exist at or near the grain boundaries due to initial forming or alloying of the matrix disrupting the usual crystal structure packing and stability. When under strain typically tensile the load is exaggerated at these grain boundaries or areas of impurity near or in the grains or grain boundaries, the atoms in these regions are already less densely packed as compared to the

matrix, atoms nearest to this areas of heightened strain are more likely to form anodic corrosion sites when exposed to corrosive environment. Stress corrosion is the term used when static or stationary stresses are involved. If cyclic or alternating stresses are involved, the failure is designated as *corrosion fatigue*. This is also a form of stress corrosion; the term identifies the nature of stress [4]. The progress of the stress activated corrosion may result in crevice or pit formation.

1.3.8 Cut Edge Corrosion

This is not defined form of corrosion as specified by Fontana [2] but is most likely to occur at the exposed surface due to the cut edge. Mass produced organic coated galvanised sheet steels are as they are inexpensive, durable, well protected and commonly used in construction industry.

Organically coated galvanised sheet steel, consists of hot dipped usually zinc coated steel that has been prepared with a paint system. The key issue with such a construction component is in situations where the sheet is cut exposing the edge, the cut edge. This cut edge is the vulnerable site on the metal that is susceptible to corrosion attack from environment usually the external outdoor environment. The sheet steel is mostly made of iron that has been treated with zinc alloy layer. Galvanicaly zinc is less noble than steel and corrodes sacrificially in preference to steel, thus giving longevity to the component. The service life is extended by coating the zinc treated sheet with an organic coating system. The organic coating usually consists of a bilayer system, primer and topcoat. Often the primer film contains corrosion inhibitors and the topcoat offers barrier protection. However the bulk of the sheet is well covered and protected from the elements of weathering the cut edge is exposed and it is here that corrosion usually initiates. Weathering often causes blistering of the paint film where there has been an ingress of moisture and or delamination predominantly at the exposed cutedge due to corrosion and cathodic disbondment. The zinc alloy layer is attacked with anodic activation of the zinc rich phase where the steel supports the cathodic reaction. Dissolution of the zinc can lead to a process of anodic disbondment of protective coatings from the protected substrate. This type of corrosion attack is called cut edge corrosion, figure 1.2 showing a typical example of cutedge corrosion failure of paint system. This is a major source of warranty claims within the painted steel sector and therefore development of enhanced zinc alloys and organic coating systems to resist this corrosion is critical.

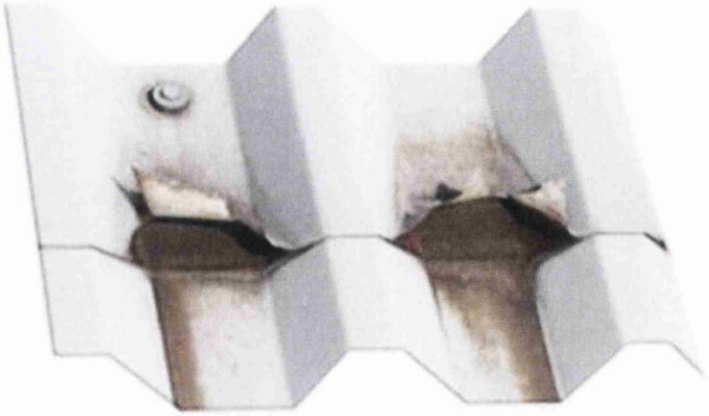

Figure 1.2 Example of cutedge corrosion failure.

1.4 Corrosion Prevention

The understanding of physical and chemical principles of a corrosive environment is crucial in order to develop protection methods. Basically, the prevention or retardation of the corrosion process is achieved by firstly the control of the corrosive environment. There are three fundamental components of an environment i.e. oxygen, water (liquid or vapour) and stimulator species. These act simultaneously and are dependent upon concentrations, temperature and exposure time which result in varying degree of corrosion attack. Therefore, removal of or minimising one of the three dominant factors slows down or stops the corrosion process. Secondly, the physically exposed metal surface or the nature of the metal is altered in a number of ways to achieve improved corrosion resistance. Metals are alloyed for a specific environment, surface treated i.e. painted, greased, oiled etc to minimise the corrosion attack.

Inhibitors are added to either the environment or to the exposed metal surface to extend the corrosion resistant properties.

1.4.1 Corrosion Inhibitors

An inhibitor is a chemical substance that when added in small quantities to an environment decreases the corrosion rate. Inhibitor chemicals react with the metallic surface or the environment giving the metal surface a certain amount of protection against corrosion. Inhibitors usually act by adsorption process on the metal surface, protecting the surface by forming a film. Inhibitors retard the corrosion process by:

- Decreasing the anodic or cathodic behaviour
- Hindering the movement or diffusion of ions to the metal surface
- Increasing the electrical resistance of the metal surface

Various types of inhibitors are described in the following subsections. Inhibitors are crucial to the metal and the environment that metal serves within.

1.4.1.1 Anodic Inhibitors

There are two types of passivating inhibitors oxidising anions and nonoxidising ions. These inhibitors cause a large anodic shift of corrosion potential, forcing the metallic surface into the passivation range. Oxidising anions such as chromate, nitrite and nitrate can passivate steel in the absence of oxygen and nonoxidising ions such as phosphate, tungstate and molybdate require the presence of oxygen to passivate steel. Anodic inhibitors increase the polarisation of the anode by reaction with the ions of the substrate metal producing either a passive thin film, or salt layers of limited solubility which coats the anode. This results in the polarisation of the corroding surface. Figure 1.3 is an Evans diagram which illustrates the effect on potential by addition of anodic inhibitor to a corroding sample. The solid line represents the anodic polarisation with no inhibitor present and the dashed line is the resultant polarisation following addition of an anodic inhibitor. With the presence of the anodic inhibitor there is a reduction in the corrosion current but an increase in the free corrosion potential, E_{corr}. Thus anodic inhibitor are considered to be dangerous inhibitors due to the associated increase in the free corrosion potential [1,3]. Concentrations of these inhibitors when applied are crucial, if the concentrations falls below critical corrosion is accelerated. Therefore it is essential that inhibitor concentrations are monitored, below critical concentration can lead to pitting and accelerated corrosion.

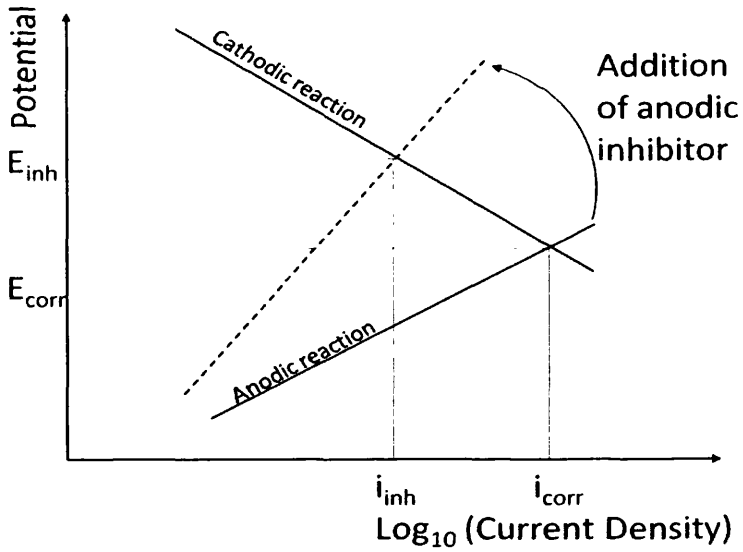

Figure 1.3 Evans diagram illustrating the change in potential and corrosion current by the addition of an anodic inhibitor.

1.4.1.2 Cathodic Inhibitors

Cathodic inhibitors retard the cathodic reaction by three different mechanisms: (i) as cathodic poisoning, (ii) as cathodic precipitates, and (iii) as oxidant scavengers. Cathodic inhibitors either slow the cathodic reaction itself or selectively precipitate on cathodic areas to increase the surface impedance and limit the diffusion of reducible to these areas. Cathodic inhibitor compounds of arsenic and antimony make recombination and discharge of hydrogen more difficult, cathodic inhibitor ions such as calcium, zinc, or magnesium can precipitate as (hydro)oxides forming a protective layer on the metal surface. The cathodic inhibitor increases the cathodic polarisation of the metal surface, as illustrated by figure 1.4. Figure 1.4 shows the decrease in the corrosion current accompanied by a decrease in the free corrosion potential. Thus cathodic inhibitors are considered to be safe. Unlike the anodic inhibitors when cathodic inhibitor is added in slight quantities the dynamics of the corrosion are still reduced.

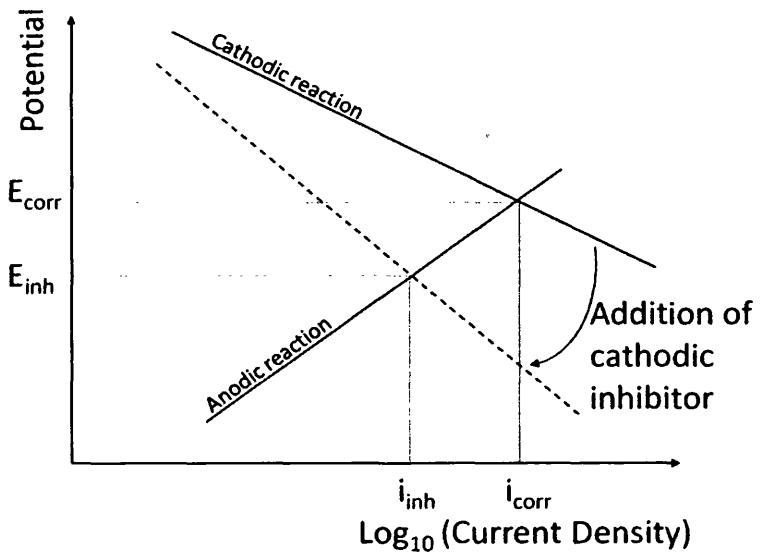

Figure 1.4 Evans diagram illustrating the change in potential and corrosion current by the addition of a cathodic inhibitor.

1.4.1.3 Adsorption Type Inhibitors

In general, these are organic compounds which adsorb on the metal surface and suppress metal dissolution or reduction reaction i.e. organic amines. These are long organic molecules with side chains which become strongly adsorbed to the metal surface. The bulky molecules can limit the diffusion of oxygen to the surface or trap the metal ions on the surface and reduce the rate of dissolution. Cathodic inhibitors are considered to be safe. Even if very small amount of inhibitor is added to the active cathode areas that reduces the overall cathodic reaction. On the other hand, anodic inhibitors are said to be risky because the addition of too little inhibitor fails to eliminate all the anode sites and as a consequence increases the corrosion rate on those which are left not covered. In general anodic inhibitors are more efficient than cathodic ones as long as sufficient inhibitor is added to the electrolyte. Modern inhibitor systems incorporate both anodic and cathodic types for greater efficiency in retarding the corrosion rate. The cathodic inhibitors impede the overall corrosion rate and allow the anodic type to seal off the anode sites.

1.4.1.4 Vapour Phase Inhibitors (VPIs)

Vapour phase inhibitors also called volatile corrosion inhibitors provide an alternative method of protecting steel components during transport. These are very similar to adsorption type inhibitors, VPIs as the name implies possess highly volatile components that possess a very high vapour pressure. As a consequence these materials can be used to suppress or inhibit atmospheric corrosion of metals (particularly steels) without being applied direct to the metal surface. Such inhibitors are placed in the vicinity of the metal to be protected, and by sublimation and condensation, spreading through the free space in a container condensing a water-repellent (hydrophobic) film on to the exposed surfaces. VPIs are usually only effective in closed spaces i.e. packaging, interior of machinery and containers during shipping, VPIs consists of compounds that are volatile organic cations, usually amine, and an anion which act as an inhibitor. On the metal surface, the cation produces a thin adsorbed film which has two important functions: it is hydrophobic, and it controls the pH of any moist layer which forms on its surface. Carbonate and nitrite are typical anions; these are carried with the volatile cation to deposit on the metal surface. In the case of free water formation on the surface or the metal component getting immersed so that the cation film breaks down, the anion acts to control the corrosion rate by polarising the electrode reactions.

1.4.2 Coatings and coating Technology

Coatings form a good barrier against corrosion. There are many different coating systems and application of coatings. This study focuses on both metallic and non-metallic coatings and how these coatings improve the longevity of the substrate (steel), the focus of this research is zinc alloy and organic coatings. The generation of zinc and zinc alloy coatings on steel is one of the commercially most important processing techniques used to protect steel components exposed to corrosive environment. From a technological point of view, the principles of galvanising have remained unchanged for over 200years. However, because of new applications in the automotive industry and construction industry, a considerable amount of research has recently been focused on all aspects of the galvanising process and on new types of zinc coatings. Tata Steel Europe products include Galvatite (GI), Galvanneal (GA), Galfan or Galvalloy, Galvalume or Zalutite and MagiZinc. These are produced via continuous production lines via hot dipping. Some products are heat treated (annealed) and some are finished with an organic colour coating system. Tata Steel Europe's colour systems commonly used are Colorcoat Prisma® and Colorcoat HPS200®.

1.4.2.1 Hot Dip Galvanised Steel (HDG)

Hot dipping is the most favoured method of applying adherent metallic coating on to steel substrates. The continuous hot dip galvanising process has three distinct stages. The first stage comprises of sheet steel (as coils) being laser stitched to tail end of previous coil. An important component of the first stage is the cleaning of the steel substrate, due to molten zinc only bonds to a chemically clean surface[5]. The cleaning and decreasing of the steel substrate is achieved by applying acid or alkali solution; rinsed with cold running water and then dipped in 10-20%HCl solution at room temperature. This is known as pickling and removes rust and scale. The second stage involves heating of the sheet steel to about 470°C in an oxygen free reducing environment of Hydrogen and Nitrogen and the remaining iron oxide films on the substrate are reduced providing a clean surface for coating. The third and final stage is dipping of the sheet steel into the zinc rich molten bath that is held at temperatures between 450-480°C. Where pure zinc baths are utilised due to the consequence of diffusion based alloying action between the zinc and steel intermetallics are formed at the interface of the two metals. The remainder of the outer layer moving away from the substrate is zinc. The The iron-zinc phase (figure 1.5) diagram shows that at normal galvanising temperatures 445-465°C, the coating consists of layers of the following phases(in order from the steel base): Γ, δ and solidified ζ –zinc [6] figure 1.6. The formation of these phases is dependent upon temperature and immersion period. Thus, there is no sudden transition from steel to zinc but a more gradual change though a series of alloy layers. Intermetallics formed tend to be very brittle subsequently dedicating the galvanised coatings formability with the zinc cracking when bent [5]. Intermetallic formation can be controlled by the addition of 0.3 wt% Aluminium to the zinc bath and is widely used in the dipping process. This aluminium addition improves fluidity of the bath and encourages the formation of Al rich intermetallic $Fe_2(Al,Zn)_5$ at the interface of the coating and the steel substrate. The intermetallic layer is very thin and also prevents the formation of further intermetallic layers resulting in the majority of the coating comprising of pure zinc. Thus the coating is easily formed with the substrate as the zinc is ductile.

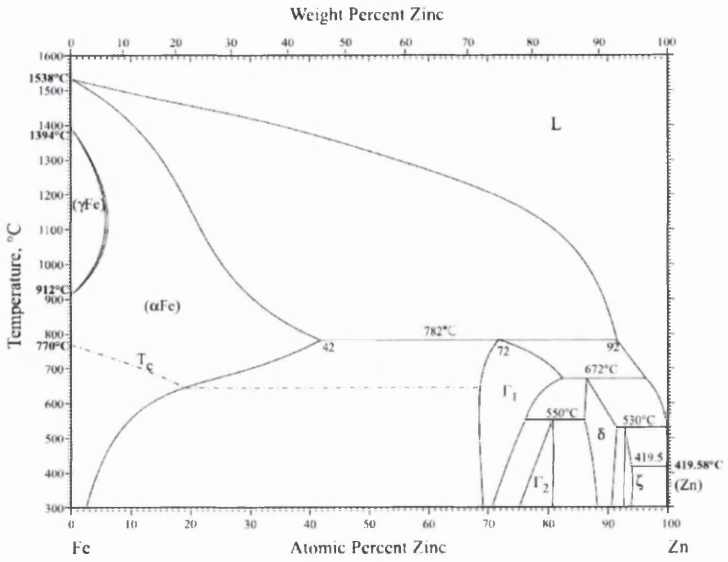

Figure 1.5 The Iron-Zinc equilibrium diagram[7].

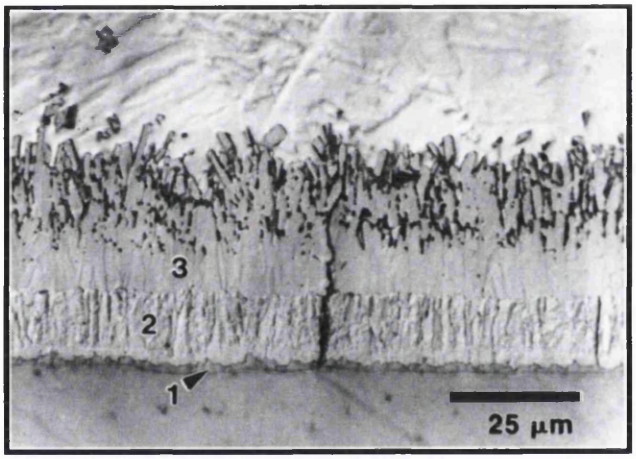

Figure 1.6 The microstructure of zinc coating formed after 300s immersion in 450°C, 0.00% Al bath on a ULC steel substrate (1) gamma (Γ) phase, (2) delta (δ) phase and (3) zeta (ζ) phase[6].

1.4.2.2 Galvalloy or Galfan

Galvalloy coated products are aimed for mainly distinct applications (building panels in rural, industrial or even tropical areas, buried artefacts and under-bonnet automotive parts. They must therefore resist corrosion damage in a wide variety of environments. As a hot dipped based zinc coating; contains 4.5-5% aluminium and up to 0.10% mischmetal. Mischmetal is comprised of rare earth elements such as Cerium and Yttrium and is added for the improvement of fluidity of the molten metal without affecting the corrosion resistance of the alloying system. The percentage of aluminium addition is significant as it near the aluminium eutectic point of the Zn-Al binary eutectic system i.e. minimum melting

point mixture. Under non-equilibrium conditions solidification occurs below this point. The Zn-Al alloy coating contains primary phase zinc rich dendrites in a Zn/Al eutectic matrix. The exact microstructure is influenced by processing and cooling rate affecting the microstructure and consequently the primary phase dendrite size. Figure 1.7 illustrates typical coating eutectic microstructures.

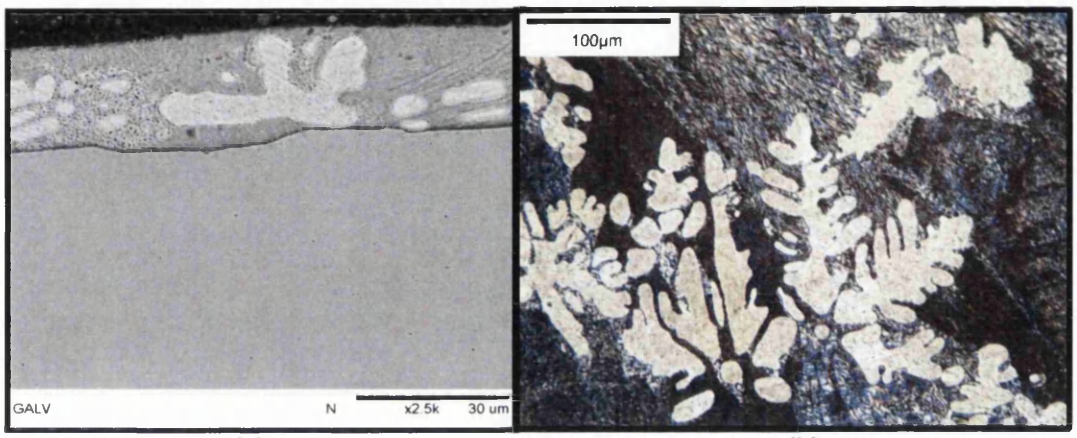

Figure 1.7 Typical Galvalloy microstructure (a) cut edge (b) Zinc dendrite and Eutectic structure

1.4.2.3 MagiZinc or Mg/Zn

The demand on the steel industry for a better, more versatile, metal coatings is ever increasing. Steelmakers are making a big effort to optimise coating composition in order to extend the life time of steel product and also save cost. Zinc and zinc alloy coatings are known to lengthen the service life of a steel product. Some of the notable Zn-Al commercial alloys like Galvalume and Galfan have good performance. Galfan has corrosion resistance of about 2-3 times more than that of a galvanised steel in most industrial and marine environments [8]. Though the addition of increased levels of aluminium have remarkably improved the corrosion resistance of these coatings, the sacrificial or cathodic protection capabilities have been proportionally compromised compared to pure zinc coatings due to reduced level of zinc in the coatings. To address the relatively low sacrificial protection offered by Zn-Al alloy coating, Nisshin in 1998 introduced the first Zn-Al-Mg alloy coating known as ZAM. ZAM retains the excellent corrosion resistance of Zn-Al alloy but also improved cathodic protection due to the presence of magnesium in the alloy. Magnesium exists as $MgZn_2$ intermetallic in this alloy which is equally active as magnesium. Tata Steel Europe and other steelmakers have been developing Zn-Mg-Al coated products for building

and automotive industries via either hot-dipping in baths containing magnesium or physical vapour deposition technology. MagiZinc, a Tata Steel Europe product, having a typical composition of Zn-(1.6% Mg)-(1.6% Al), figure 1.8 illustrates the microstructure of the alloy coating. The Zn rich phase is the first phase to form on cooling with dendrites nucleating and growing the steel substrate and alloy coating interface. The binary eutectic is next to form and is comprised of $MgZn_2$ and Zn with the final ternary eutectic phase solidifying. The Ternary phase comprises of lamellar of $MgZn_2$, Zn and Al nodules. $MgZn_2$ has been shown to be the dominant Mg containing phase within hot dipped coatings of this composition with no Mg_2Zn_{11} [9]. The formation of $MgZn_2$ over the equilibrium phase Mg_2Zn_{11} due to non-equilibrium freezing condition during fast cooling on production lines [10]. Tata Steel Europe first introduced a product based on MagiZinc in May 2008. Tata Steel Europe are currently offering this with the following coating weight: ZMA100 (100g/m^2) - ZMA200 (200g/m^2) and thickness: 0.4 – 2.0 mm. The addition of magnesium to the Zn-Al system resulting in a ternary alloy has been proved to give increased corrosion protection over the standard HDG in standard industry corrosion Pre-painted Zn-Al-Mg alloy coated steel sheet subjected to Salt Spray tests and Cyclic corrosion Tests and 16 months of natural weathering resulting in improved corrosion performance than existing systems [10,11].

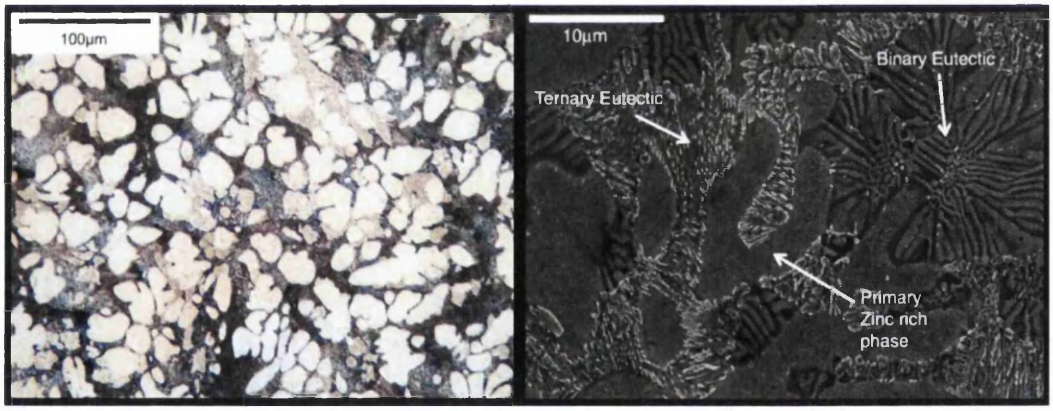

Figure 1.8 MagiZinc microstructure

1.4.2.4 Non-metallic Coatings – Organic Colour Coatings

The role of non-metallic coatings in corrosion protection is to isolate the substrate from the environment. Organic coatings in combination with sacrificial metal coating are the most popular method of protecting the steel against atmospheric corrosion. Such duplex coating systems are best suited for the sheet coil industry. The corrosion resistance of such systems can be attributed to the synergy between the cathodic protection provided by the zinc alloy coating and combined barrier resistance of the metal and organic coating. The organic

coating system comprises of three layers that are applied to the substrate in sequence, by continuous coil coating line figure 1.9. The coating line can be subdivided in three main sections, the entry section, the process section and the exit section.

In the entry section the tail end of the coil in process is joined to the front end of the following coil to be coated. An accumulator is used as a substrate reservoir which allows the process to remain operational whilst two coils are joined. The process section can also be subsectioned into two zones, pretreatment and paint application.

On entry into the coil coater within the pretreatment zone the galvanised steel is alkali cleaned, followed by a hot water rinse to remove all excess alkali and surface impurities. It is then roller coated with a 1μm thick layer of pre-treatment and dried. In the case of most products for external applications a chemical conversion is carried out traditionally by a chromating process. Due to increasing regulations regarding chromate use for pre-treatments, with phosphate alternatives becoming increasingly more common, in this case the substrate is subjected to a conditioning process prior to phosphating. Application of a conversion coating serves a dual purpose, to further increase the corrosion resistance of the substrate by inhibiting the spread of underfilm corrosion and to modify the surface to improve primer and topcoat application. The continuously moving strip is coated with the chemical conversion coating by a roller coater and then heated to approximately 80°C to remove the water content from the coating.

The pretreated substrate is lead into the paint application zone, where firstly the substrate proceeds through to the priming stage. A layer of primer (5-30μm thick) is applied to enhance the corrosion resistance of the coated product and prepare the substrate surface for the finishing coat. The substrate then passes through the primer oven set at 400°C, on passing through the oven at line speed (30-150 m/min) the substrate reaches a peak metal temperature (PMT) of ~220°C thus ensuring it is fully cured. The primers used in the coil coating process are based on epoxy, polyester or acrylic resins pigmented with a sparingly soluble corrosion inhibitor. Due to tightening legislation the use of traditional strontium chromate or calcium chromate based pigment is restricted; powder of Trizinc Bis (orthophosphate) is finding increasing use as primer pigment. The final stage in the paint application zone is where the coil is quenched and passed through to the finish coater where the topcoat is applied by a roller coating process. The application parameters and thickness of the topcoat is dependent on the formulation of the resin and added constituents. It is generally 25-100μm thick on the exterior surface and significantly thinner on the backing coat of the steel and is controlled by the distance between metering and

coating rolls in relation to the line speed and coating viscosity. The coated coil is cured in the finishing oven which is often multi-staged, tailoring the temperatures to the coating system used. The total curing time is dependent on the topcoat used but is on average 25-35 seconds. If further processing such as embossing is required, then it is carried out on the cured coil prior to the final quenching and drying process.

The finished coated material is then inspected for quality and recoiled in the exit section. Excess strip is held in the exit accumulator whilst shearing of the desired length of coil occurs; use of accumulators alleviates the need to stop the coil coating process.

In the coil coating process, it is possible to apply a top coat and backing coat simultaneously. In this case the strip must remain unsupported during the primer and finishing coat curing processes, this is achieved using a catenary oven system which maintains tension in the coil using bridle rolls. The backing coat system of organically coated steel is comprised of similar layers as the topcoat system. The galvanised substrate is coated with a pre-treatment and primer identical to that of the exterior coating, and a thin final layer of paint – which is frequently a different polymer system. The topcoat and or the backing coat offer mostly barrier protection to the underlying substrate.

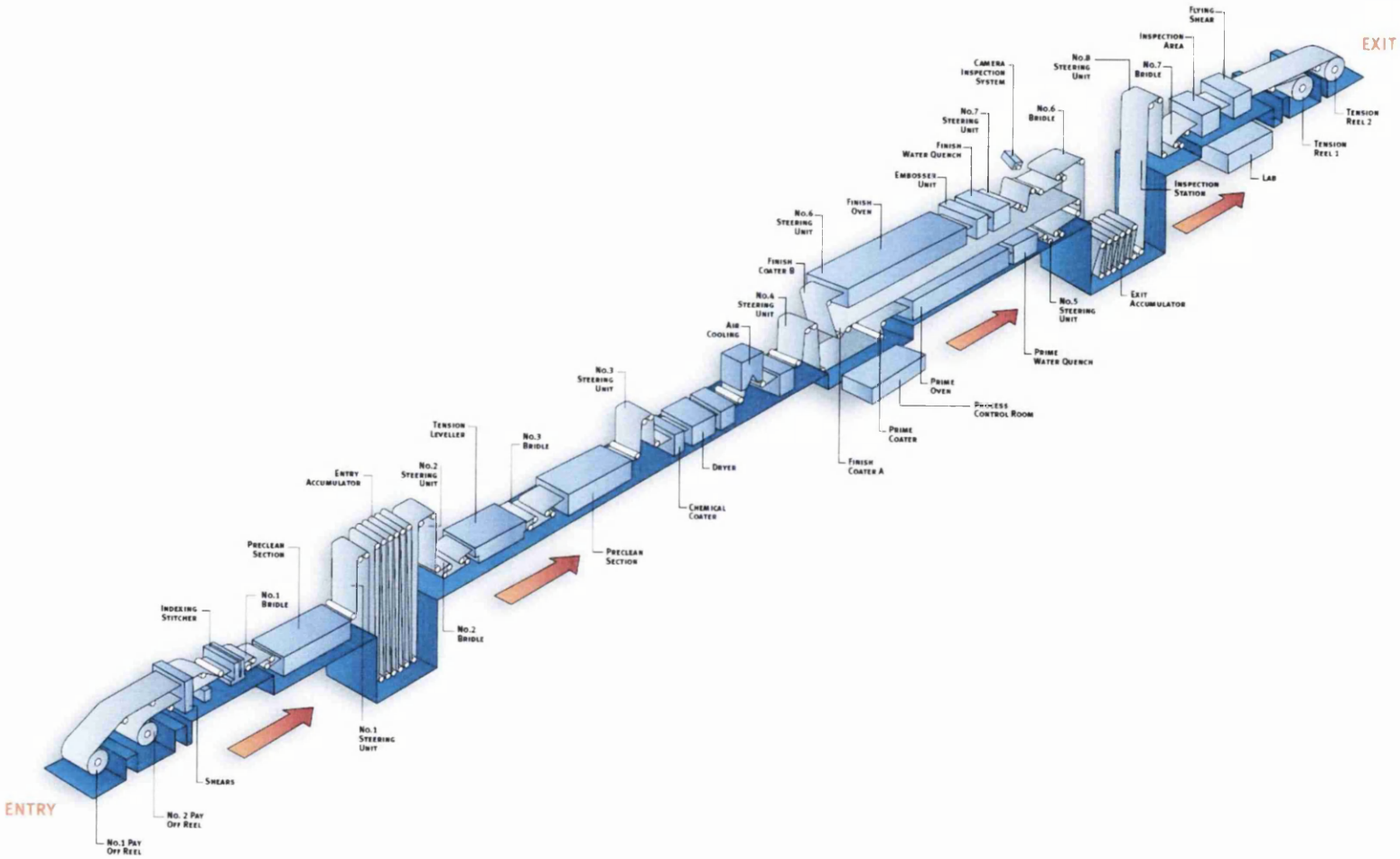

Figure 1.9 A schematic of a typical coil coating line.

A typical commercial organic coating consists of numerous ingredients that can each be categorised in one of four groups (i) organic binder (resin), (ii) volatile component (solvent), (iii) pigment and (iv) additive. The binder is a component of the matrix which eventually solidifies to form the dried paint film. Typical binders include synthetic or natural resins such as acrylics, polyurethanes, polyesters, melamines, oils, or latex. The volatile component or diluent serves to adjust the viscosity of the paint. It is volatile and does not become part of the paint film examples are alcohols, ketones, esters and ethers. Pigments typically a fine powder are added to a binder, which is a relatively neutral or colourless material that is film forming component of the system. Powdered metals can also be used as pigments to give added anodic or cathodic protection to the overall system. The corrosion protective properties can be influenced by manipulation of any of the ingredients even if the ingredient is designed to impact an aesthetic quality e.g. gloss and not corrosion performance as such. Paint systems can have a wide varity of miscellaneous additives, often included in small quantities these may contribute towards control of surface tension, improve adhesion and ultraviolet stability. Plastisol is a generic name for the PVC based paint coating that is applied to the steel substrate in liquid form. Plastisols are available in a huge choice of colours and finishes and are widely used for internal and external construction applications, as well as general engineering. Tata Steel Europe's brand name for its range of plastisol products is Colorcoat®. Within this range there are a number of well-known trademarked products, such as Prisma® and HPS200®. Figure 1.10 shows a schematic of the different layers of a pre-finished steel product. There is an ongoing drive to improve the performance of coatings to extend the product life.

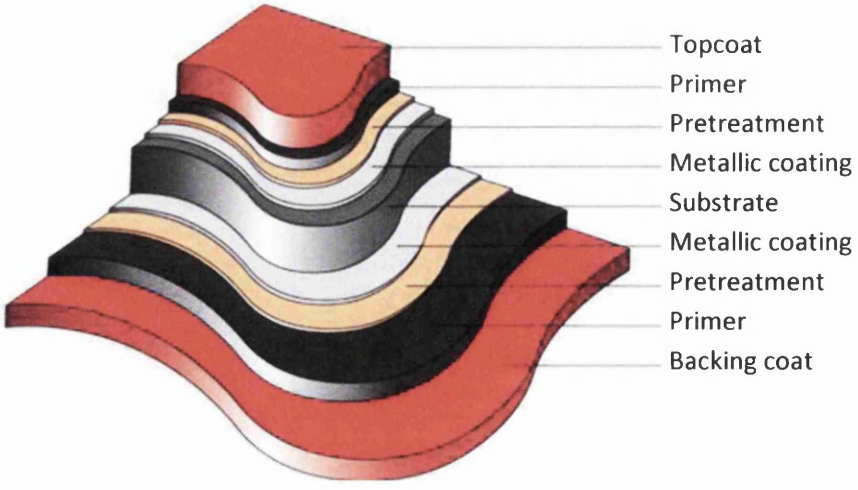

Figure 1.11 Schematic of the layers of a typical paint system.

1.4.3 Use of chromate based Inhibitor and challenges of suitable replacements

In order to optimise the anticorrosion performance of organically coated steel sheets pigments based on hexavalent chromium, chromate salts (Cr(VI)) have been used extensively in organic coating systems. Registration, Evaluation, Authorisation and Restriction of Chemicals (REACH) a European Union Regulation founded 18 December 2006 addresses the production and use of potential chemical substances that can harm both human health and the environment. REACH has identified Cr(VI) as a substance of very high concern due to the negative impacts on human health and environment.

Corrosion of OCS used in construction predominantly occurs at the exposed cut edges. Construction materials typically cladding coated with organic over layers and primer layers pigmented with hexavalent chromate salts (Cr(VI)) typically strontium chromate ($SrCrO_4$). In such materials the anodic activity is localised on the zinc (alloy) layer underlying the thicker organic coating with the cathodic activity focused on the steel. The chromate based pigments function well under non acidic, neutral pH corrosive conditions. Initially the anodic sites are focused upon the zinc alloy layer. The pH localised to the anodes becomes acidic, chromate pigments subsequently leach out reacting to form soluble dichromates of ($Cr_2O_7^{2-}$). Dichromates are also oxidising agents and passivate the exposed surfaces and so reduce the rate of corrosion. Ferrous and zinc ions in solution are also oxidised by the dissolved dichromate ions forming ferric hydroxide and chromic hydroxide. These are both insoluble and precipitate onto the exposed metal surface. The surface becomes electrically insulated from the environment, thus restricting corrosion process. At cathodic vicinity the presence of alkali (hydroxyl ions) can cause the zinc hydroxides to redissolve and from zincates. This could lead to an incremental loss of inhibition. Strontium (from strontium chromate pigment) can form a sparingly soluble hydroxide that is slightly alkaline, thus inhibiting formation of more alkali at the cathodic locality [12,13].

There is considerable work focused upon discovering a suitable replacement for Cr(VI) inhibitor. Replacements such as rare earth metal cation salts namely cerium Ce(III), lanthanum La(III) and yttrium Y(III) have been tested to be efficient inhibitors [12,13]. Properties of corrosion inhibition of various phosphates based pigments such as aluminium triphosphate, calcium phosphate, calcium zinc phosphate and zinc phosphate have been subject of much research. Phosphate based inhibitors also show a promising prospect as a replacement for Cr(VI) [14,15]. It has been demonstrated that ion-exchange pigment technologies have been exploited for retarding corrosion. Ion-exchange minerals also called smart-release pigment are incorporated with an organic polymer with gaining appeal with

inherent ability to release inhibitor species and hinder aggressive ions only when a corrosive aqueous environment exists. Typical example of an ion-exchange pigment that is commercially available is an exchangeable calcium-containing silica pigment [16,17]. Electroactive conducting polymers (ECPs) represent a class of interesting materials being explored for use in corrosion control coating systems, possibly as a replacement for Cr(VI)-based coatings [18-20].

1.5 Accelerated Corrosion Testing

The information of a product and durability or expected in-service life can be predicted via accelerated testing. Natural atmospheric weathering 3-5 years testing usually give most precise results. However, there is a need to rapidly predict or evaluate the corrosive resistance of a product. There are a number of accelerated tests, which give extrapolated results on performance of a coating in a smaller time frame. Such tests aim to increase the corrosion rate whilst giving a satisfactory correlation between the accelerated rate and the natural rate of corrosion without introducing new corrosion reactions that may give misleading results [5]. These tests simulate the natural corrosion mechanism as closely as possible whilst accelerating the corrosion rate allows technically useful results to be obtained from a short test duration. In such laboratory tests the combination of dominant factors that produce corrosion must be focused such that enhancing the actions of these dominant factors [21]. In order to attain valid informative results, design of the exact test conditions is crucial, some vital consideration are:

- The test must accelerate the corrosion process without changing the corrosion mechanism.
- How will acceleration be achieved?
- What are the limits of the test?
- Prarameters to take into account include temperature variations, humidity, amount of rain fall (surface water), drying out periods, chemical environment, pH etc.

The following subsections briefly describe some of the traditional accelerated corrosion tests.

1.5.1 Salt Spray (Fog) Test

The salt spray test is a method of testing protective coatings on iron or steel to determine their probable performance in coastal atmospheres. The test consists of subjecting specimens to a mist of 3, 5 or 20 wt% sodium chloride (NaCl) solution at 20-40°C and

observing the amount of attack after a given time interval [5]. The recommended period of exposure in salt spray test is 16, 24, 48, 98, 200, 240, 500 or 1000 hours or mutually agreed upon by individuals concerned. It has been suggested that the salt spray test is unreliable as a means of evaluating corrosion resistance performance in a seacoast atmosphere model [5,21]. However this test is widely recognised and used for the purpose of comparison of different metals and coating performance in various concentrations of mist, salt spray.

1.5.2 Prohesion Test

Prohesion test is a measure of degradation of a paint layer; paint system failure is by blistering or delamination caused by physical and chemical attack. This is a less severe adaptation of the standard salt spray test. The method typically involves the test panels mounted in a chamber into which is introduced an aqueous solution of salts in form of a fine aerosol. The method differs from the standard salt spray test in that the salt solution used in the prohesion test is relatively dilute and the panels are not continuously exposed. This method involves exposing the samples to an aqueous solution containing 0.35% ammonium sulphate ($(NH_4)_2SO_4$) and 0.05% sodium chloride (NaCl) solution. The test cycle consist of 1 to 3 hours exposure to the salt mist at ambient temperature followed by 1 hour drying at 35°C. This test was employed successfully [22,23], resulting a good simulation of natural exposure.

1.5.3 Sulphur Dioxide (SO_2) Test

Sulphur dioxide accelerated tests are used to model corrosion in industrial atmospheres where attack from moisture and acidic gases are dominant. It is certain that corrosion is promoted by the combination of high humidity and presence of sulphur dioxide. Sulphur dioxide in atmosphere can transfer to surface of the metal via rain or dew formation producing acidic aqueous solution on the metal surface. This acidic solution accelerates metal dissolution quite considerably causing more rapid corrosion at industrial sites due to both increased electrochemical reaction process from greater ionic conductance and decreased pH. The sulphur dioxide accelerated tests are generally performed in conditions of 25°C, above 95% humidity with 0.5-2% SO_2 by volume in air for periods of 6-24hrs at temperatures 20-40°C [21]. It has been reported that concentration values of sulphur dioxide are crucial [21], if sulphur dioxide concentration is exceeded, the SO_2 reacts as a solution species (i.e. HSO_3^-), and this results in corrosion reaction (and products) that differs remarkably from natural process. Thus sulphur dioxide concentration is crucial to quantitatively speed the corrosion rate forming sulphate on the metal surface.

1.5.4 Humidity Test

In a tropical environment where there is relatively high humidity and daily temperature cycles rapid corrosion of metals can occur. This corrosive environment may be simulated in laboratories by inducing humidity cycles in an enclosed chamber. Condensation can be influenced by the use of temperature or humidity cycles; typically humidity is held constant and change in temperature, this results in condensation forming on the metal surface initiating corrosion. Usually Humidity is held at approximately 90% with the temperature cycle from 25°C to 50°C accomplished in 30min [5]. The cycle is repeated every 2 hours allowing condensation to remain on the surface for a predefined duration. Several variances exist for this test i.e. temperature range, hold or cycle repeat time etc.

1.5.5 Recent Works on Accelerated Corrosion Tests

The requirement of corrosion performance data of metallic materials and relative long time needed to acquire measurable corrosion results exposed to natural environment led to many methods of accelerated corrosion tests. It has been assumed that the rates of corrosion are increased by appropriate means and a satisfactory correlation is established between the accelerated rate of reaction and natural corrosion rate.

Accelerated tests and outdoor exposure of coiled galvanised sheet steel tests have been compared [24]. Galvanised steel sheets were subjected to various tests, such as, resistance to chemicals (i.e. 5% NaOH, 5% HCl solutions), salt fog exposure, humidity exposure and outdoor exposure test (panels exposed to marine and continental-industrial locations). They have at first evaluated the performance of coated galvanised steel systems with and without chromates as pigment in primer and pretreament through laboratory tests and outdoor exposure and secondly they have correlated the results of accelerated tests with outdoor measurements to predict failures in service of these anti corrosion technologies. They have reported that water borne primers provide a high initial barrier effect, however in high chloride concentration, blistering of the paint film and corrosion of zinc was unavoidable [24]. The diffusion of chloride ions to the paint-galvanised steel interface has resulted in increased electrochemical activity of zinc and consequently its dissolution. It was also established that the chromates were effective inhibitors for zinc anodic dissolution particularly in the standard polyester topcoat and strontium chromate primer. In aqueous environment, the chromates diffused towards the zinc surface where they were reduced to trivalent chromium that precipitated forming a passive layer. With the passage of time, the paint permeability increased maintaining the corrosion protection of the

substrate metal [24]. Chromates in the standard primer continued to inhibit zinc corrosion after two years of outdoor exposure, whereas water based epoxy Cr(III) primer protection was exhibited in the initial 6 to 12 months that was related to total Cr content [24]. It is concluded that the standard polyester topcoat and strontium chromate primer paint system provides higher corrosion protection than the polyester and water based epoxy Cr(III) primer. It is generally understood and reported else were [5,21,24] that accelerated tests are used for estimating a ranking of performance in service and do not reproduce the characteristics of outdoor degradation, however both aree considered as complementary.

The cut-edge corrosion of coil coated sheet cladding utilising salt spray, prohesion and novel wet/dry cyclic tests have been investigated [22]. Tests were performed on a number of organically coated steel sheets; Zalutite with PVC coating, Galvalloy with PVC coating, Hot Dip Galvanised (HDG) steel sheet with PVC coating. Results from these tests were compared with specimens subjected to natural weathering, 2 years and 5 years, exposure at severe marine site and at industrial-marine site respectively. The results of the investigation showed that the outcome of the novel cyclic and salt spray tests were varied; prohesion tests were more consistent. These tests delivered undercut data and blistering area measurements. Scanning electron microscope analysis of the samples suggest that Zalutite performed better than HDG followed by Galvalloy. They concluded that large variations and scatter of results for identical specimens were observed for some of the test highlighting the tests consistency in the their prediction of long term behaviour, however in this case it is reported that the prohesion test offers a good compromise between realism and adequate acceleration of atmospheric corrosion [22].

1.5.6 Scanning Electrochemical Techniques

Scanning electrochemical techniques are fairly common practice and effective in studying the kinetics and mechanisms of metallic corrosion in aqueous environments. There are small differences in various techniques but typically operate via the scanning motion of a probe above the corroding surface submerged in solution. The probe is a scanning microtip electrode that usually is a small distance away from the corroding surface and attains data such as local potential, potential gradient or current. From such data corrosion kinetics and active anodes/cathodes are observed and analysed. The data area interpreted using specialised software and presented as topographic area map or spatially resolved representations that are used to infer local differences in surface current density and reactivity. There are three variants of the technique most commonly employed; the Scanning Reference Electrode Technique (SRET), the Scanning Vibrating Electrode

Technique (SVET) and the Scanning Kelvin Probe (SKP). SRET and SVET permit assessment of immersed sample surfaces in solution and SKP allows investigation of corrosion activity beneath organic coatings or moisture films.

The electrochemical technique SRET is utilised for the study of the surface corrosion, in brief the potential in the solution is measured generated due to the flow of ionic current from anodes to the cathodes. The technique is able to locate the corrosion activity however its sensitivity and spatial resolution is limited. With the advancements of technique SVET is now favoured, SVET is similar in operation to SRET. The SVET is relatively more sensitive and provides higher spatial resolution. SVET is described in greater detail in the following section and measures the vertical component of current flux generated by the surface corrosion phenomenon under solution. The SKP technique is based on scanning capacitor measurements of the corroding surface. This technique is well suited for measurements of corrosion reactions beneath organic coatings but less competent to investigate corrosion occurring on immersed surfaces.

1.5.6.1 The Scanning Vibrating Electrode Technique

The SRET is the forerunner to and replaced by the SVET. The SVET has been shown to be invaluable tool in the study mechanistic investigation of corrosion in organic coated steels and specifically, cut edge corrosion [25,26].

A corroding metal in an aqueous environment can result in localised corrosion features on the surface. On the metal there are localised anodic sites and cathodic areas, and ionic current flow is established between these sites. The distribution of ionic current through the electrolyte originate from a localised anode and is envisaged as lines of current flux passing from the anode to the cathode. The conducting circuit is completed by electron flow through the substrate metal, the resistance of which is negligible in comparison to the electrolyte and thus metallic surface is a plane of constant potential. The solution or the electrolyte having considerable higher resistance than the metal, the movement of ionic current through the solution consequently produces ohmic potential gradients. These can be represented as series of lines of iso-potential lying normal to the lines of ionic current flux as shown in figure 1.12.

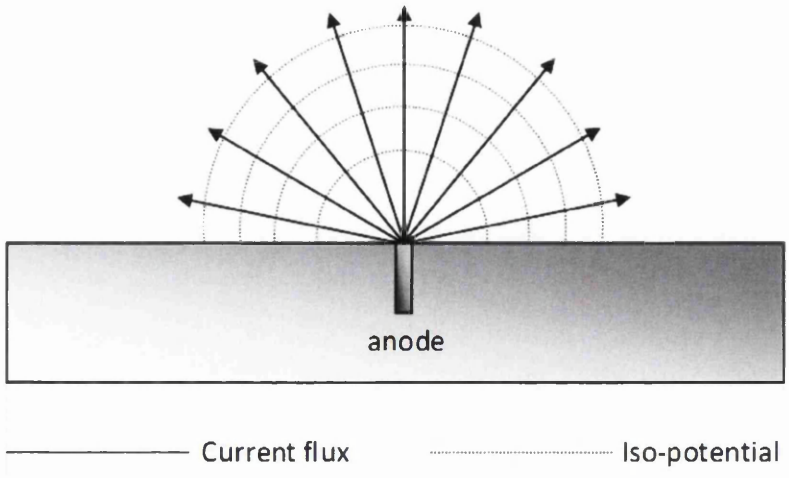

Figure 1.12 Schematic diagram showing lines of ionic current flux emanating from a localised anode setting up lines of iso-potential. The cathode in this instance is assumed to be "remote" giving radial distribution of current flux.

The distribution of the potential and ionic currents is theoretically derived by the Laplace equation:

$$\nabla^2 E = 0 \tag{1.7}$$

where *E* is the electrical potential, and Ohm's Law,

$$i = -\kappa \nabla E \tag{1.8}$$

where *i* is current and κ the solution conductance. Except in the very simplest of cases solutions to this problem are non-trivial and no general analytical solution is possible. However, analytical solutions may readily obtained in the case of point current sources *i* situated at height z = 0 on a non-conducting x, y plane with the current drain at infinity. It is shown that the potential at any point (x,y,z) in solution is inversely proportional to the distance from the source and is given by

$$E = \frac{i}{2p\kappa\sqrt{(x^2 + y^2 + z^2)}} \tag{1.9}$$

The vibrating probe converts the normal component of the potential into AC voltage by means of mechanical motion and can therefore register a signal. The magnitude of the current flux is directly proportional to corrosion intensity and therefore the changes in corrosion activity are recorded. Considering the anodic point current source the normal electric field strength (F) measured by the SVET vibrating probe perpendicular to the sample surface is given by the z differential of the equation (1.9), is given by

$$F = \frac{dE}{dz} = \frac{iz}{2\pi\kappa(x^2 + y^2 + z^2)^{1.5}} \quad (1.10)$$

Furthermore, the maximum field strength (F_{max}) will be obtained SVET probe is directly over the point source (x=y=0):

$$F_{max} = \frac{i}{2\pi\ \kappa\ z^2} \quad (1.11)$$

It can be concluded from equation (1.11) that there is an inverse square relationship between the maximum field strength (F_{max}) and the probe height and thus making critical the control of probe height above the surface. Theoretical spatial resolution of the SVET is determined by calculating the signal peak width at half maximum peak height (*whm*). Considering a quantity r as the distance from a point current source on the x,y plane then,

$$r = (x^2 + y^2)^{0.5} \quad (1.12)$$

The value of r where F is equal to half the maximum value is found by combining equations (1.11) and (1.12) and thus,

$$0.5F_{max} = \frac{iz}{2\pi\kappa(r^2 + z^2)^{1.5}} \quad (1.13)$$

The ratio of equations (1.10) and (1.12) gives

$$r = z\,(2^{2/3} - 1)^{0.5} \quad (1.14)$$

and the width of the SVET response peak is 2r hence,

$$whm = 2r = 1.533z \quad (1.15)$$

The theoretical maximum spatial resolution of the SVET at a scan height of 100μm is 153μm.

In the work described here the probe is formed of a platinum electrode microtip (diameter 125μm) insulated with a glass sheath enclosure. The probe tip is attached to a moving coil loudspeaker cone that induces controlled vibrations. This probe assembly including the loudspeaker is moved by a tri-axial micro-manipulator stage controlled by a personal computer that also serves as a data logging device. Vibrations of the tip are controlled by a lockin amplifier oscillator ensuring correct frequency and phase of synchronous detection. The lockin amplifier also registers the ac signal detected by the probe that is recorded to a personal computer.

1.5.6.2 Recent Corrosion Analysis using the SVET

The SVET has increasingly been utilised in the study of corrosion phenomena. This technique allows an in situ measurement of current density close to the surface of immersed sample under investigation in an electrolyte. Current density maps determined by SVET offer a method of observing the onset and progress of corrosion. Being an *in situ* technique, mapping of current density is used to locate spatially distributed corrosion sites and to quantify its progress as it grows [27]. The SVET has been deployed to study electrodeposited Zn and Zn-Co-Fe alloy coatings to protect steel both galvanically and due to passivation in dilute chloride solutions [27]. The SVET analysis of immersed high strength steel sheet of 1mm thickness cut unto strips 2.5 x 5.0 cm^2 with partial electroplated Zn and Zn-Co-Fe coating in 10mM NaCl electrolyte for 30min, 1.5hrs, 3hrs, 24hrs and 27hrs. They compared the performance of the two partially coated steel strips one with Zn coating and other with Zn-Co-Fe coating. The first SVET measurements (after 30min) of immersion showed that the Zn coating acted as the active anode. After 1.5hrs of immersion, the main anodic peak shifted to another side and the intensity of the current density also diminished, after 3hrs of exposure time the intensity of the anodic current density has decreased sharply while the relatively large area of sample showed reasonable uniform but negative (cathodic) values.

In the case of a partially Zn coated sample the local electrochemical corrosion process consisted of mainly zinc dissolution as an anodic process and oxygen reduction on the steel as the cathodic process. It is well discussed in literature [28] that Zn^{2+} ions dissolved in the electrolyte can effectively act as cathodic inhibitors. The reduction of oxygen or water that produces hydroxyl ions result in an increase in local pH that further leads to non-uniform precipitation of $Zn(OH)_2$. The decrease in the anodic and cathodic current densities and variation of active sites on Zn surface with the time of exposure was attributed to the formation of a barrier layer of $Zn(OH)_2$ that blocks further dissolution of zinc. After 24hrs of immersion, the anodic and cathodic activities were wide spread on the whole sample area and zinc coated area is no longer distinguishable, indicating the laps of protective capability of Zn coating. It is implied from that the passive layer formed over the surface is transformed and no longer able to protect. Exposure of sample for 27hrs showed further increase in corrosion activities in terms of SVET measured increased anodic and cathodic current densities.

The Zn-Co-Fe alloys coating samples were prepared with three alloy concentrations mainly varying the Co content. It is concluded with the aid of SVET measurements that anodic and cathodic activities can clearly be distinguished at the coated and uncoated areas of the sample as well as changes in the location and magnitude of the associated current densities with time of exposure. The sacrificial properties and the protection range decreased with the increase of Co content in the alloy layer. Further to the above they derived that for higher content of Co in alloy layer, the coating becomes more noble to steel and loses its sacrificial protection. The barrier resistance of the coatings increases with higher Co content in the alloy coating. It is found that a barrier layer is formed for the Zn-Co-Fe alloys during immersion in 10mM NaCl solution that covered the surface and reduced corrosion activities. For both Zn and Zn-Co-Fe alloy layer with low Co content both white and red rust became apparent after 24hrs exposure. The Zn-Co-Fe alloy layer with the highest Co content 32%wt + 1%wt Fe, the coating tended to be anodic compared to the coupled steel during early exposure time. However after dezincification the presence of a stabilised hydroxide barrier in conjunction with the presence of greater amount of Co on the surface enhanced overall barrier resistance of the coating. There was no white or red rust present near the Zn-Co-Fe alloy coated area and the coating demonstrated it was able to protect the exposed steel to a certain distance in a corrosive environment [27].

The corrosion resistance was evaluated of bis-[triethoxysilypropyl] tetrasulfide (BTESPT) doped with cerium nitrate pre-treatment by the use of electrochemical techniques. One such technique deployed was the SVET during immersion in NaCl solutions [29]. It was found that adding Ce gave aluminium 2024 alloy and hot dipped galvanised substrates increased protection via two mechanisms. Firstly addition Ce improved the barrier performance of the coating by increasing the coating density. Secondly Ce inhibited cathodic activity. Analysis of the SVET data revealed that the addition of Ce to the coatings had reduced the corrosion currents present on the substrate surfaces [29]. By introducing a defect in the coating SVET examination resulted in location and intensity of corrosion currents occurring at the defect site. SVET immediately detected the anodic currents associated with galvanic corrosion occurring upon creation of the defect site. Findings suggest reduced cathodic activities due to Ce encouraging formation of hydroxide/oxide layer and local increase in pH. The use of electrochemical impedance spectroscopy and scanning electron microscope confirmed this hypothesis and showed evidence of deposits of cerium and oxygen in the locations where intermetallics were present.

1.5.7 Metal Runoff Analysis Technique

Organically coated galvanised steels are commonly used in the construction industry. These materials are considered to be low maintenance, have long lifetime and are easily adapted to various designs. Zinc galvanising is used as surface coating to prolong structural integrity by improved corrosion resistance. Metal salts based on chromates (Cr(VI)) are used in organic coating systems for exterior as adhesion promoters and in the form of corrosion inhibitor pigments[30]. When exposed to atmospheric conditions these materials are subjected to a corrosion process in which corrosion products form on the surface. The composition and nature of these products depends upon exposure conditions in terms of humidity, temperature, dry and wet deposition of gaseous and particulate pollutants. During a rain event, soluble corrosion products are removed from the surface. The run-off water is collected and the metallic leachants in the run-off analysed for various ions present. The leachant metal quantification is made possible with the use of inductively coupled plasma (ICP) combined with mass spectrometry.

1.5.7.1 Inductively Coupled Plasma – Mass Spectrometry (ICP-MS)

Inductively coupled plasma (ICP) is an analytical technique used for the detection of and quantify trace elements (metals) in an aqueous sample. The aqueous sample is transformed into an aerosol via a nebulizer. When measuring metal content in the liquid sample; the nebulizer jets gas at right angles over the exit of the tube containing the liquid. The gas shears the liquid forming very small droplets. The droplets are fed through a spray chamber that only allows droplets of a particular size and velocity. The sample aerosol is introduced into path of ICP torch/plasma within the hardware. The plasma is generated by coupling the energy from a radio frequency generator into a suitable gas (argon) and by introducing electrons emanating from a spark by Tesla coils, which is accelerated via a magnetic field induced through copper coil. This combination of circumstances ionise the argon gas atoms resulting in a self sustaining plasma. The plasma is characterised by intense heat ~10000K. The interaction of the plasma and aerosol results in the formation of ions at atmospheric pressure. There exists an interface consisting of two cones with an opening in each of the cones of 1mm in diameter. The interface is held at vacuum and the plasma tuned to allow the ICP induced ions to flow through the aperture into the Mass spectrometry Quadrupole compartment. Mass spectrometry works on the basis that ions of an element are deflected in a magnetic field with the amount of deflection dependent

on the mass/charge ratio of the ion. The quadrupole mass spectrometer works by allowing only one mass of ions to pass through to the detector at any given time. The quadrupole essentially sorts ions based on their mass/charge ratio, by setting the correct combinations of voltages and radio frequencies to guide the ions with the selected mass/charge ratio towards the detector. The ions strike the active surface of the detector, known as a dynode, an electron is released each time an ion impacts the surface. An array of conversion dynodes or electron multipliers is utilised to induce a cascade effect of electron release until a measurable pulse is produced. Pulses generated are monitored and the system counts the analyte ions that hit the first dynode. The output from the detector is recorded and interpreted using a desktop standard computer. The ICP-MS software enables the desired elements for analysis to be easily selected and then tested on an elemental composition, with quick response time.

1.5.7.2 Recent Studies of Zinc Runoff

The increasing awareness in society of the potential adverse effects that release of metals from diffuse sources may have on man and environment. As a result, several legislative actions and restrictions have been implemented against the use of certain metals and metal groups. Corrosion induced metal runoff from buildings and metallic structures are considered to be one of the major sources of diffuse dispersion of metals. A successful way to improve corrosion resistance of metallic structures is to apply cathodic protection. Cathodic protection is achieved by several methods for example; compressed current, sacrificial aluminium or magnesium or zinc anodes. The uses of galvanised steels or steel structures with sacrificial zinc modules are commonly used for marine and outdoor structures.

The impact of zinc dissolution (anodic activity) in runoff on marine sediment for metallic contamination has been investigated [31]. Sacrificial zinc anodes are widely used to protect ships and steel metallic components in harbour structures. It is reported that increased shipping traffic combined with lower renewal of the seawater by tides due to harbour design contributes to an increase of water zinc level. Concentrations reached up to $25\mu gL^{-1}$, dependent upon tide exposition, whereas the zinc average concentration in open ocean are reported to be less than $0.5\mu gL^{-1}$ [31]. A 12 month experiment using carbon steel and natural sea water was conducted to evaluate the potential zinc contamination of sediment and sea water. The zinc toxicity depends on its total concentration but also on its mobility and reactivity with the ecosystem constituents. The investigation focused on cathodic protection and calcareous deposit formation on carbon steel samples in natural sea water

and buried in sediment. The cathodic protection potential provided by the zinc anode was maintained at -1V/AgAgCl. A 70L container with natural marine sediment and sea water continuously circulated at a rate of $5m^3h^{-1}$ allowing good oxygenation of the water, an additional supply of fresh sea water which represents 5% of the sea water rate leading to total tank renewal every 4 hours. Sea water and sediments were collected from 400m from the Luc-Sur-Mer shore, Normandy France. A total of 10 steel samples were studied, 2 samples were removed after 1, 3, 6, 9, and 12 month exposure. Steel samples were submersed in water and some were buried under sediments. Sea water and sediments were also periodically monitored. Sediments were collected from three zones: superficial sediments (in contact with water), sediments close to the steel structure (15cm from water/sediment interface) and deep sediments (30cm from water/sediment interface). Zinc concentrations in collected water were determined using inductively coupled plasma atomic emission spectrometry. Sediments were leached by optimised sequential chemical procedure. The levels of elements measured were greater than expected due to the water and sediment used in the experiment that were sampled near the shore and is most likely contaminated due to excessive human activities.

In the course of the experiment no significant concentration variations were reported for any of elements except for zinc. It was noted, that during the first month of experiment the zinc concentration had risen from $0.04mgL^{-1}$ to $1.09mgL^{-1}$, highest level measured during the experiment. The initial increase of zinc concentrations after 1 month of cathodic protection is correlated to dissolution of 10 zinc anodes, the first month corresponds to the cathodic protection establishment when the current demand and the anode dissolution are both at their highest rate. In the following months a regular decrease of zinc concentrations were recorded, except for the 9 months sampling revealed an incremental increase. The progressive decrease of zinc concentration in the 3^{rd} and 6^{th} month intervals were reported to be due to lower current demand resulting from calcareous formation on the steel structure. The zinc anode had undergone the formation of zinc oxide surface barrier layer which in conjunction with calcareous formation simultaneously reduce the zinc dissolution into the water. The reduction of zinc concentration was also attributed to removal of two anodes at the 3^{rd} month interval and two more at the 6^{th} month period. The water renewal also limited the increase of zinc concentration due to dilution effect. Sample from the 9^{th} month revealed elevated zinc concentrations; these were due to cleaning operation of the remaining anodes. The cleaning performed was such that the zinc oxide layer was removed into the water in the tank, and dispersed. This caused the increase in zinc concentration as

this layer is probably partially soluble. At the end of the experiment the water contamination by zinc is observed to be 0.24mgL^{-1}, which is 6 times higher than the initial value 0.04mgL^{-1}. They concluded that sacrificial anodes used in the experimental conditions induced a significant increase of the water zinc concentration.

Similarly the sediments were studied and it was reported that initial increase of zinc concentrations on all sediments was observed attributed zinc compounds forming and settling to the sediment layer. In the following months the progressive reduction was noted due to dilution and formation of passive layer on the anodes. It is concluded that the use of sacrificial zinc anodes for cathodic protection induce a significant water contamination by Zn^{2+} ions. Some of the zinc ions may form zinc hydroxide or other compounds and precipitate or interact with the sediment and sea water constituents. The implications of zinc concentrations in natural environment introduce potential toxic environment affecting the ecology.

For the purpose of this study only one aspect, the zinc runoff from samples has been considered, of a multi disciplinary investigation focused on corrosion induced zinc runoff and its interaction with soil [32]. Various zinc and zinc alloy coated samples were investigated; samples of 300cm^2 surface area were exposed single sided at 45° to the horizontal in Stockholm, Sweden. All the cut edges were sealed with zinc free paint system to minimise any contribution from the edge effect. Energy dispersive spectroscopy (EDS) technique was used for compositional and quantitative analysis of the runoff water.

It is reported that the zinc runoff rate on a long term perspective is relatively constant considering pollutant levels and annual rain fall quantities at the experiment site over a 5 year exposure [32]. The observed average annual runoff rates for: zinc sheet 1.9g^{-2}yr^{-1}, galvanised sheet steel with chromate 1.8g^{-2}yr^{-1}, galvanised sheet steel with thin organic coating (TOC) 0.8g^{-2}yr^{-1}, general galvanised sheet steel 2.5g^{-2}yr^{-1}, Galfan 1.1g^{-2}yr^{-1}, Galfan with TOC 0.6g^{-2}yr^{-1}, Galvalume 0.5g^{-2}yr^{-1}, Galvalume with TOC 0.3g^{-2}yr^{-1}. The observed differences in annual runoff rates between materials are related to combined effect of changes in surface properties in terms of coating degradation and corrosion product formation. Corrosion product formation was observed on bare zinc sheet, on general galvanised steel, primarily in zinc rich areas of Galvalume and on Galfan sheets.

Analysis of corrosion products revealed formation of zinc carbonates and aluminium hydroxide as the main constituents. Surface treated samples (i.e. chromate inhibitor and TOC) recorded a lower of zinc runoff rate from the underlying substrate in contrast to the

untreated samples. It was noted by the authors that galvanised steel with chromate inhibitor did initially display good corrosion resistance but lost its barrier properties by consumption of chromate species with increasing exposure time, 5years. The barrier effect provided by TOC also declined with time but still presented a degree of protection against atmospheric corrosion damage after 5 years of exposure. Similar function of TOC barrier was noted for Galfan and Galvalume. Alloying with aluminium resulted in generally lower runoff rates of zinc compared to zinc sheet. Higher runoff rates were measured for Galfan as compared to Galvalume. It is reported for Galfan that zinc runoff is perhaps due to dissolution of primary zinc rich phases at surfaces formed at depressed eutectic cell boundaries and for Galvalume it is the dissolution of zinc rich phases of interdendritic areas. They conclude that the presence of a barrier such as a paint system, a layer of chromate, or TOC does reduce the runoff rate as long as the barrier properties are kept intact.

1.6 Recent studies of Cut Edge Corrosion

Mass produced organically coated galvanised sheet steel (OCS) is popular in the automotive and construction industry due to ease of manufacture, flexibility, relative low cost and aesthetics. The primary mode of failure for OCS by means of corrosion at the exposed cut edges as highlighted previously in section 1.3.8. Primarily when the OCS product is guillotined for manufacture purposes a certain amount of the bare metal is exposed. The exposed area of bare metal was subjected to corrosive attack providing the initiation site for the corrosion cell. Once corrosion initiates, the applied organic coating prematurely fails due to the underlying corrosion processes. The failure of organic coating is usually due to blistering or delamination, the continued deterioration of the organic paint system by disbondment exposes more of the metallic substrate resulting in the increase of corrosion attack. Corrosion inhibition at cut edges is a problem for automotive, construction industries and for the coil coated steel manufacturers. Therefore, development of the OCS systems is required to limit these effects and ensure improved performance of the products.

Corrosion inhibition of galvanised steel cut edge by the use of phosphate pigments has been investigated [33]. The study considered the performance of sodium phosphate as corrosion inhibitor for cut edges of galvanised steel. A number of examination techniques were employed to gain an understanding of mechanism protection offered by sodium phosphate. Phosphates are commonly classified as non-oxidising anodic inhibitors, it is

generally accepted that phosphate ions in solution react with metal cations released from the metallic surface and precipitate as a barrier film at anodic areas.

Cross cut samples of electro-galvanised steel with a zinc thickness of 7μm on each side of a 800μm thick steel sheet samples with an approximate length of 1cm were investigated. The electrochemical study was performed at room temperature using a naturally aerated 0.01M NaCl solution with a 0.01M Na_3PO_4 solution concentration of inhibitor. The experimentation observed was two part, with no inhibitor in the solution and with inhibitor in electrolyte solution for SVET ionic current mapping to gain understanding and performance of inhibitor. Mapping of ion currents over the cut edge using SVET with no inhibitor in electrolyte revealed that in most cases activation of zinc only occurs in one of the edges. Initially a small anodic site develops in the zinc region with intense anodic currents due to smaller anodic site as compared the larger cathodic steel area. With continuous exposure a decrease in the reaction rate was measured as the anodic site grew accompanied by the formation of zinc corrosion products precipitating on the steel. The initial white zinc corrosion product layer ($Zn(OH)_2$), which became apparent after few minutes of immersion grew away from the anodic site onto the steel substrate, with decreasing anodic current. After 24 hour exposure another anodic site developed on the opposing zinc surface. For the system with no inhibitor it is understood that cathodic polarisation presented above the bare steel results in further build up of zinc corrosion product precipitates mostly zinc hydroxychloride (simonkolleite).

Given the anodic inhibition provided by phosphates there was a likelihood of zinc passivation and consequent loss of sacrificial protection of steel; however that was not the case. In the presence of phosphate inhibitor, the process on the surface was greatly affected. It was observed upon immersion anodes nucleated at the zinc surface, causing zinc ions to be released that become entrapped by the phosphate, precipitating as zinc phosphate. Zinc thus became anodically protected by this primary phosphate layer. This was not the sole factor for improved corrosion performance, on the steel cathodic area. The drop of cathodic reaction was attributed to a combination of thin layer of zinc phosphate and calcium phosphate (calcium present in the steel). These precipitates were responsible for the reduced access of oxygen to the surface therefore limiting the cathodic reaction rate. They concluded that sodium phosphate is capable of inhibiting galvanic corrosion at electro-galvanised steel cut edges. The protection mechanism mostly is the formation of zinc phosphate precipitating at the anode, hindering the zinc dissolution and diffusion. This zinc phosphate layer if locally damaged allows for the development of micro

anodes at the zinc surface forming further zinc phosphate gel like deposit. This does not result in total loss of sacrificial protection but only in the reduction of the galvanic current. This action at the anode hinders the diffusion of zinc cations to the cathode. When inhibitor is added to an already active cut edge, where zinc ions diffuse over the surfaces, zinc phosphate precipitation occurs more readily over both cathodic and anodic areas giving better inhibiting efficiency [13,26,34-38].

1.7 Microstructure manipulation via ultrasonic melt treatment

Metals and alloys are rarely uniform in composition or structure. There are many techniques that can be employed to refine the microstructure. The refinement to microstructure can be beneficial or detrimental to the properties of the metals. Microstructure manipulation is often carefully arranged to suit specific applications optimizing the metal for a particular function. Microstructure treatment or manipulation can be achieved by different techniques for example, alloy constituents, melt temperature, cooling rates, stirring etc. Ultrasonic melt treatment was identified long ago, 1950s. This technique of melt treatment has been increasing in support and adopted by the industry. Ultrasound is cyclic sound pressure with a frequency greater than the upper limit of human hearing, of approximately +20KHz. Ultrasonic vibration can be used to refine the solidification structure. The vibration of solidifying melts leads to structural refinement of metals and can result in improvement of their properties. Ultrasonic effects can be summarised as follows [39]:

1) Reduction in the mean grain size;

2) Disruption of columnar structure and induce formation of equiaxial grains;

3) Distribution of phases;

4) Improvement of material homogeneity;

5) Improved distribution of non-metallic inclusions.

Steels and generally all metallic materials show a rather high ultrasonic treatability.

The most likely cause of grain refinement via the ultrasonic treatment results from a combination of phenomena stimulated by the ultrasonic probe notably the mechanical shock and stirring. A shock front propagates from the ultrasonic source breaking the formed and forming dendritic arms from the primary stalk. Mechanical stirring is the action induced by the ultrasonic source within the melt which can also result in the breaking of the dendritc arms. Stirring causes bending of the dendritic arms. The secondary dendritic

arms are relatively shorter and are in some alloys narrower at their roots. It is reported that localised temperature is increased by several degrees causing remelt of the roots this is due to the forces imposed on the roots and result in the breaking of the secondary arms[40]. Another widely accepted opinion about dendritic solidification is that each dendrite grows from a one centre. Hence the degree of grain refinement is dependent upon the number of real solidification centres. The numbers of solidification centres in a melt depend on active solidification nuclei wetted with matrix liquid and able to form solidification centres. Ultrasonic melt treatment develops cavitations in the melt, and promotes wetting of the dispersed impurities and their introduction in the solidification process as an active material for the formation of solidification centres. Ultrasonic treatment increases the number of matrix liquid wetted nuclei as solidification centres resulting in more nucleation sights and finer more homogenous microstructure [41]. Figure 1.13 shows as an example of ultrasound refined microstructure.

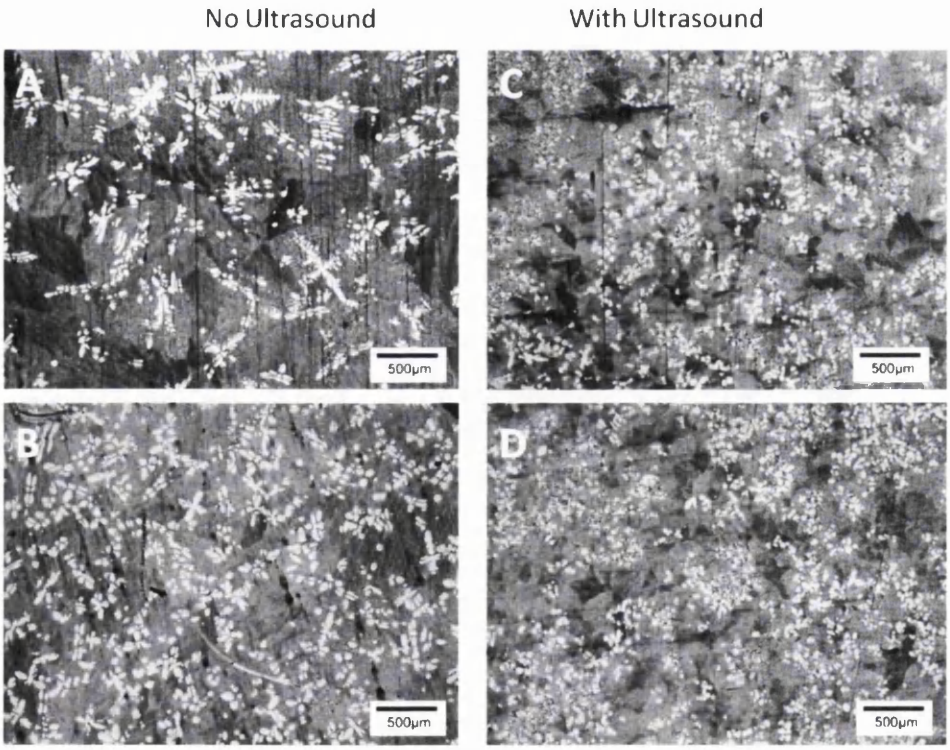

Figure 1.13 Optical micrographs of Zn – 4.8wt% Al Alloy solidified with no ultrasound (A and B) and with ultrasound (C and D) at two distances away from the ultrasound horn in order to evaluate the effect of the irradiation with distance. The distances are 20 mm (A and C) and 40 mm (B and D).

1.8 Aims of investigation

The work presented in the following chapters investigates:

- The metallic runoff from the cut edges of a variety or organically coated galvanized steels for a fifteen month duration. A novel exposure technique is used to maximize the cut-edge length per unit area to enable realistic results to be obtained from small coupons. ICP-MS is used to detect levels of metal ions in runoff solutions obtained.
- Development of reliable accelerated laboratory testing procedures in an attempt to model long term external weathering of zinc/organically coated steels in a short time scale.
- Detailed study and attempt to gain an understanding of the mechanisms of corrosion on pure zinc using the SVET in dilute salt solution
- Corrosion behaviour of various organically coated steels using the SVET in a dilute salt solution. Mass loss measurements from the SVET are used to develop further accelerated laboratory trials to mimic external weathering. Determine which components and combination of a paint system have crucial impact upon the longevity of the product.
- Examination of microstructure resulting from ultrasonic melt treatment. Subsequently a mechanistic corrosion analysis of the modified microstructure via SVET experiments.

1.9 References

(1) Trethewey, K. R.; Chamberlain, J. Corrosion : for students of science and engineering; Longman Scientific and Technical, 1988.
(2) Fontana, M. G. Corrosion engineering; 3rd ed. ed.; McGraw-Hill: New York, 1986.(3) Shreir, L. L. E. Corrosion Vol. 1. - 2; 2nd edition. ed.; Butterworths: [S.l.], 1976.
(4) Bosich, J. F. Corrosion prevention for practicing engineers; Barnes and Noble ; London : Distributed by Chapman and Hall: New York, 1970.
(5) Burns, R. M. a. B.; Bradley, W. W. Protective Coatings for Metals ... Second edition; pp. xiv. 643. Reinhold Publishing Corporation: New York, 1955.
(6) Marder, A. R. Progress in Materials Science 2000, 45, 191-271.
(7) Nakano, J.; Malakhov, D. V.; Purdy, G. R. Calphad 2005, 29, 276-288.
(8) Edavan, R. P.; Kopinski, R. Corrosion Science 2009, 51, 2429-2442.
(9) Sullivan, J.; Mehraban, S.; Elvins, J. Corrosion Science 2011, 53, 2208-2215.
(10) M. Vlot, m. Z., M. Toose, L. Elliot, R. Bleeker, T. Maalman International conference Proceedings paper GALVATECH 2007.
(11) K. Ueda, A. T., Y. Kubo International conference Proceedings paper GALVATECH 2011.
(12) Powell, S. Surface Engineering 2000, 16, 169-175.
(13) McMurray, H. N.; Powell, S. M.; Worsley, D. A. Br. Corros. J. 2001, 36, 42-48.
(14) Zubielewicz, M.; Gnot, W. Progress in Organic Coatings 2004, 49, 358-371.
(15) Mahdavian, M.; Attar, M. M. Progress in Organic Coatings 2005, 53, 191-194.
(16) Williams, G.; McMurray, H. N.; Loveridge, M. J. Electrochimica Acta 2010, 55, 1740-1748.
(17) Williams, G.; McMurray, H. N. Electrochimica Acta 2012, 69, 287-294.
(18) Spinks, G. M.; Dominis, A. J.; Wallace, G. G.; Tallman, D. E. Journal of Solid State Electrochemistry 2002, 6, 85-100.
(19) Tallman, D. E.; Spinks, G.; Dominis, A.; Wallace, G. G. Journal of Solid State Electrochemistry 2002, 6, 73-84.
(20) Williams, G.; Holness, R. J.; Worsley, D. A.; McMurray, H. N. Electrochemistry Communications 2004, 6, 549-555.
(21) Barton, K.; Duncan, J. R. Protection against atmospheric corrosion : theories and methods; Wiley-Interscience: London, 1976.
(22) Howard, R. L.; Lyon, S. B.; Scantlebury, J. D. Progress in Organic Coatings 1999, 37, 91-98.
(23) Howard, R. L.; Lyon, S. B.; Scantlebury, J. D. Progress in Organic Coatings 1999, 37, 99-105.
(24) Zapponi, M.; Elsner, C. I.; Actis, F.; Di Sarli, A. R. Corros. Eng. Sci. Technol. 2009, 44, 119-127.
(25) Worsley, D.A.; Mcmurray, H. N. Research in Chemical Kinetics 1997, 4, 149-202.
(26) Worsley, D. A.; Williams, D.; Ling, J. S. G. Corrosion Science 2001, 43, 2335-2348.
(27) Lodi, Z. F.; Mol, J. M. C.; Terryn H. Materials and Corrosion 2008, 59 no.10, 802-810.
(28) Proskurkin, E. V.; Gorbunov, N. S. Galvanizing, sherardizing and other zinc diffusion coatings; Technicopy Ltd in association with Zinc Development Association: Stonehouse, Glos., 1975.
(29) Cabral, A. M.; Trabelsi, W.; Serra, R.; Montemor, M. F.; Zheludkevich, M. L.; Ferreira, M. G. S. Corrosion Science 2006, 48, 3740-3758.
(30) Belghazi, A.; Bohm, S.; Sullivan, J. H.; Worsley, D. A. Corrosion Science 2002, 44, 1639-1653.
(31) Rousseau, C.; Baraud, F.; Leleyter, L.; Gil, O. Journal of Hazardous Materials 2009, 167, 953-958.

(32) Bertling, S.; Odnevall Wallinder, I.; Leygraf, C.; Berggren Kleja, D. Science of The Total Environment 2006, 367, 908-923.
(33) Simões, A. M.; Torres, J.; Picciochi, R.; Fernandes, J. C. S. Electrochimica Acta 2009, 54, 3857-3865.
(34) Böhm, S.; McMurray, H. N.; Powell, S. M.; Worsley, D. A. Electrochimica Acta 2000, 45, 2165-2174.
(35) Penney, D. J.; Sullivan, J. H.; Worsley, D. A. Corrosion Science 2007, 49, 1321-1339.
(36) Loveridge, M. J.; McMurray, H. N.; Worsley, D. A. Corros. Eng. Sci. Technol. 2006, 41, 240-248.
(37) Worsley, D. A.; McMurray, H. N.; Sullivan, J. H.; Williams, I. P. Corrosion 2004, 60, 437-447.
(38) Worsley, D. A.; Powell, S. M.; McMurray, H. N. Corrosion 2000, 56, 492-500.
(39) Abramov, O. V. High-intensity ultrasonics : theory and industrial applications; Gordon and Breach Science Publishers: Amsterdam, The Netherlands :, 1998.
(40) Campbell, J. International Materials Reviews 1981, 26, 71-108.
(41) Eskin, G. I. Advanced Performance Materials 1997, 4, 223-232.

Chapter 2

Experimental Procedures

2.1 Metallographic Investigation

Galvalloy is a Tata Steel Europe product that is an alloy of Zinc 95.2 wt%, Aluminium 4.8 wt%. The addition of aluminium advocates the formation of primary zinc rich phase in the form of dendrites within aluminium and zinc lamellar eutectic. the alloy coating exhibits significantly improved life over that of ordinary pure zinc coating in atmospheric and aqueous exposure[1].

Chemically pretreated with chromate containing and chrome free agents, Galvalloy coated steel (0.51 mm gauge) were manufactured in coil coating trials at Tata Steel Colors Shotton works in North Wales. Table 2.1 lists the test samples prepared for investigation. The sample matrix included reference production line material for comparison with the trial samples as a reference (sample ID KK1 and KK2). The reference sample had been pretreated with a chromate pretreatment, applied with a 5μm primer containing chromate inhibitor and a topcoat with a 200μm poly-vinyl chloride (PVC) plastisol on one side following application of a 15μm single coat polyester backing layer. The remaining samples had varied pretreatment, primer and topcoat combinations. These variances are not critical for the metallographic work and the findings are presented in chapter 3.

Metallographic investigation provides a thorough examination of the microstructures to quantify the observed structure and microstructure morphology. The study of microstructural evolution in the metallic coatings during coil manufacture revealed primary phases present and facilitated understanding of the corrosion mechanistic processes.

Table 2.1 Galvalloy samples details for metallographic inspection.

Sample Identification	TATA Identification	Metallic coating Galvalloy	Cleaner agent std=standard, f=fresh & (concentration %)	Pretreatment	Pretreatment weight (mg Ti or Cr/m^2)	Primer Code name	Primer Target DFT (µm)	Topcoat	Topcoat Target DFT (µm)	Gauge (mm)
KK-1	8ZM045	265 gm^{-2}	Novamax 187U (std)	NR6022 (Cr)	20-30	Coilprime HS	5	HPS200 Ultra - GWG	5	0.48
KK-2	8ZM073	265 gm^{-2}	Novamax 187U (std)	NR6022 (Cr)	20-30	Active B (Akzo)	5	HPS200 White - Active	5	0.58
KK-4	7ZM072	265 gm^{-2}	Novamax 187U (std)	G1455 (0Cr)	8-10	ANNP – IN7UD987	5	HPS200 Ultra	5	0.51
KK-5	7ZM080	265 gm^{-2}	Novamax 187U (std)	G1455 (0Cr)	8-10	BASF – CP71	5	HPS200 White	5	0.51
KK-6	7ZM082	265 gm^{-2}	Novamax 187U (std)	G1455 (0Cr)	8-10	ANNP – IN7UD987	5	HPS200 White	5	0.51
KK-7	7ZM083	265 gm^{-2}	Novamax 187U (std)	G1455 (0Cr)	8-10	BASF – CP71	5	HPS200 Ultra – GWG	5	0.49
KK-9*	9KR092	275 gm^{-2}	Novamax 187U (std)	NR6022 (Cr)	20-30	Coilprime HS	5	HPS200 Ultra	5	0.50

*Sample KK9 is MagiZinc metallic coating weight of 275g/m^2, remaining samples are Galvalloy metallic coating weight of 265g/m^2.

Novamax 187U is commercially available cleaner agent by Henkel, important constituents are sodium hydroxide and sodium xylenesulphonate.

NR6022 is commercially available pretreatment by Henkel, important constituents are dichromic tris(chromate) and chromium trioxide.

G1455 is commercially available pretreatment by Henkel, important constituents are dihydrogen hexafluorotitanate(2-) and phosphoric acid.

Coilprime HS is commercially available primer by BASF, important constituent is strontium chromate.

Active B is commercially available primer by Akzo Nobel, important constituent is strontium chromate.

ANNP-IN7UD987 is commercially available primer by Akzo Nobel, important constituents were unknown due to commercial sensitive reasoning.

BASF –CP71 is commercially available primer by BASF, important constituent are trizinc bis(orthophosphate) and a calcium ion exchange additive.

2.1.1 Preparation of Metallographic Samples

The samples for microstructural investigation were prepared, first 10mm x 10mm coupons were guillotined. The coupons were then immersed in dichloromethane to remove the Poly-Vinyl Chloride topcoat. The coupons were subsequently pressure mounted in Bakelite. Each of the samples were then subjected to careful investigation described below.

2.1.2 Primary Volume Fraction

The initial examination involved confirmation of the average volume percentage of primary zinc solid solution phase within the alloy coating for each sample. Samples were polished using a 1μm diamond polishing compound and then etched. After each controlled polish the specimen was rinsed with tap water and ethanol before etching. The microstructure was revealed by the use of 2% Nital solution (98% ethanol and 2% concentrated nitric acid). This step highlighted the details in the microstructure of the different phases present in the metallic coating. The etching process showed the microstructure by selective dissolution of the structure, starting at the surface and proceeding inward. The surface was treated with Nital solution for approximately 3-5 seconds after which the specimen was rinsed by tap water and ethanol. To examine the microstructural changes as a function of depth in the coating the samples were first indented with a Vickers Hardness Tester diamond in three places on the specimen surface approximately 5mm apart. The depth into the coating was estimated following careful polishing and by measuring the extreme diagonals of the indent, which decreased after each consecutive polish. Applying trigonometry and knowing the diamond's indentation angle (136°) the depth was calculated and corresponding images were recorded. This process is schematically described in figure 2.1. The images of the microstructure were recorded at known positions within the metallic coating using an Olympus E330 SLR digital camera (set for 5 mega-pixel, 2650x1920 resolution) attached to a Reichert optical microscope. The images obtained were imported into Corel Paint Shop® Pro (2005 edition). The primary phase was then meticulously coloured white using the various tools available in Corel Paint Shop software. Sigma Scan® Pro (version 5) was used to measure the areas of the white coloured regions consequently quantifying the amount of primary phase accurately in each image by overlaying an intensity threshold. This was performed for each depth and then averaged to give a total volume fraction for each sample.

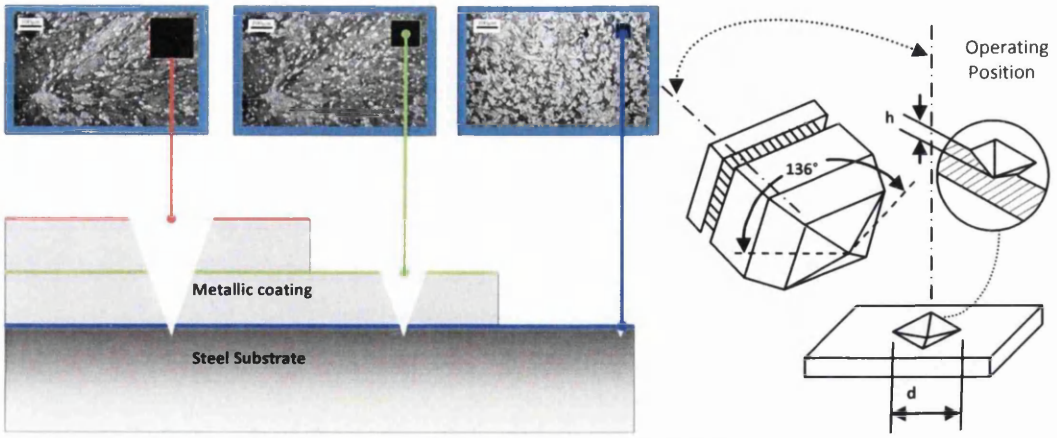

Figure 2.1 Calculation of depth through metallic coating using Vickers hardness indent.

2.1.3 Quantifying the number of dendrites

Images taken from the steel substrate and coating interface, typically similar to those in figure 2.2, were used to estimate the average number of primary phase zinc solid solution dendrites per square mm. The enhanced images from Corel Paint Shop Pro imported into Sigma Scan, by overlaying and manipulating the intensity threshold functions within the software a total count of enhanced objects, dendrites in black, can be obtained; typical example in figure 2.2(3). Since the images were calibrated, the number of objects (dendrites) was recorded as number per unit area. This quantity is subsequently normalised to give a dendrite number per square mm.

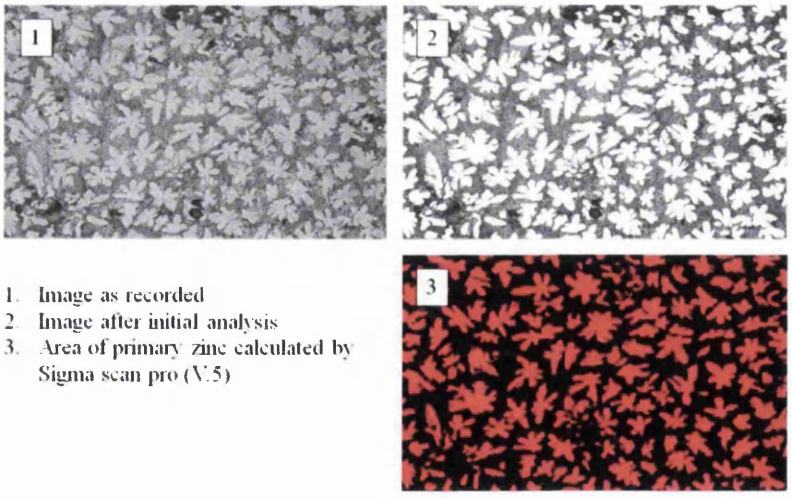

Figure 2.2 Calculation of area percentages of dendrites and number of dendrites.

2.1.4 Calculating the average dendrite size

This was achieved by calculating the percentage area of primary phase at the coating and steel interface (described above) and dividing it by the number of solid solution dendrite crystals within the same area. This process yielded an average dendrite size. An assumption was made that the dendrite sizes remained relatively constant throughout the sample.

2.2 External Run off experimental work OCS Cut-edge

There were two techniques organized, one was external or outdoor weathering relying on the natural rain cycles, humidity, temperatures and ambient air quality variations. The second method was a more controlled laboratory experiment utilising a rain simulator and temperatures were monitored at ambient room conditions.

The conventional technique for external exposure of such materials commonly entail exposure of 100x150mm test panels at a 45° (in accordance with the BSNEN 13523-19:2004 and BSN 13523-21:2003) with a 500mm of cut edge length. The levels of metallic ions leached from such a length would be too small to be easily detected by even the most sensitive of techniques. Organically coated galvanised steels (OCS) were obtained from Tata Steel Europe. An alternate method for study of cut edge outdoor exposure was adopted [2], the OCS samples listed in Table 2.1 were cut to an initial diameter of 120mm. An array of 72 holes was then punched in the coated samples imitating the shearing of a normal guillotine. The array of holes and the overall circumference of the disc combine to give an total cut edge length of 1.5m for each sample whilst maintaining a 87.5% of the sample surface area. Each of the sample discs was then secured to a polyethylene funnel by nylon cable ties such that the circular coupons were horizontal. The funnels had a 150mm diameter wide entrance ensuring the rainfall passing over the sample was collected. The funnels were secured to 5ltr Polyethylene Jerrican by means of drilling the Jerrican lid allowing the narrow neck of the funnel to be pushed through and bonded with marine resin, figure 2.3. One blank was also set up as described above minus the OCS cut edge specimen. A total of 7 samples (table 2.1) were exposed for 18 months and one blank. The samples were exposed at Swansea University Engineering building roof top that is in close proximity to the Swansea bay hence a marine environment. Blank samples of water have been collected and analysed in order to eliminate any potential background variations in metallic contamination in the rainwater. The runoff water from each sample was collected every month and analysed for metal ions using ICP-MS.

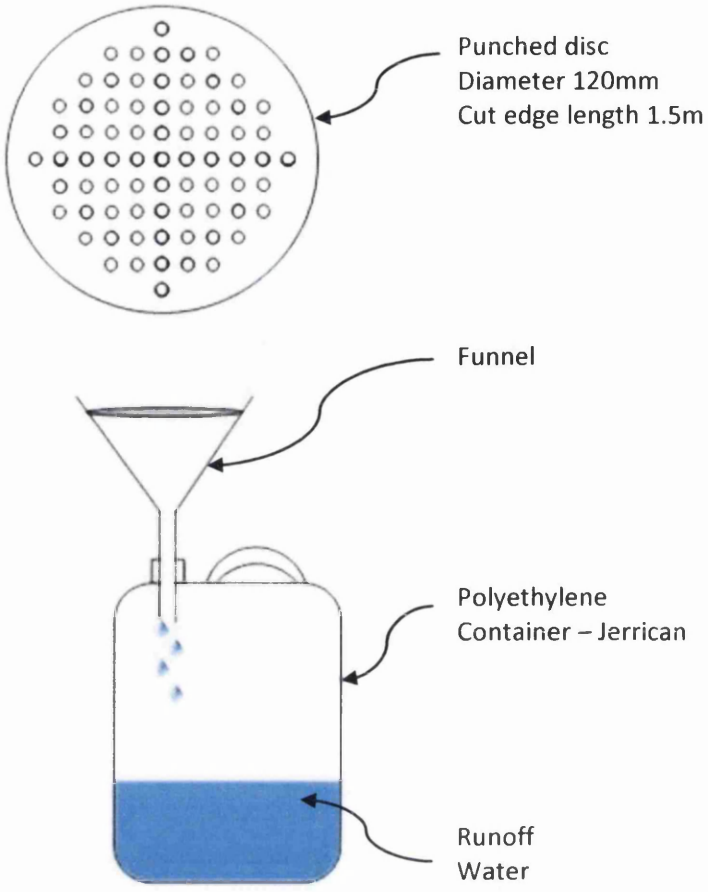

Figure 2.3 Schematic and photograph of external runoff apparatus.

2.3 Accelerated Run off experimental work OCS Cut-edge

Accelerated corrosion tests were performed on 120mm diameter OCS coupons prepared in the same manner as for the external cut edge corrosion work. A specialised rain simulator was constructed in order to expose the OCS coupons to a recirculating electrolyte solution. The rain simulator consists of two chambers: a reservoir section which also houses the platform for mounting the sample and a top chamber which incorporates the shower matrix. The equipment consisted of Masterflex Tygon tubing supplied by Cole Parmer. The electrolyte from the reservoir is recirculated via the rain-shower matrix over the coupons by means of a peristaltic pump. This is illustrated schematically in figure 2.4. The fittings were designed such as to minimise evaporation. The flow rate through the rain-shower matrix was averaged to be 13ml/min (equivalent rainfall 0.17mm/h). The electrolyte solution used for each test was 2 liters of distilled deionised water and samples of solution were taken after 24hours, 72 hours and 120 hours. The solution samples were then subjected to ICP-MS analysis.

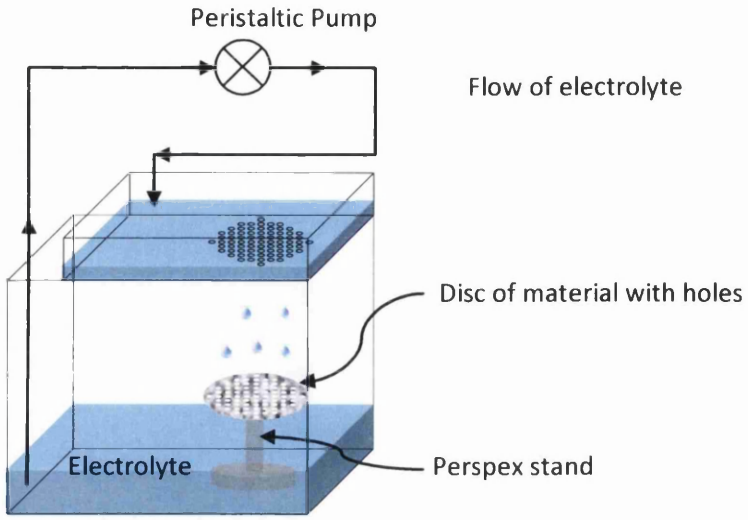

Figure 2.4 diagram of accelerated testing apparatus (Rain simulator).

2.4 Scanning Vibrating Electrode Technique

The SVET has been used a great deal with a view to understand as fully as possible the corrosion mechanisms on the cut edge of the samples in aqueous solution. The SVET is an invaluable tool in the mechanistic investigation of corrosion in organic coated steels and specifically, cut edge corrosion [3-8]. The SVET resolves localised corrosion events occurring in a solution utilising a movable microtip electrode. The SVET detects an alternating potential at the vibration frequency, which is proportional to the potential gradient in the direction of the vibration emanating from the current sources in solution [3]. Localised corrosion on galvanised surfaces in chloride electrolyte has distinct regions of anodic and cathodic sites and SVET is deployed to detect these anodic and cathodic events as a function of time. Employing SVET gives access to corrosion behaviour of a variety of metallic coating systems. It has the versatility to determine the location and intensity of anodic and cathodic activities occurring at the metal surface. Data collected from the SVET are used for a semi-quantitative assessment of metal loss during the 24 hour experiment allowing comparisons to be drawn between the coating systems efficiency in hindering the corrosion progression.

2.4.1 SVET application for cut edge corrosion

The cut-edge samples were prepared from panels supplied by Tata Steel Europe and were guillotined into 20x10mm coupons and were then embedded in a Struers two component acrylic resin (DuroCit). The resin was selected due to its electrical inert non conductive properties with no shrinkage. The coupons were mounted on their edge to enable investigation of cut edge corrosion and to aid handling and polishing with relative ease. The resultant sample was then polished to reveal one metallic cut edge with the rest of the sample completely insulated from exposure to the electrolyte used for SVET. Before the immersion of the sample in the electrolyte the polished edge was subjected to optical microscopic examination (magnification 100x) to ensure that sample was scratch free and that there were no crevices at the metal and resin interface.

The SVET was configured to scan over the surface once every hour for 24 hours. The glass encased 125 μm platinum wire microtip was used for scanning at a constant height of 100 μm across the corroding sample surface immersed in 0.1% $NaCl_{(aq)}$ electrolyte. The dissolved oxygen concentration in the bulk of electrolyte solution was assumed to be constant at $2.8x10^{-4}$ mol dm^{-3} (~9 ppm) [9]. The microtip electrode was set to vibrate at a frequency of 140Hz normal to plane of the scan (polished cut-edge surface) with amplitude of 30 μm. A lockin amplifier (EG&G Instruments 7265 DSP) was used to control the frequency, amplitude and also measured the detected signal from the microtip probe. The microtip probe was attached to a glass push rod using a Teflon holder. The push rod was attached to the speaker cone that provides the vibration to the microtip. The speaker and push rod were encased in a mu-metal head, which reduced electromagnetic leakage to a minimum. The probe assembly was mounted on a tri-axial micromanipulator that used linear bearings driven by stepper motor. Computer controlled operations of the tri-axial platform movement through x, y and z directions, ensured a consistent area was scanned by probe over the sample surface. A schematic illustration of SVET equipment used is seen in figure 2.5. The sample under examination was secured to the Perspex levelling table, inside a Perspex tank containing the 0.1% $NaCl_{(aq)}$, which was unstirred at room temperature and exposed to air.

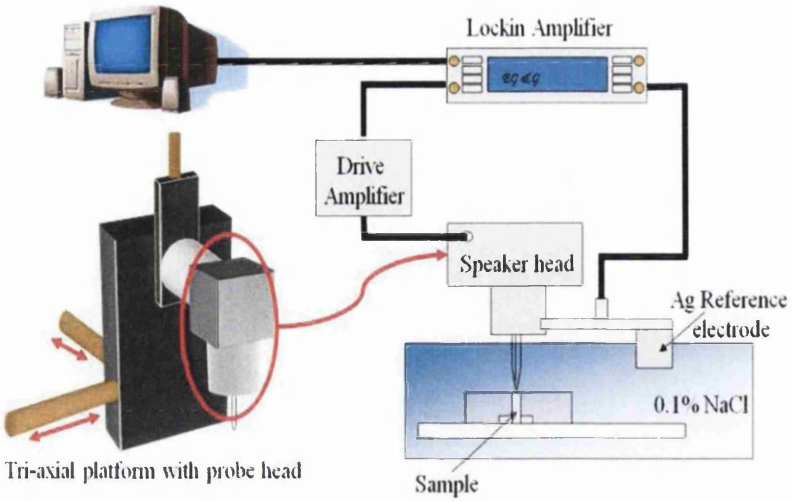

Figure 2.5 Schematic of the SVET equipment.

2.4.2 SVET application for zinc localised corrosion

The corrosion testing was done with the scanning vibrating electrode technique (SVET) that showed it suited well the purposes of the work. It measures potential differences in solution created by ionic fluxes originated by the corrosion process. The technique possesses the great advantage of resolving the anodic and cathodic distributions on the surface of a metal, which is of remarkable value in corrosion research.

Commercial-purity zinc samples (99.99% purity) obtained from Goodfellows were prepared guillotined into 10x10mm coupons (thickness 1.0mm) and were then embedded in a Struers two component acrylic resin (DuroCit). The resin was selected due to its electrical inert non conductive properties with no shrinkage. The coupons were mounted such as to enable investigation of surface and to aid handling and polishing with relative ease. The resultant sample was then polished to a very smooth level surface with the reverse side and edges of the coupon completely insulated from exposure to the electrolyte used for SVET. Before the immersion of the sample in the electrolyte the polished surface was subjected to optical microscopic examination (magnification 100x) to ensure that sample was scratch free and that there were no crevices at the metal and resin interface.

The SVET was configured to perform a total of five continuous scans over the surface. The SVET platinum microtip was used for scanning at a constant height of 100 µm across the corroding sample surface immersed in four differing concentrations of $NaCl_{(aq)}$ electrolyte, notably 1.0%, 0.1%, 0.01% and 0.001% $NaCl_{(aq)}$. The dissolved oxygen concentration in the bulk of electrolyte solution was assumed to be constant at 2.8×10^{-4} mol dm^{-3} (~9 ppm) [9].

The microtip electrode was set to vibrate at a frequency of 140Hz normal to plane of the scan with amplitude of 30 μm. A lockin amplifier (EG&G Instruments 7265 DSP) was used to control the frequency, amplitude and also measured the detected signal from the microtip probe. Microtip attached to a computer controlled tri-axial platform ensuring consistent area over the sample surface was scanned. The 10x10mm surface was scanned over by microtip using a step size of 0.1mm giving a matrix of 100x100 scan points over the surface area. The sample under examination was secured to the Perspex levelling table, inside a Perspex tank containing the electrolyte, which was unstirred at room temperature and exposed to air. A prior calibration (described in section 2.4.3) permits conversion of the measured potential differences to current densities.

2.4.3 SVET Calibration

The SVET measures the normal component of the current flux generated at current source in solution. This is done by vibrating the microtip at a constant height, amplitude and frequency directly above the point current source. The potential measured by SVET microtip is proportional to the electrical field strength, F, or potential gradient in the direct of vibration. Equation 2.1 describes the relationship between field strength, F, and distance from the point current source (i).

$$F = \frac{dE}{dz} = \frac{iz}{2\pi\kappa(x^2+y^2+z^2)^{1.5}} \tag{2.1}$$

Where κ is the electrolyte conductivity and x, y, and z are distances in the horizontal and vertical planes.

$$F_{max} = \frac{i}{2\pi\kappa z^2} \tag{2.2}$$

The value for F is therefore at its maximum when the microtip is directly above the point current source shown by equation 2.2.

Calibration was achieved using two compartment cell shown schematically in figure 2.6. Each compartment contains a $1cm^2$ Pt electrode and the specified electrolyte used in the investigation. The compartments are linked by a vertically orientated glass tube. The setup was calibrated by positioning the SVET microtip inside the vertical bore of the glass tube, the microtip probe was inserted 5mm downward into the tube lumen with the large area low-impedance silver reference electrode (2.5 x 2.5 cm) immersed in electrolyte contained in the Perspex tank. Different currents were applied through this glass tube using a nano-galvanostat and the current density calculated for the internal area of the glass tube. At an

electrolyte concentration of 0.1% NaCl and for galvanostat induced currents -50 to +50 μA and consequently current densities -2.76 to +2.76 Am^{-2}, plots of SVET voltage signal versus current density provide straight lines, linear, correlation coefficient value of >0.998. The gradient of a plot of current density versus SVET voltage provides a calibration factor for the instrument, typical calibration plot figure 2.7. The use of this tube cell for calibration is rapid and consistent.

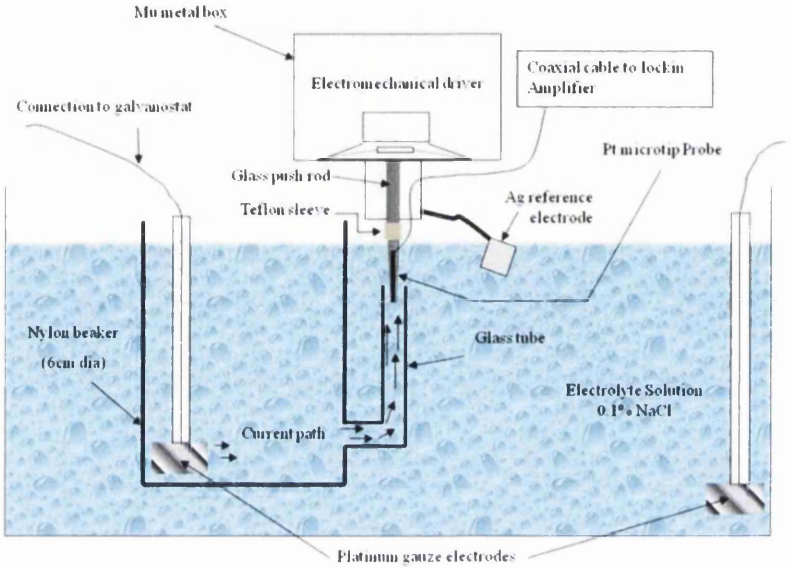

Figure 2.6 Schematic representation of the calibration set up.

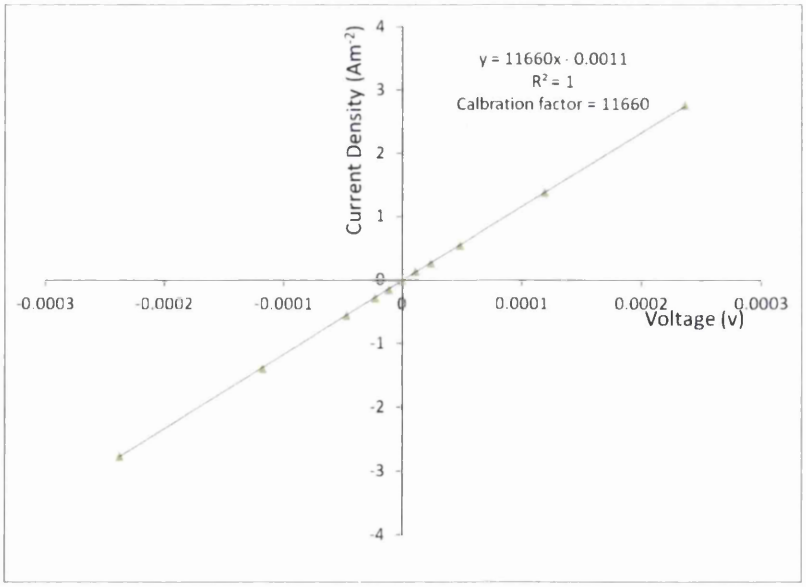

Figure 2.7 SVET calibration plot measured in 0.1%NaCl electrolyte.

2.4.4 SVET Data Rendering

The raw data collected from the SVET experiment were used in calibration as discussed in previous section to convert nV into A m^{-2}. The calibrated data from the SVET experiments allow Faraday's law to be employed in order to calculate metal loss during each test by assuming the corrosion activity occurring on the sample surface remains constant in the intervals between scans and that the corrosion in the samples studied occurs preferentially on the primary zinc phase [5,10]. The SVET logfile processor a part of the SVET software suite was used to estimate metal loss which integrates the area under the positive going voltages (anodic) measured by SVET. At each point of measure the SVET delivers a value of potential voltage in nV that can be converted to Am^{-2} by multiplying the potential by the calibration factor described above giving a value in Am^{-2}. This current density is then integrated over the area of the scan to give a total current, A. By multiplying this current value by time of an hourly scan (3600 seconds) converts the data into charge. The charge value obtained can now be converted into mass using Faraday's law and knowledge of the corroding ions' charge and atomic weight. It is therefore possible to calculate an estimated total zinc loss (tzl) for 24 hour experiment that is the sum of each scan through the experiment life, equation 2.3.

$$tzl = \frac{Q}{nF} \times A_r \qquad (2.3)$$

Where Q = charge (C)

F = Faraday's constant, 96485 $C.mol^{-1}$

n = number of electrons lost during corrosion, 2 for Zn

A_r = atomic weight, approximately 65 for Zn

It is possible to track the number of anodic events, their respective intensity, activity period and location during the 24 hour experiment. A standard personal computer is used in tandem, which records the signal detected by the SVET microtip probe from the lockin amplifier in respect the stored scanning grid. The individual hourly scan files from SVET after calibration function is applied is scrutinised further by determining the location of each anodic event, their intensity and any variation of their activity in the individual hourly scan over the entirety of the experiment duration. Thus, this interrogation of the data makes it possible to a) determine of the life time of anodes and b) assess any variation in intensity of corrosion during the life time of the anodes. In this case, samples investigated in which primary zinc dendrites are preferential corrosion sites [10,11]. It is possible to link dendrite size and number with corrosion activity.

2.4.5 SVET Limitations

As with most techniques the SVET and associated analysis routines have a few limitations in its application. There is an issue with the detection efficiency, in a situation where the spatial separation of anode and cathode are less than the *whm* value, spatial resolution of the SVET, such that the current loops from the point sources do not pass through the plane of SVET scan. Hence in cases of general corrosion the SVET underestimates metal loss. A single hourly scan for a cut edge sample approximately 2.5x 22 mm in scan surface areas is produced over a period of time about 7 minutes. The time between scans is one hour, due to the nature of activation and passivation of corrosion activity. It is possible that certain anodic events are missed. Therefore, the value of corrosion rate, metal loss and other derived corrosion activity values may be an under estimate of the actual corrosion performance. Hence, the SVET is described as semi-quantitive technique that can provide indicative trends of corrosion activity as opposed to actual values. That said, for galvanised steels in sodium chloride solution other works proved that SVET measured and ICP-MS measured zinc loss differs only by ~20% [10].

2.5 Microstructure manipulation via ultrasonic melt treatment

The ultrasonic irradiation experiments were performed at the Tata Steel, Galvanising line in Shotton, UK. Graphite Crucibles were pre-heated in an oven to 100°C and 1kg of Zn - 4.8 wt% Al alloy was taken directly from the galvanising bath using a ladle and poured into the crucible. The ladle was pre-heated through immersion in the bath to ensure solidification did not occur in the ladle. The ultrasound probe with a titanium horn was then lowered into the molten metal to a depth of approximately 0.5 cm below the melt line and held steady using a clamp stand as shown schematically in figure 2.8.

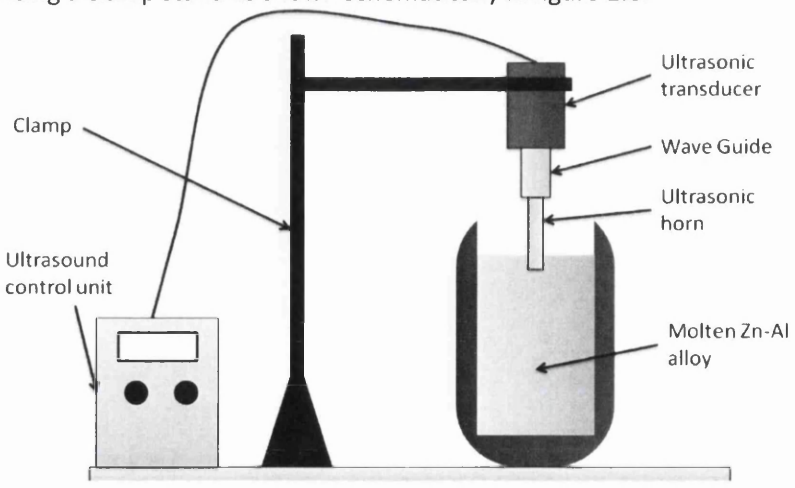

Figure 2.8 Schematic of apparatus used to ultrasonically irradiate the Zn-4.8wt% Al melt.

The ultrasonic horn was pre-heated to 100°C using a blow torch and measured with an infra red thermometer prior to introduction to the melt in order to reduce cooling effects produced by the titanium horn. Ultrasonic irradiation was then applied to the melt using the control unit for the transducer at the full power of the unit with no pulsing of the ultrasound to ensure 100% applied power during the cycle. The horn was gently moved laterally periodically to assess the condition of the melt and removed once a mushy / semi-solid state was achieved. This generally was within 90 seconds of the application of the molten metal to the crucible. The experiment was repeated with another crucible, molten metal added and the ultrasonic horn heated and lowered into the melt but this time no ultrasonic irradiation was applied in order to assess the control solidification behaviour of the alloy whilst replicating any cooling effect the introduction of the horn may have had. After solidification and cooling had completed the casts were removed from the crucibles and sectioned in half. The sections were then polished on the cut face to a metallographic finish to enable the microstructure of the alloy to be assessed at various depths through the casting directly below ultrasonic horn.

2.5.1 Analysis of microstructures

The cut face of each section of casting was polished to a 1μm metallographic finish using progressively finer emery papers and diamond slurry. The section was then etched using 1% Nital and an example of such sectioned cast samples with ultrasonic irradiation is shown in figure 2.9.

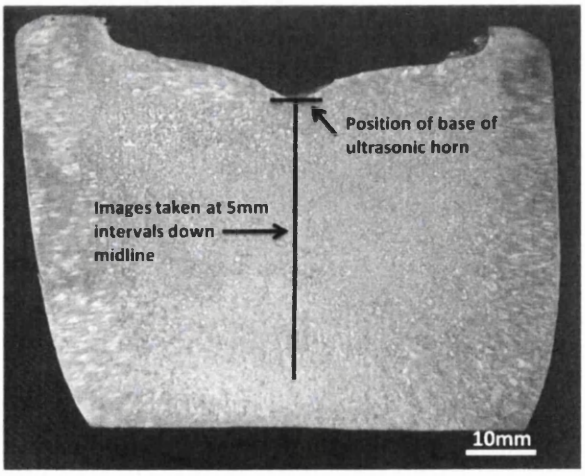

Figure 2.9 Cut face section of casting polished to a 1μm metallographic finish and etched.

The structure of the cast samples were then analysed initially macroscopically with digital images taken using a Nikon Coolpix digital camera mounted on a height adjustable gantry. Microstructures were then assessed using a MEF3 Reichert optical microscope at a variety of magnifications. To assess primary phase numbers, volume fractions and size images at 20 times magnification were taken at 5 mm increments from the bottom of the ultrasonic horn down the centre of the casting to a distance of 40 mm from the horn. To quantify the primary phase properties image analysis software, JSAC Paint Shop Pro X, was used to colour the primary phase white in each image. Sigmascan Pro 5 software was then used to count the number of primary phase instances and also work out the area fraction of primary phase per image. This data was then used to calculate the average size of the primary phases.

In order to examine the finer morphology of the primary and eutectic phases images were taken at times 100 magnification using the Reichert optical microscope with higher resolution images obtained from a JEOL 6100 scanning electron microscope (SEM) and a Hitatchi TM8000 desktop SEM.

2.5.2 Assessment of corrosion behaviour using SVET

The Zn-4.8wt Al alloy used in this section of work is not used as bare galvanised product and in service it is always over coated with organic coatings. Therefore, the failure mechanism is always down to cut-edge corrosion rather than surface corrosion. In order to assess the castings produced in this investigation in terms of cut edge corrosion a 3mm groove was machined into a section of material from the centre of each casting and a mild steel strip inserted into the groove thus allowing corrosion tests to be performed that mimicked cut-edge corrosion whereby anodic dissolution of the zinc alloy is driven by cathodic protection of the exposed steel. The steel (3mm width) was inserted with great care ensuring that no crevices existed between the inserted steel and the alloy casting. The microstructure of the material either side of the steel insert was examined to ensure that the manufacture of the false cut-edge had not changed the structure in any way and this was found to be the case for both the irradiated and un-irradiated castings. An example of the sample prepared in this manner in shown in figure 2.10. The portion of casting with a false cut-edge was then polished flat and to a mirror finish using progressively finer emery papers and 1μm diamond slurry to ensure reproducible surfaces for SVET testing. The sample was then masked using PTFE tape to leave an area of $7.5x10^{-5}m^2$ exposed for SVET experiments. The area was masked carefully to ensure a ratio of 1.5mm to 3mm in terms of

exposed Zinc alloy to steel in order to simulate a realistic cut-edge. The area scanned by the SVET was 15mm along the false cut edge and 5mm perpendicular to this across the edge. The SVET probe made 100 measurements along the length of the cut edge and 50 measurements across the samples width generating a matrix of 5000 data points for each scan. Three areas of the each casting were scanned namely the top which was closest to the point of application of the ultrasound probe (5mm from horn), the middle (25mm from horn) and the bottom (45 mm from horn) to assess the effect of distance from horn on corrosion resistance. The SVET tests were carried out in 0.1%NaCl solution and one scan was taken every hour for 24 hours and three repeat tests for each material were carried out. The dissolved oxygen concentration in bulk solution was assumed to be constant at 2.8 x 10^{-4} mol dm^{-3}, the equilibrium concentration for air saturated water, and all tests were carried out at 25°C.

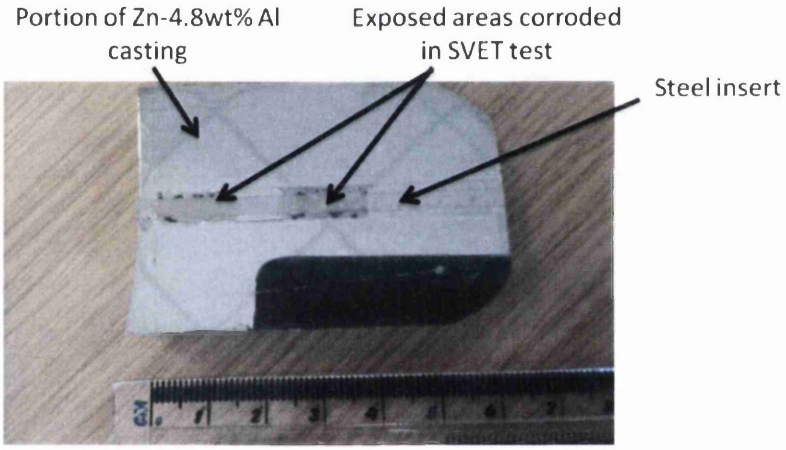

Figure 2.10 Portion of Zn-4.8wt% Al alloy casting with steel insert to create a false cut-edge for corrosion testing with SVET.

2.6 References

(1) Jones, D. A. Principles and prevention of corrosion; 2nd ed. ed.; Prentice Hall ; London : Prentice-Hall International: Englewood Cliffs, NJ, 1996.

(2) Böhm, S.; Sullivan, J. H.; Worsley, D. A. Materials and Corrosion / Werkstoffe und Korrosion 2001, 52, 540-545.

(3) Worsley, D. A.; McMurray, H. N. Research in Chemical Kinetics 1997, 4, 149-202.

(4) McMurray, H. N.; Powell, S. M.; Worsley, D. A. Br. Corros. J. 2001, 36, 42-48.

(5) Worsley, D. A.; Williams, D.; Ling, J. S. G. Corrosion Science 2001, 43, 2335-2348.

(6) Z. F. Lodi, H. Z., J. M. C. Mol, H. Terryn and J. H. W. de Wit Materials and Corrosion / Werkstoffe und Korrosion 2008, 59 no.10. 802-810

(7) Cabral, A. M.; Trabelsi, W.; Serra, R.; Montemor, M. F.; Zheludkevich, M. L.; Ferreira, M. G. S. Corrosion Science 2006, 48, 3740-3758.

(8) Williams, G.; McMurray, H. N. Journal of The Electrochemical Society 2008, 155, C340-C349.

(9) Bonnel, A.; Dabosi, F.; Deslouis, C.; Duprat, M.; Keddam, M.; Tribollet, B. Journal of The Electrochemical Society 1983, 130, 753-761.

(10) Elvins, J.; Spittle, J. A.; Worsley, D. A. Corrosion Science 2005, 47, 2740-2759.

(11) Challis, M.; Worsley, D. A. British Corrosion Journal 2001, 36, 297-303.

Chapter 3

Metallographic Investigation

3.0 Introduction

Metallography is the study of the physical structures and components of metals using microscopy. The specimens were prepared by various systematic grinding, polishing and etching techniques to reveal different alloying components and their respective phases. A sophisticated technique detailed in section 2.1 was implemented and careful image analysis allowed evaluation of the alloy microstructure. The microstructure study was undertaken to develop an understanding of the evolution and morphology of the microstructure within the alloy layer and to insure that the specimens examined that had the alloy layer applied were under similar production line parameters. The likeness in the microstructure of the alloying layer for individual samples and the associated corrosion inhibition contributions will be comparable subsequently any difference in corrosion performance can then be attributed to the following cleaning, pretreatment, primer and topcoat combinations.

3.1 Metallographic observations

The microstructure morphology was examined at a number of stages through the Galvalloy coating quantifying:

(i) the volume percentage of primary zinc,

(ii) the number of the primary dendrites,

(ii) the average dendrite size.

Figure 3.1 shows the equilibrium phase diagram for zinc-aluminium alloys with a eutectic point at just over 5% aluminium relevant to the coating alloy composition and the solidification patterns of the alloys. The typical images of microstructure through the coating are shown in Figure 3.2. Similar images were also recorded for the six Galvalloy samples listed in table 2.1. In Figure 3.2, the images were taken from near the coating surface (~5μm in depth), the centre of the coating (~20 μm in depth) and close to the coating and substrate interface (~30 μm in depth). In these images the zinc dendrites are shown as lighter areas. The remainder of the Galvalloy coating consists of a two phase eutectic structure predominantly of lamella morphology with alternating sheets of Zn and Al. Observations revealed little primary zinc (light colour) is exposed at the surface of the Galvalloy coating, consequently the surface in contact with the paint system is mostly eutectic composition (dark colour). Further into the coating away from the surface towards the alloy and steel substrate interface via progressive polishing the amount of primary zinc

phase visible is much greater and the dendritic features become apparent. This observed change in microstructure with the depth reflects how the coating forms as it solidifies. The primary zinc phase containing >98% zinc is first to nucleate. The nucleation events occur at the steel surface. The remaining alloy liquid becomes progressively richer in aluminium until the eutectic composition is reached at which point this liquid solidifies surrounding the primary phase with a two phase Zn/Al lamellar eutectic.

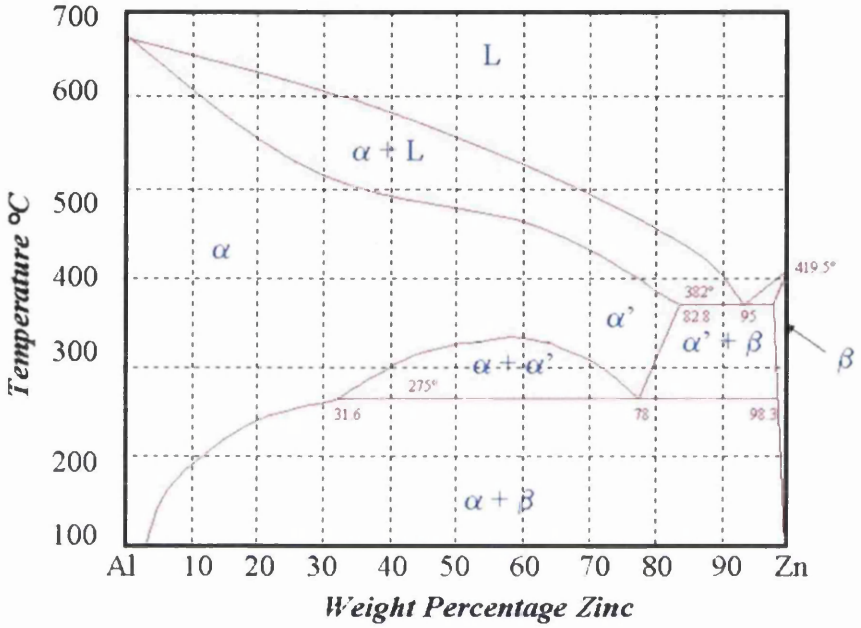

Figure 3.1 The Zn – Al equilibrium phase diagram.

The distinctive microstructure of MagiZinc (sample identification KK-9) is shown in Figure 3.3, images were taken from near the coating surface (~8 µm in depth), the centre of the coating (~20 µm in depth) and close to the coating and substrate interface (~30 µm in depth). The zinc rich dendrites correspondingly revealed themselves to be lighter areas, the remainder of the coating, where the Zn grains are surrounded by a eutectic. The introduction of magnesium to the Zn-Al alloy bath causes a depression in the eutectic temperature as well as a displacement of the eutectic composition towards a higher Al level thus leading to an increased primary zinc phase solidification. An SEM image of the microstructure shown in figure 3.4 highlights the differing phases present. Zinc rich dendritic phase is the first phase to form upon melt solidification, with dendrites nucleating at the steel substrate. The Binary eutectic comprising of lamellar of $MgZn_2$ and Zn is next to form from the remaining melt with the final solidification of ternary eutectic of a lamellar formation consist of $MgZn_2$, Zn and Al nodules [1].

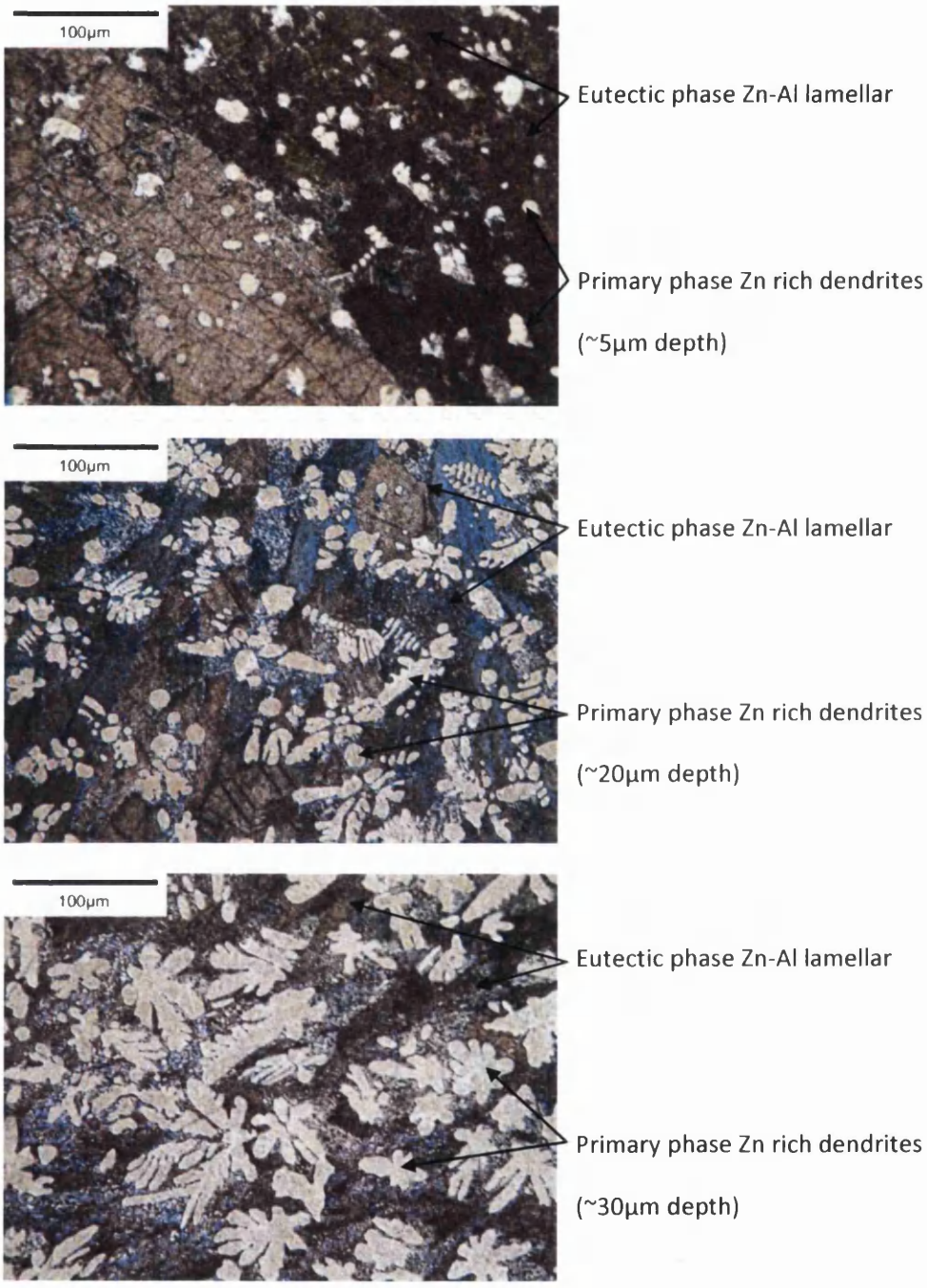

Figure 3.2 Optical microscopic images of KK-4, Galvalloy coating.

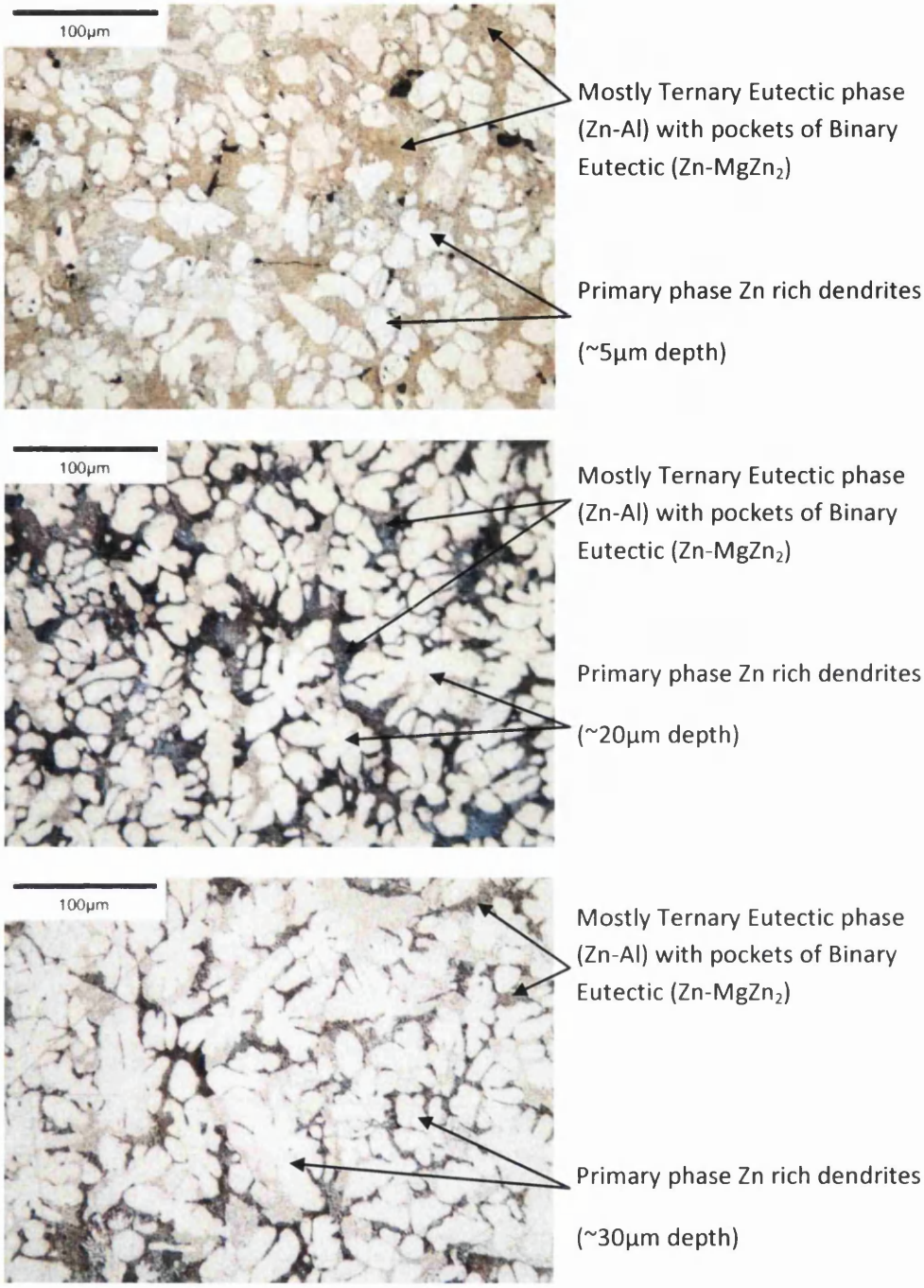

Figure 3.3 Optical microscopic images of KK-9, MagiZinc coating.

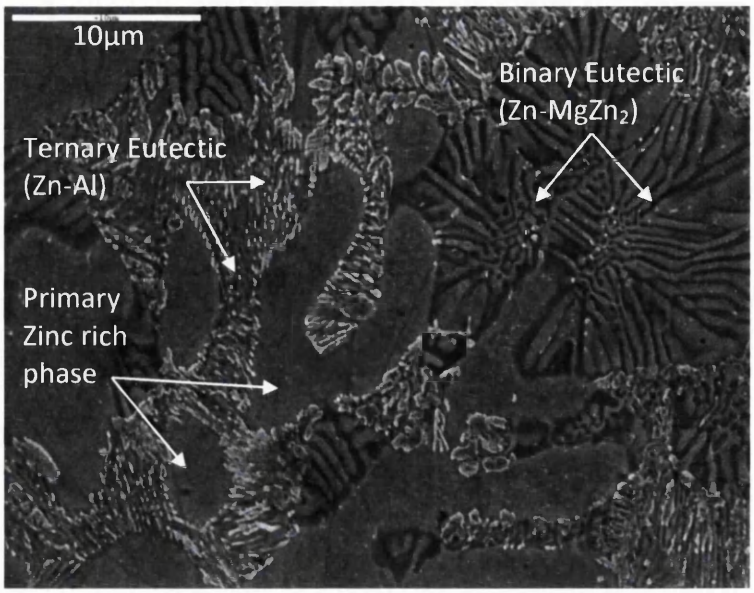

Figure 3.4 Scanning Electron Microscope image of MagiZinc alloy coating.

The average number of primary Zn dendrites at the coating and substrate interface was determined from the microstructure images near the coating and steel substrate interface, figure 3.5. An average number of dendrites 245 (±25) dendrites mm^{-2} was observed for the samples that is consistent with other published work [2,3]. This suggests that the nucleation rate for all the samples was similar and thus they had been produced using similar production line conditions. There was only exception of MagiZinc where the average number of dendrites was observed to be relatively higher than that of standard Galvalloy coating due to the greater percentage of zinc in the alloy. A typical value of ~325 dendrites mm^{-2} was observed for MagiZinc, KK-9, that is consistent with figures reported elsewhere [3].

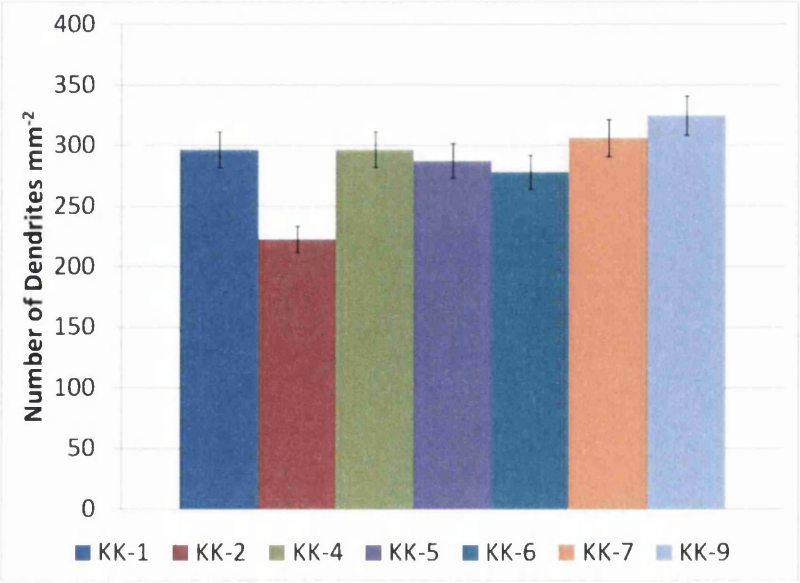

Figure 3.5 Average number of primary Zn dendrites at the coating and substrate interface.

Average dendrite size was calculated by analysing the primary Zn dendrites at the various depths through the coating, figure 3.6. The observed average dendrite size was 68 μm^2 with a spread of ±10 μm^2 between the Galvalloy samples. This consistency of dendrite size again suggests that the materials had been produced with similar line conditions allowing similar nucleation and growth of the alloy. MagiZinc (KK-9) had a larger average dendrite size of 186 μm^2. This increase in dendrite size was due to modification of the binary alloy by the addition of Mg.

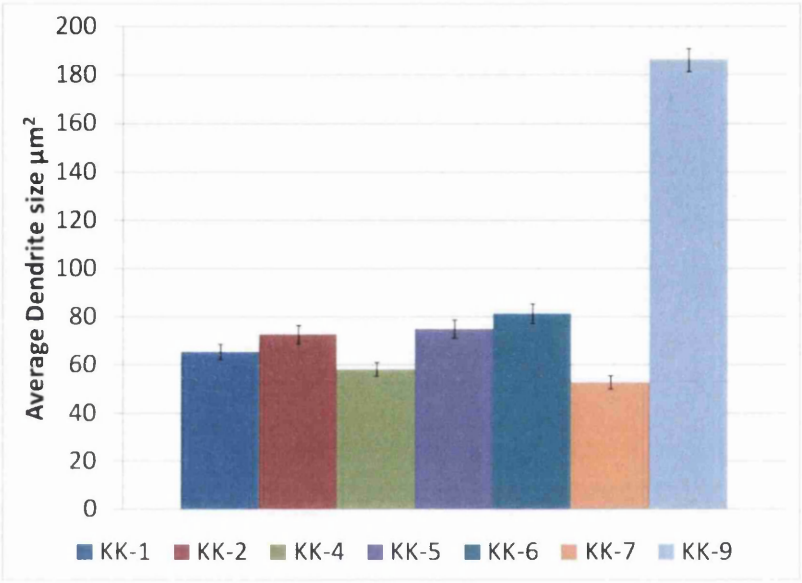

Figure 3.6 Average Dendrite size through the alloy coating.

The average volume fraction of primary Zn phase in the coating was calculated from the average percentage area of primary Zn at each depth from a number of images taken from different positions in the coating, a summary of these results is presented in figure 3.7. The quantitative volume fractions for each of the samples were similar with the exception of KK-9. However further scrutiny of data exhibited an abnormal value for sample KK-6. This was due to the sample images used for volume calculation being closer to the substrate rather than evenly spread. The higher volume of primary Zn found in KK-9 was expected due to greater zinc percentage within the alloy. The addition of Mg to the Zn-Al alloy induced a depression in the eutectic temperature and a displacement of the eutectic composition to a higher Al level thus leading to increased volume percentage of primary Zn solid solution phase. The increase was brought about due to an extended freezing range

that allowed an increase in precipitation and growth of the primary Zn phase. The observed increase in primary phase volume fraction was consistent with other published research [3,4].

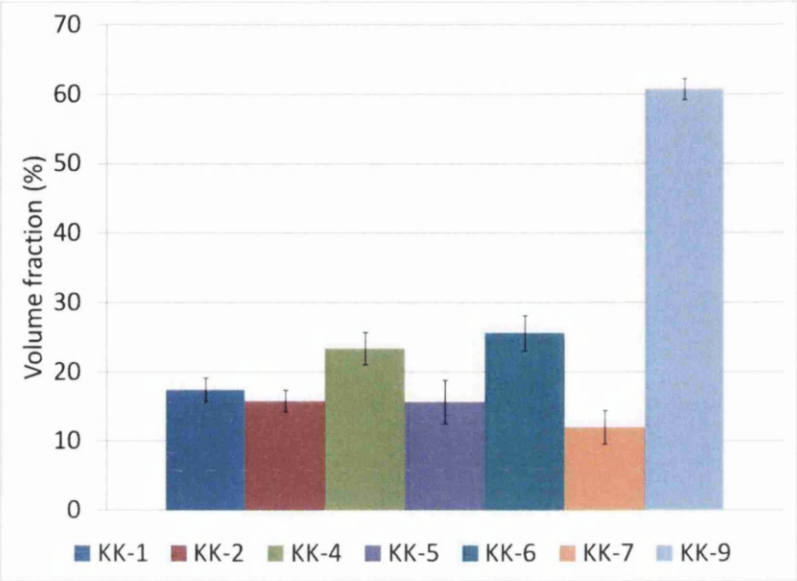

Figure 3.7 Primary Zn volume fractions for the alloy coating.

The microstructure investigation has revealed that the average area of primary zinc was found to be increasing as the coating substrate interface is approached. This reflects that the nucleation of Zn dendritic phases in the coating was at the steel substrate surface. The images of different depths for Galvalloy showed a likeness in primary phase structure, i.e. the morphology was found to be similar except for KK-9, MagiZinc. The MagiZinc sample consistently displayed greater number of dendrites, higher percentages of primary Zn and consequently greater percent volume fraction of Zn dendrites. The similarity in the microstructures of the six Galvalloy materials was of critical importance in the assessment of the effect of organic coatings on the cut edge corrosion performance. It has been shown previously that microstructural changes in Galvalloy can have a large effect on cut edge corrosion resistance [2,3,5]. The in depth microstructure analysis was not performed for all the subsequent samples however the microstructure morphology at a given depth was examined and compared within the specific batches of trails. The microstructure was found to be similar in features of the primary phase structure and distribution. The relationship between the number of interfacial dendrites and the corrosion rates is critical, it is reported elsewhere that an interfacial dendrite count of 180-280 (±25) mm^{-2} will result in a certain level of contribution towards the overall corrosion mechanism. This level of corrosion contribution associated with the number of interfacial dendrites remains

relatively unchanged for the stated range of interfacial dendrite count [2] . For the six Galvalloy samples examined the interfacial dendrite number is listed in table 3.1, the average count of 245 (±25) mm^{-2} interfacial dendrites was observed that is within the limits of 180-280 (±25) mm^{-2} for which the corrosion contributions will be alike and thus rate influences of interfacial dendrite numbers is restricted. Thus, by comparing samples with similar microstructures, the true effect of the subsequent organic coatings was assessed with confidence.

Table 3.1 Average interfacial dendrite number

Sample ID	Average Dendrite size (mm^{-2})
KK-1	297
KK-2	222
KK-4	297
KK-5	287
KK-6	278
KK-7	306
KK-9	324

3.2 Conclusions

The metallographic investigations of the samples confirm that the substrate and the Zn-Al alloy layer applied were comparable, except for KK-9. The similarities of the microstructure morphology for the specimens examined with the exception of KK-9 confirm that the individual sample substrates had undergone the same production line parameters. Sample KK-9 was applied with a Zn-Al-Mg alloy layer and the microstructure examination revealed a consistent dendrite size through the alloy layer. In contrast, the remaining six samples, the microstructure morphology differs significantly to KK-9. It was observed that dendrite nucleation occurred at the substrate to alloy interface and the dendrite size decreases further away from the substrate alloy interface.

Hence the corrosion inhibition contributions associated with the alloy layer would be similar and any difference in corrosion performances can be attributed to the subsequent cleaning, pretreatment, primer and topcoat combinations.

3.3 References

(1) Sullivan, J.; Mehraban, S.; Elvins, J. Corrosion Science 2011, 53, 2208-2215.
(2) Penney, D. Thesis, Univeristy of Wales Swansea, 2006.
(3) Elvins, J.; Spittle, J. A.; Sullivan, J. H.; Worsley, D. A. Corrosion Science 2008, 50, 1650-1658.
(4) Schuerz, S.; Fleischanderl, M.; Luckeneder, G. H.; Preis, K.; Haunschmied, T.; Mori, G.; Kneissl, A. C. Corrosion Science 2009, 51, 2355-2363.
(5) Elvins, J.; Spittle, J. A.; Worsley, D. A. Corrosion Science 2005, 47, 2740-2759.

Chapter 4

Zinc runoff from organically coated sheet steel

4.0 Introduction

Organically coated galvanised steels (OCS) have become popular building materials in the construction sector due to the possibility of rapid construction, flexibility and relative low cost [1]. OCS sheets are used increasingly in place of bare galvanised materials due to their aesthetic appeal. The primary mode of failure of such materials occurs due to metallic corrosion at the exposed cutedges and subsequent delamination of the polymer coatings. Currently chromate Cr(VI) containing inhibitor systems are effective at retarding such corrosion for extended time periods but due to legislation there is a drive to remove chromate Cr(VI) based inhibitors from existing systems and replace with alternative inhibitor systems that must be evaluated. This chapter evaluates the different anticorrosive performance of the chromate Cr(VI) containing and Chrome-free based OCS systems by means of monitoring the monthly zinc runoff induced by natural weathering and subsequent rain events and zinc runoff from laboratory accelerated rain chamber experiment. The aims of this section of work were to evaluate the levels of soluble zinc runoff from such materials, relate runoff to the exposure conditions and material composition and assess their respective corrosion inhibition performance. In this section of work an attempt has also been made to develop an accelerated version of weathering test that can give a ranking order based on the levels of runoff at a fraction of the time for traditional weathering trials.

The metal runoff is a phenomenon that has been recognised as being the dissolution of soluble corrosion products that may form on the exposed metal surface. When metal corrosion products form by weathering or during accelerated testing, they are dissolved by rain, dew or an electrolyte liberating the metal ions from the corroded surface and disperse into the immediate environment via a liquid medium.

4.1 External exposure

Seven material samples plus a blank have been exposed for 18 months to assess the metallic runoff due to cutedge corrosion of the materials. Table 2.1 lists the organically coated steel substrates exposed at Swansea University Engineering building roof top, which is in close proximity to the Swansea bay and therefore considered to be marine environment. The samples all have a Galvalloy metallic coating composed of Zn-4.8wt% Al except sample KK9 which has a Zn-1.6wt%Al-1.6wt%Mg alloy coating. The zinc runoff was monitored and the coating performance was assessed using a novel technique explained in detail in chapter 2.

4.1.1 Comparison of zinc runoff levels of various organically coated steels

Samples listed in Table 2.1 were subjected to atmospheric corrosion. Zinc runoff levels for all samples were recorded over an 18 month timeframe (1-06-2010 – 30-11-2011) with zinc runoff levels measured from accumulating runoff rain water at the end of each month. Figure 4.1 illustrates levels of zinc ions detected for each sample every month and figure 4.2 shows the cumulative zinc runoff levels in milligram per meter of cutedge for each of the sample. In all cases it was seen that following relatively rapid zinc ion release in the first four months of exposure, the samples then showed a decrease in rate of zinc runoff. The stabilisation in zinc ion release coincides with the build up of corrosion products and the onset of corrosion inhibition by the chromate or chrome free based coatings, which reduce the available surface area for electrolyte contact. This observation implies that, in the absence of large scale organic coating delamination, this type of material may potentially exhibit the majority of its zinc runoff during the first few months after assembly. There is reduced impact thereafter until the coating system becomes seriously degraded and allows further corrosion to become established. This observation mirrors measurements made during corrosion performance evaluations of the freshly prepared edges that rapidly develop (hydroxide) based film after short term exposure [2,3].

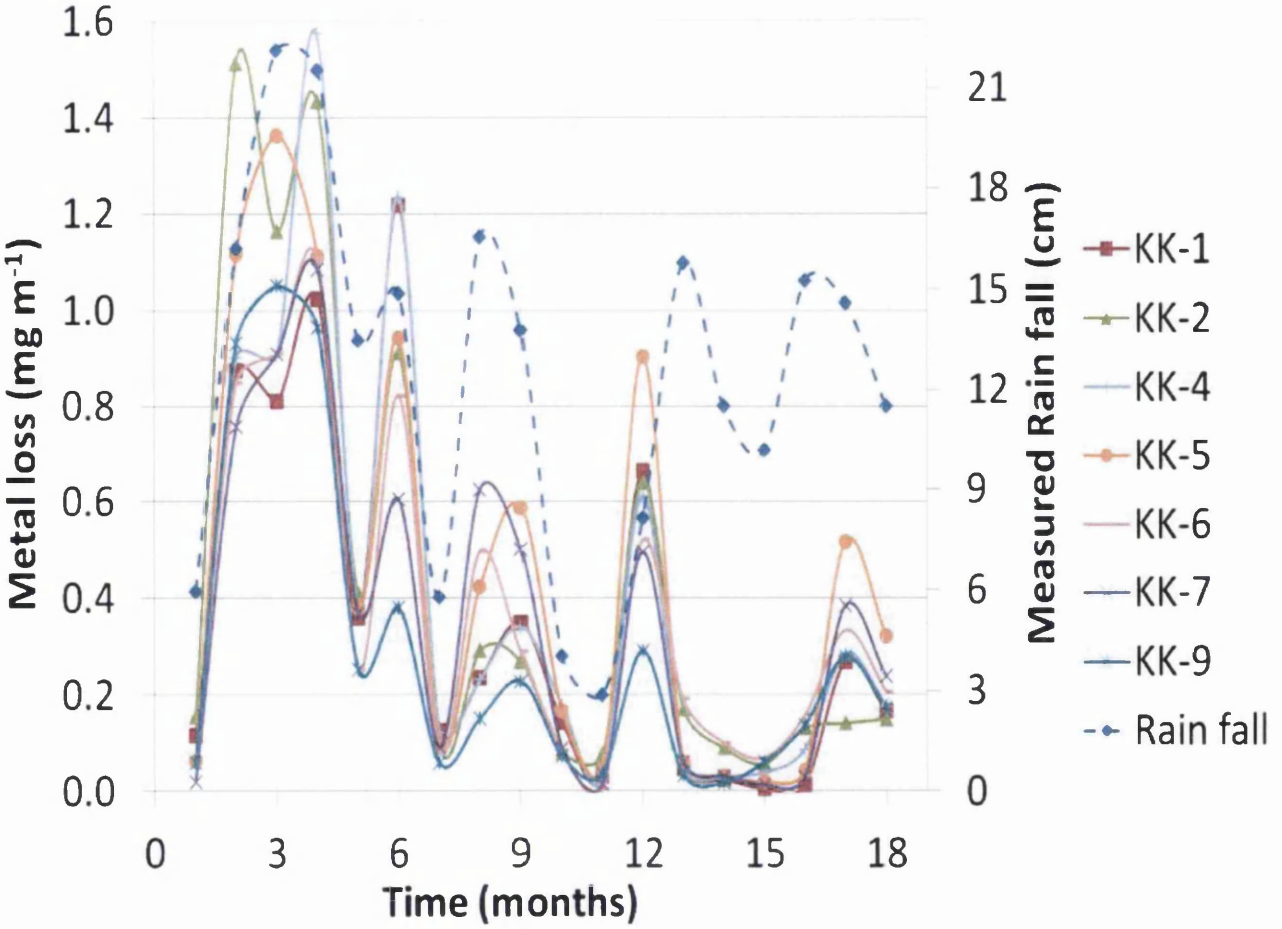

Figure 4.1 Monthly recorded Zinc runoff profiles from materials exposed at the Swansea University weathering site for 18 months.

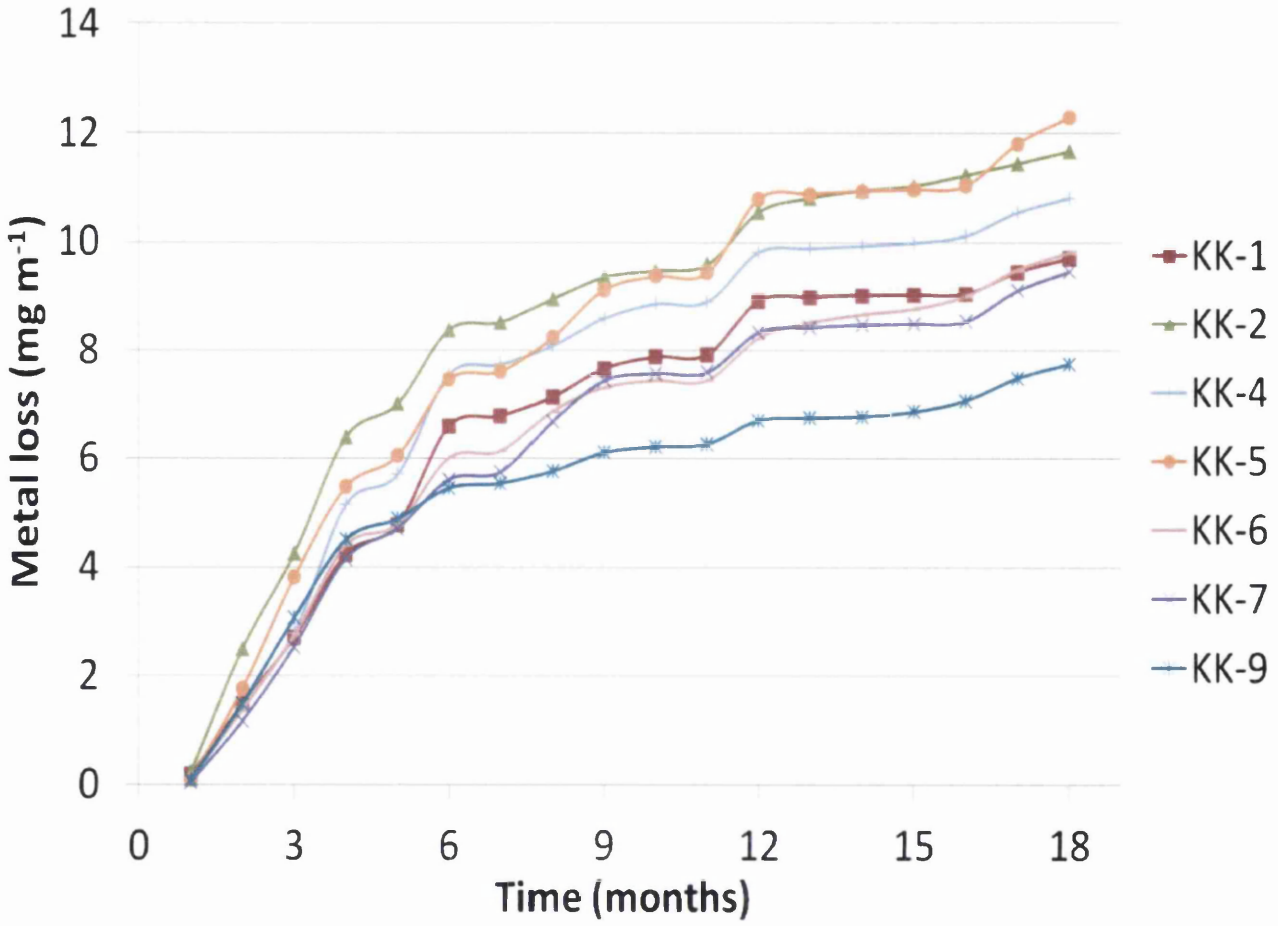

Figure 4.2 Cumulative Zinc runoff profiles from materials exposed at the Swansea University weathering site for 18 months.

The zinc runoff levels measured for samples exposed at the Swansea University site were induced mostly by rainfall and chloride ions. The location is considered to be marine in character due to its proximity to the sea (<500m). The zinc runoff levels ranged from 0.005 – 1.574 mg m^{-1} (cutedge) for the various materials over the 18 months exposure. The Galvalloy based OCS are considered to possess improved resistant to corrosion than systems based upon hot dip galvanised, also a common construction material. The most common mode of failure for such materials is due to cutedge corrosion, which may lead to delamination of the organic coating. The microstructure of Galvalloy described in chapter 3 was composed of Al/Zn eutectic with primary zinc rich dendrites. The cutedge corrosion phenomenon consists of several interactions, corrosion of Al and Zn as well as inhibition from other components of the paint system. This includes the formation of an adherent Al_2O_3 layer over the exposed coating that has high corrosion resistance. The passive aluminium oxide layer formed upon initial exposure of the coating is followed by galvanic zinc corrosion. The presence of exposed primary zinc rich dendrites at the cutedge can be attributed to the source of the zinc runoff [3-5]. The primary Zn dendrites within the Zn-Al lamellar eutectic matrix emanating mostly from the steel substrate are susceptible to localised corrosion events. These initiated localised corrosion sites are established and also remain active until all the Zn in the local dendrite has been consumed. This phenomenon is due to the relatively large cathodic area (steel) exposed at the cutedge. The oxidation reaction underpinning the corrosion attack on Zn dendrites can lead to conditions that favour further continued localised corrosion attack and can establish the formation of a pitting type corrosion event. The active localised Zn anodic site soon gets exhausted of Zn, consequently, new anodic attack initiates to another neighbouring Zn rich dendrite. This process continues until sufficient corrosion products are formed from the oxidation reactions of aluminium in the Zn-Al eutectic and of zinc in the primary phase.. The formation of corrosion products hinders further corrosion due to high diffusion resistance of electrolyte and oxygen through the newly formed oxide layer [3,6].

The samples before and after weathering appear to be intact with no measurable delamination seen at the cutedges from visual inspection month on month. The cumulative Zn runoff shown in figure 4.2 has revealed a relatively high Zn content in the runoff during the initial period of exposure. This was due to galvanic cells that are set up between the substrate steel and the Zn/Al alloy layer containing pockets of Zn rich dendrites. The establishment of galvanic cells is due to the presence of moisture on the exposed cutedge. The more frequent sources of moisture are dews, mist and rain. Rain is contaminated by

soluble substances of the atmosphere (pollutants) and in this way reflects the prevailing character of the localised environment. It is known fact that near the sea, rain is somewhat saline and acidic in nature. The measured average pH values for rain ranged from 5 – 6.5. Specific corrosion products of zinc are dependent on the prevailing atmospheric conditions and associated rain water. The atmospheric corrosion products of zinc consist of initially zinc oxide/hydroxide. Moisture and CO_2 play an important role in atmospheric corrosion of zinc. Various researchers reported that the corrosive effect of CO_2 is caused by the acidification of the surface electrolyte, giving rise to higher surface conductivity and an enhanced dissolution of metal surface films [2,7,8]. With CO_2 present in ambient air, the main corrosion products that can form are zinc hydroxycarbonate and Hydrozincite. Occurrence of trace sulphur dioxide in atmosphere tends towards conversion of zinc hydroxycarbonate to hydroxysulphate. The marine character of the location and affecting rain water ensures presence of chloride anions. Water containing Cl^- adsorbs onto the surface's existing corrosion product film or becomes retained in fine capillary moisture layers and interacts with the existing corrosion product film. Ordinarily the Cl^- anions undergo a degree of repulsion from the negative surface charge of zinc hydroxycarbonate, zinc hydroxysulphate, zinc hydroxide, zinc hydroxychloride and zinc oxide. However, prolonged Cl^- anion association can lead to precipitation of insoluble simonkolleite and hydrozincite [2,9,10]. These corrosion products can offer anticorrosion protection via film formation on the exposed surface that has good cohesion and adhesion and provides a protective barrier. The initial higher runoff period ends when a coherent layer of corrosion products has formed to sufficient volume to offer a degree of barrier protection to the metallic coating and steel substrate.

Reference samples KK-1 production line material and KK-2 Tata laboratory prepared were both chromate containing systems. The corrosion mechanism may differ a little from that described above due to the interaction of the chromate inhibitor. The substrate had been treated with Henkel's NR6022 pretreatment. This is a chromic acid solution that interacted with surface of the overlying alloy layer. When in contact with electrolyte the chromate ions were adsorbed on the active parts of the surface and reduced forming compounds of trivalent and hexavalent chromium. The substrates were also applied with chromate containing primer. The chromate pigments used in the primer were strontium chromate ($SrCrO_4$), which is an acid salt that is slightly soluble in water. The mechanism of inhibition by chromate was: initial adsorption of chromate ions on the exposed surface transported via the electrolyte to the cathodic sites, followed by formation of a passive film containing

chromium oxide (Cr_2O_3) and Iron oxide (Fe_2O_3) [11]. The alloy layer consists of mostly Zn and in presence of electrolyte zinc hydroxide ($Zn(OH)_2$) was formed. The combination of events listed above provided the hindrances to corrosion attack. The described mechanism holds true for MagiZinc sample KK-9 which too had been treated with a chromate containing system. The combination of MagiZinc alloy coating and chromate containing paint system offered a marked improvement over the traditional Galvalloy coated steel substrate treated with chromate based paint system. Figure 4.2 shows that sample KK-9 exhibited the lowest cumulative metal loss demonstrating the best anticorrosion characteristics from the batch of samples tested. The improved anticorrosive nature of the system of sample KK-9 in comparison to reference samples KK-1 and KK-2 is mostly due to the difference in the metal alloy coating of the steel substrate. Sample KK-9 was not further compared with remaining samples due to the significant difference in metallic alloy coating but demonstrates the potential of this type of alloy for future use as a metallic coating for steels.

The remaining systems, KK-4 to KK-7 were chrome free. Galvanic coupling was present between the underlying steel and Galvalloy coating. The most protection was provided by the barrier effect of the applied paint system. During production samples had been subjected to Henkel's Bondrite 1455 pretreatment. This was applied to form a corrosion resistant titanium dioxide (TiO_2) and zinc phosphate ($Zn_3(PO_4)_2$) [12]. The liquid phase deposition treatment forms films that add to the barrier protection as well as provide a surface for primer application. Samples KK-4 and KK-6 had been applied with Akzo Nobel IN7UD987 primer, whereas samples KK-5 and KK-7 had been applied BASF CP71 primer. The IN7UD987 primer offers mostly barrier protection due to lack of any active inhibitor within the primer matrix, it also provides a suitable surface for the topcoat. The CP71 primer contains the trizinc bis orthophosphate, this has been substituted in place of lead and chromium as an anti rust pigment. Inhibition is offered by promoting the formation of protective film. The inhibition mechanism is cathodic in nature and deposition of sparingly soluble zinc phosphate reduces the exposed cathodic area [11,13]. The mechanisms of under paint corrosion for organically coated steels are complex and are not fully understood. Active ions from the inhibitor are thought to form a covering passivating film and therefore preventing ion egress from metal to electrolyte [13]. The topcoat applied offered straightforward barrier protection to the underlying substrate.

The cumulative zinc runoff from the cutedge for all the samples is presented in figure 4.2. The initial corrosion rate was observed to be relatively high and was maintained for the

first 4-6 months after which a reduction in corrosion rate was noted. Samples KK-1 and KK-2 both reference samples and both containing chromium based inhibitor show an initial accelerated corrosion rate which then reduces to a lower rate after 6 months. Sample KK-2 exhibited a greater magnitude of overall zinc runoff than KK-1 and this was due to the difference in gauge of the substrate, KK-1 was gauge 0.48mm and KK-2 was of a higher gauge 0.58mm. The higher gauge substrate would in result have a relatively larger cathodic area exposed at the cutedge which would perhaps drive the anodic dissolution of zinc from overlaying alloy layer [3]. Sample KK-4 when compared with KK-5 showed a relatively higher extent of total zinc runoff suggesting that the sample KK-4 that had been treated with IN7UD987 primer provided less corrosion protection than the CP71 that was applied to KK-5. A similar observation was apparent when KK-6 was compared with KK-7. Sample KK-6 had been applied with IN7UD987 primer and KK-7 had been treated with CP71. A conclusion can be derived that CP71 offers improved corrosion protection to the substrate than the IN7UD987 due to CP71 containing trizinc bis orthophosphate. Primer CP71 promotes the formation of an adherent protective zinc phosphate based film. Samples KK-4 and KK-6 were applied with a HPS200 Ultra White topcoat and samples KK-5 and KK-7 where applied with a HPS200 Ultra Goosewing Grey. The total zinc runoff observed also implies that the HPS200 Ultra Goosewing Grey offers improved corrosion barrier protection than the HPS200 Ultra White.

In chromate containing systems the hexavalent chromium (Cr^{6+}) plays a significant role as the inhibitor in corrosion resistant coating. Chromate compounds provide excellent corrosion resistance however Cr^{6+} is known to be toxic. With tightening regulatory requirements the economic significance of implementation of chrome-free and non toxic alternatives is clearly important. Reference samples KK-1 and KK-2 both containing chromate based inhibitors set the standard for the chrome free systems to match in performance or show improved anticorrosion characteristics. After 18 months exposure the cumulative zinc runoff detected for samples KK-1 and KK-2 were 9.7 mg m^{-1} and 11.7 mg m^{-1} respectively. Sample KK-2 is of a thicker gauge by about 20% than sample KK-1; that is the steel substrate gauge for KK-1 was measured to be 0.48mm and KK-2 steel substrate gauge measured to be 0.58mm. In order to compensate for the effect of thicker gauge on the recorded zinc runoff it may be a good approximation to factor down by 20% the zinc runoff associated with sample KK-2 resulting in ~9.4 mg m^{-1} of Zn runoff for the 18 months exposure. From the outdoor weathering data it was clearly evident that the chrome free systems applied to samples KK-4 and KK-5 showed comparatively high cumulative zinc

runoff values for the duration of 18 months exposure, 10.8 mg m^{-1} and 12.3 mg m^{-1} respectively. The zinc runoff from chrome free systems applied to KK-6 and KK-7 where 9.8 mg m^{-1} and 9.5 mg m^{-1} respectively. Anticorrosion performance of samples KK-6 and KK-7 were very closely matched with the reference samples KK-1 and KK-2. Sample KK-7 proving to be the best from the chrome free systems subjected to 18 months of outdoor weathering with equivalent performance to chromate containing inhibitor systems. Samples tested can be ranked according to the levels of Zn runoff observed via the accelerated testing; samples listed at the top being most corrosion resistant, see table 4.1.

Table 4.1 Samples tested ranked in order from top of the table with lowest Zn runoff levels observed via the outdoor weathering tested.

Sample ID	Zn Runoff (mg m^{-1})
KK-9 (Zn/Al/Mg) (Cr)	7.8
KK-7 (Cr Free)	9.5
KK-1 (Cr)	9.7
KK-6 (Cr Free)	9.8
KK-4 (Cr Free)	10.8
KK-2 (Cr)	11.7
KK-5 (Cr Free)	12.3

Table 4.1. highlights some important results in that the Cr free systems are performing well in comparison with the Cr containing coatings over the 18 months of exposure. This is encouraging for the Industrial sponsors who need to match existing warranties based on Cr containing systems with Cr free coatings. The performance of the new Zn-Al-Mg alloys coating (KK-9) is also an interesting result and highlights the potential benefits that such alloys may confer to construction systems going forwards.

4.1.2 Effect of rainfall

Figure 4.1 show profiles of monthly recorded zinc runoff vs. rainfall quantity for each material at the Swansea University roof top site. From these zinc runoff plots it can be seen that there is a general temporal trend between the zinc runoff level and precipitation quantity for each month for all the materials. Generally, higher quantities of rain produce more runoff but it is difficult to obtain direct quantitative correlations as other environmental conditions, such as Cl^-, SO_2 and NO_x levels, will contribute to the runoff quantities observed. It is also interesting to note general falling levels of runoff from all the samples tested. The reason behind this is twofold. Initial exposure will result in rapid removal of zinc rich dendrites in the aluminium zinc alloy layer. It is also anticipated that

longer-term exposure will lead to inhibitor leaching and inhibition of the cut edge corrosion that will reduce the runoff rate further.

4.2 Modelling of external weathering zinc runoff

In this section of work an attempt was made to develop a mathematical model to predict runoff behaviour for this class of materials and therefore potentially offer the industrial sponsor some idea of performance before manufacture. The experimental data of zinc runoff as function of time for period of 18 months (1-06-2010 – 30-11-2011) on the roof of the Swansea University building is plotted figure 4.2 The data can be best presented by an n^{th} order negative exponential equation (Eqn. 4.1), where y is the cumulative zinc runoff (mg m^{-1}) and t is the time of exposure (hrs). This mathematical expression has previously reported in modelling of stress corrosion cracking, however in this instance has been applied to model the levels of zinc runoff [2,14].

$$y = a_0\left(1 - e^{-(a_1.t)}\right)^n \tag{4.1}$$

Where a_0, a_1 and n are arbitrary constants reflecting physio-chemical resistances experienced by cut-edge sample of prepared coated steel sample to the dissolution process. These constants are evaluated using built-in function "Solver" of Microsoft office 2007(Excel) by minimizing the predefined objective function "sum of square of percentage errors between experimental measured data and calculated using equation 4.1. The formulation of mathematical function (Eqn. 4.1) is based on various corrosion resistances, coating, oxidant diffusion, galvanic protection (Zn and Al-Zn), formation of protective layer of Al_2O_3, etc. Each resistance is presumed to be the best represented by a first order system. The overall protection system of material constitutes of combination of n interacting simultaneous corrosion resistant systems that can be modelled by simple and most adequate expression (Eqn. 4.1). All the data were represented with an average absolute error of less than 5% and correlation coefficient value of 0.9999.

$$OF = \sum_{i=1}^{n}\left(\frac{\left(y_{\exp} - y_{cal}\right)\times 100}{y_{\exp}}\right)^2 \tag{4.2}$$

The rate of dissolution is evaluated by the differentiation of equation 4.1 as:

$$\frac{dy}{dt} = n.a_0.a_1.e^{-(a_1.t)}\left(1 - e^{-(a_1.t)}\right)^{n-1} \tag{4.3}$$

Equations 4.1 and 4.3 describe the continuous function of dissolution of zinc for the experimental period and simulated data can be generated and used for any time interval for investigation of real mechanism for both experimental conditions, natural rainfall and simulated rain chamber runoff. Figure 4.3 illustrates the predicted zinc runoff levels for the samples by the use of the model equations based on experimentally measured values compared with the experimentally measured Zn loss due to outdoor exposure. These equations can be used further by extrapolation to indicate rates for longer time based on the experimentation data history. The extrapolated data may be interpreted with caution as the model presently only reflects the experimental of 18 months. Figure 4.3 illustrates the predicted zinc loss based on model expression equation 4.1. The corrosion mass loss (y) as a function of time determines the corrosion rate $\frac{dy}{dt}$ (equation 4.3 from equation 4.1). Figure 4.4 shows as an example, the calculated corrosion rates for the organically coated steels exposed to external weathering derived from the model equation 4.1. The model equation 4.1 proposed fits well with the external weathering data with respect to levels of zinc runoff recorded for organically coated steel induced by atmospheric corrosion. The formula gives possibilities to predict the metal mass loss due to external weathering. Although proposed model equation has been validated against 18months of data further long term data confirmation will provide a more refined solution for longer term prediction of organically coated steels. Such a model equation can be utilised by the industry i.e. TATA Steel, in product development as well as giving an edge over competitors in delivering newer products rapidly to the market with confidence in the products life expectancy.

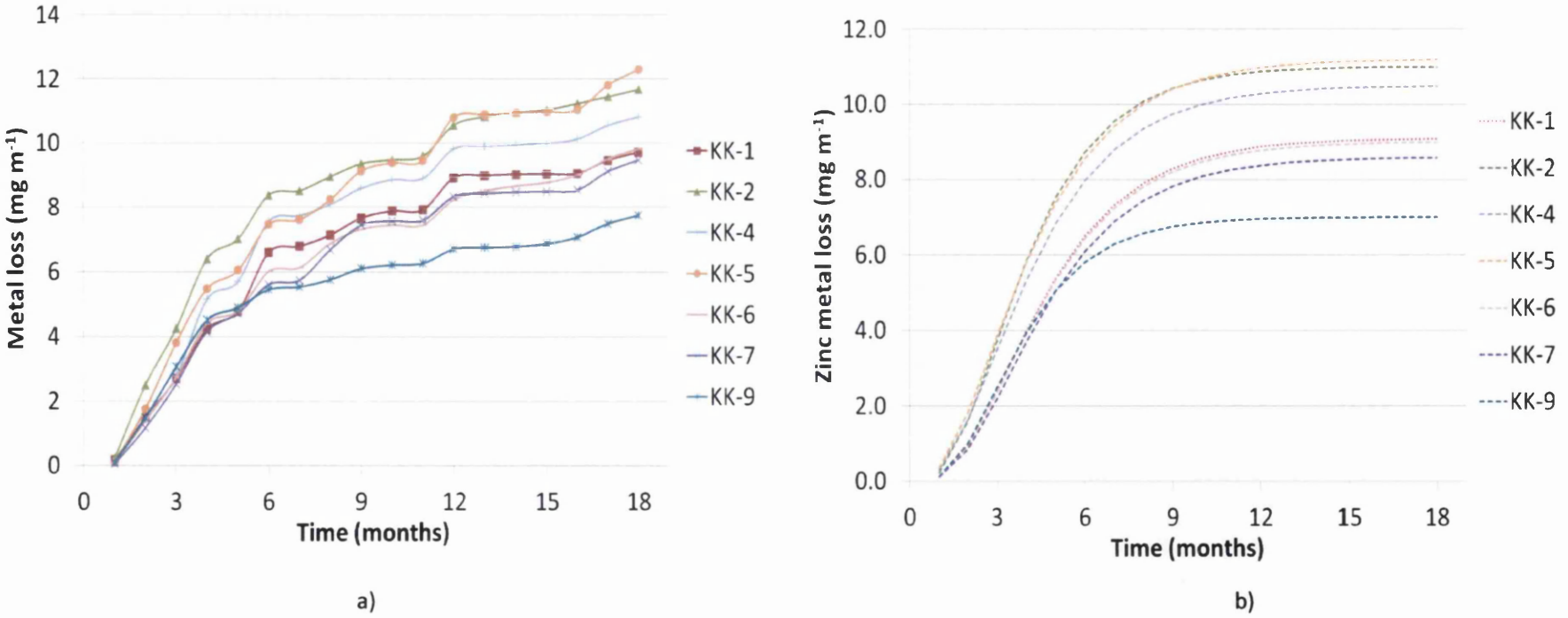

Figure 4.3 a) Measured Zn runoff of samples exposed outdoors b) Predicted Zinc based on the model expression (eq. 4.1).

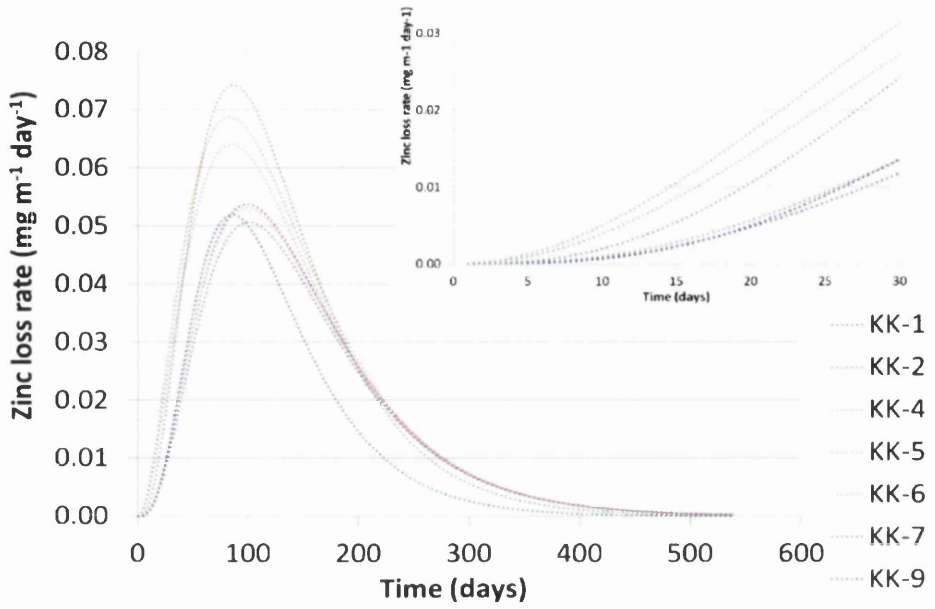

Figure 4.4 of corrosion rate (mg m^{-1} day^{-1}) from equation 4.3 as function of time in days.

4.3 Accelerated runoff experiment – Rain simulator

In this section, experimental work based on the realistic accelerated laboratory tests that has been developed to simulate the external weathering induced zinc runoff behaviour from the cutedges of organically coated galvanised steels as presented in section 4.1 are compared and discussed.

Accelerated tests have been carried out on the set of materials given in table 2.1 with 2 litres of re-circulated distilled water sprayed at 13ml/min (equivalent to an average of 0.17mm/h rainfall) onto coupons of material with an exposed cut-edge of 1.5m held perpendicular to the falling simulated rain for 120hrs. A detailed description of these tests and apparatus used is given in section 2.3. The composition of distilled water electrolyte used in the accelerated tests is tabulated in Table 4.2. From this data it can be seen that small quantities of ionic species are present in the water that can increase the conductivity of the electrolyte initiating electrochemical processes on the materials. The accelerated experiments have been repeated numerous times and the results shown are an average of these tests. The repeatability between tests proved to be within 15%. As with the external exposure tests zinc has been the major detectable ion detected in the runoff waters.

Table 4.2 Composition of distilled water electrolytes used in accelerated tests obtained from ICP-MS analysis at time zero.

Element	Concentration (ppb)
Na	<0.5
Cl	<0.5
Mg	<0.5
Cr	<0.5
Fe	<0.5
Zn	2.0
Al	5.5

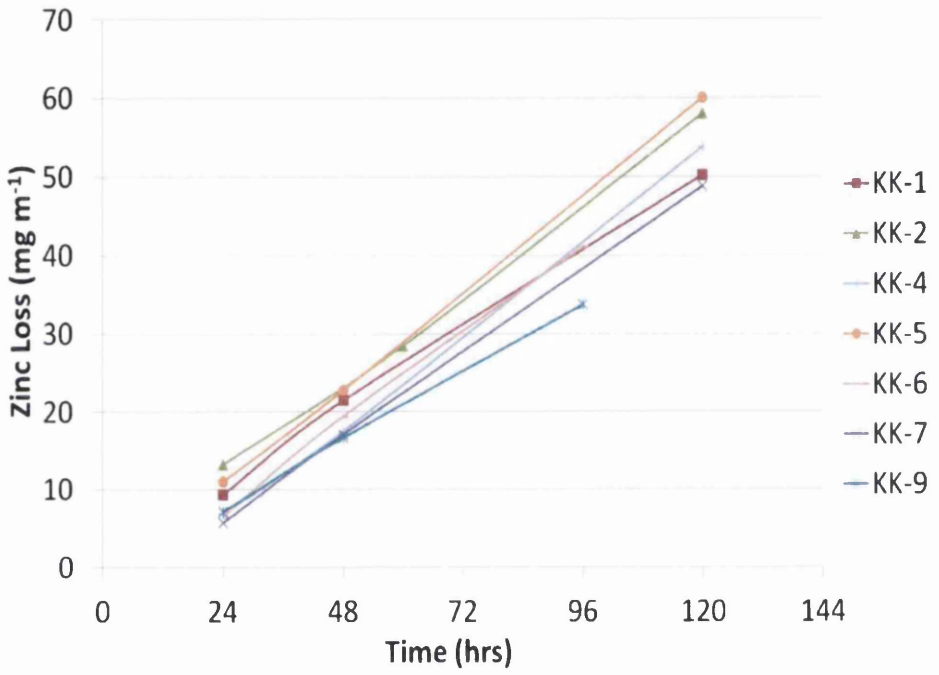

Figure 4.5 ICP-MS measured Zinc runoff data from accelerated test.

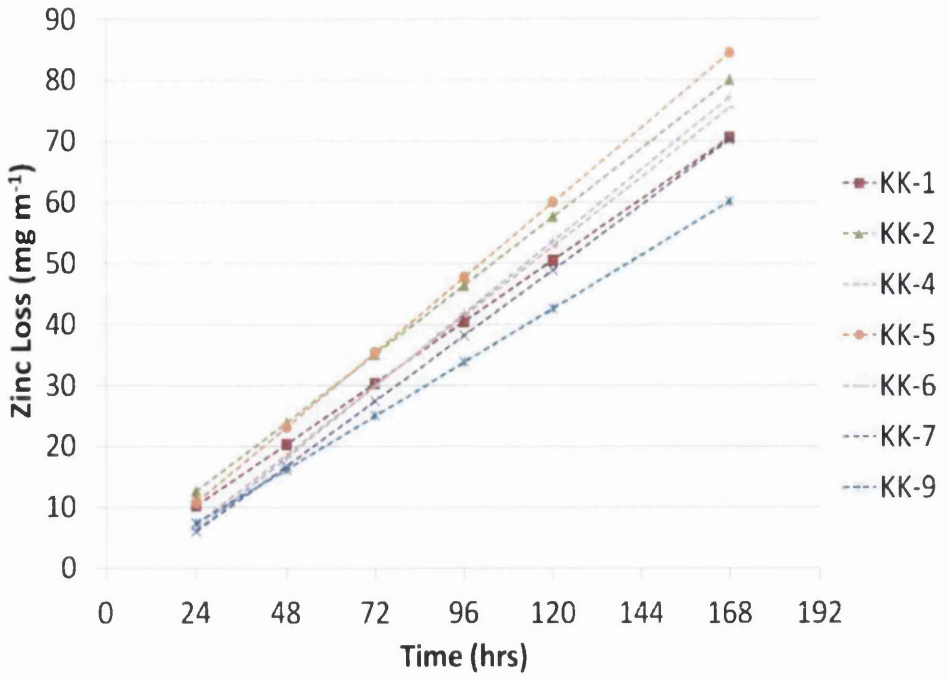

Figure 4.6 Extrapolated Zinc runoff derived from accelerated test data.

Figure 4.5 shows the actual data collected from the accelerated rain chamber test. The data points from the accelerated runoff for each sample allowed a linear relationship to be identified. The linear relationship was then used to extrapolate the runoff up to 168 hours illustrated in figure 4.6; providing constant time interval for the uniformity of the data. All the samples subjected to accelerated testing showed no visible signs of paint degradation or delamination. Samples KK-1 and KK-2 are both reference samples (chromate containing), KK-2 was of a thicker gauge hence showing greater Zn runoff than KK-1 with the difference in gauge was about 20%. Similar trends were observed as per the outdoor weathering data. Sample KK-9 having the least measured Zn loss, KK-9 was the MagiZinc alloy prepared substrate with the chromate based inhibitor. Samples KK-7 from the chrome free systems performed equally if not slightly better than chromate containing samples with Zn loss levels comparable to reference sample KK-1. Sample KK-6 from the batch of chrome free systems exhibited the next best performance. Accelerated test results show overall similar trends to those observed via the external weathering. Samples tested can be ranked according to the levels of Zn runoff observed via the accelerated testing, see table 4.3. Samples are ranked in order of most resistive to corrosion at top of the table with lowest Zn runoff levels observed via the accelerated tested. The ranking order for the samples is in the same order to that observed by means of outdoor weathering also shown in table 4.3.

Table 4.3 Samples ranked in order of most corrosion resistant from top of the table with a comparison between the laboratory and external runoff tests showing that the same order of performance was observed in both tests.

Sample ID	Total Zn Runoff 168hrs Accelerated test (mg m^{-1})	Total Zn Runoff 18 months External weathering (mg m^{-1})
KK-9 (Zn/Al/Mg) (Cr)	60.1	7.8
KK-7 (Cr Free)	70.3	9.5
KK-1 (Cr)	71.6	9.7
KK-6 (Cr Free)	75.5	9.8
KK-4 (Cr Free)	77.3	10.8
KK-2 (Cr)	80.1	11.7
KK-5 (Cr Free)	84.6	12.3

The zinc runoff levels observed through the accelerated testing were significantly greater than those obtained from outdoor weathering. The most probable cause of higher levels of zinc runoff observed in accelerated testing than the external weathering are due to passivation of the substrate in external weathering and the averaging of the corrosion rate over a longer period in the external weathering and shorter period for the accelerated test. The higher levels of zinc runoff in accelerated test can be due to the nature of the electrolyte used, in this case distilled water. Once the water has been vaporised and condensed back to liquid state majority of the soluble and non volatile contaminants are removed from the water leaving the distilled water with few trace amounts of dissolved solids and is starved of ions. Therefore in the accelerated test when the electrolyte comes into contact with the metallic substrate there is a relatively rapid ion exchange and resulting corrosion products if any will be quickly dissolved in the ion starved electrolyte, thus distilled water is an aggressive corrodent. Another contributor to the raised levels of zinc runoff from the accelerated test was due to the continuous wetting of the samples. The credible cause for higher zinc runoff levels is perhaps the combination of the factors outlined above. The ranking order of samples in table 4.3 matches the outdoor weathering results.

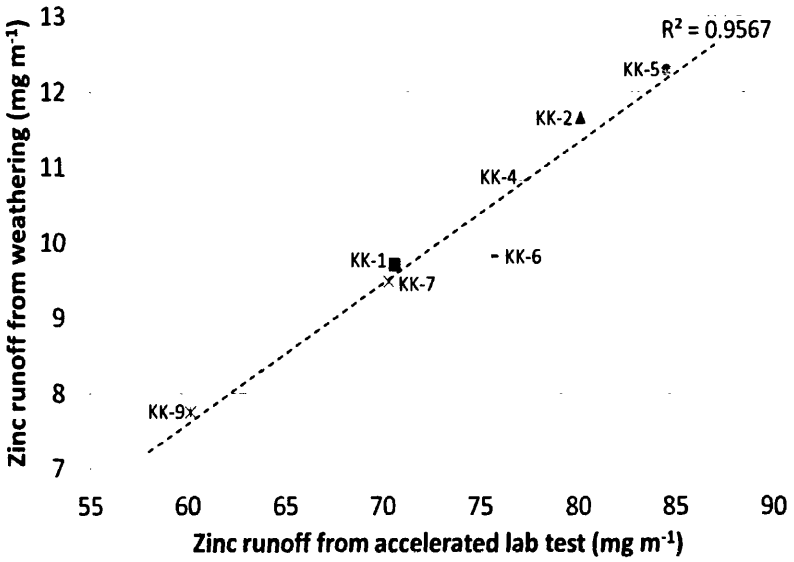

Figure 4.7 Comparison of 18 months external weathering with 168 hr accelerated lab test.

The results of accelerated test runoff data (mg m^{-1}) have been further compared with the external weathering runoff data for the samples tested. The comparison of 18 months of external weathering with the accelerated test shows a good correlation, illustrated in figure 4.7. The relationship between the data sets is encouraging, the accelerated tests predicting the measured level zinc runoff from external weathering convincingly well. This suggests that the laboratory developed test could be used to predict 18 months performance of similar materials but also be a useful ranking tool of performance for materials developed in the future based on similar coating systems.

4.4 Conclusions

Coupons of differing zinc coated steels have been exposed for 18 months at the Swansea University roof top site to assess metallic runoff. Zinc has been the major quantifiable runoff ion over the experimentation time.

The levels of zinc runoff from the coupons, when exposed to the natural weathering, showed that there was a general trend between the zinc runoff level and precipitation quantity for each month for all the materials. Generally, higher quantities of rain produce more runoff. There is an initial period of about 5months where the corrosion rate is relatively high and then starts to plateau. The higher corrosion rate observed at first is due to onset of galvanic corrosion. Primary zinc rich dendrites are exposed at the cutedge surface that are the source of the zinc runoff and even though only a small surface are of

the dendrite may be visible at the edge the corrosion can persist through the coating until all the zinc dendrite has dissolved. At the exposed cutedge the dissolution of the primary zinc dendrites occurs during the initial exposure until the aluminium from the AL-Zn eutectic corrodes promoting the development of an adherent Al_2O_3 layer, which posses a high corrosion resistance and also followed by the zinc corrosion products on top this oxide layer. Although samples were left for 18 months there were no visible signs of paint film delamination, it would be fair to assume that with prolonged exposure eventually the organic coating delamination would occur thus exposing more of the metal and subsequently resulting in higher rates of corrosion. From the perforated coupons tested in the simulated laboratory examination, it is evident that sample KK-9 (Magizinc) with the chrome containing system performed the best for the exposed period. However the chrome free inhibitor system combination of BASF's primer CP71 and HPS200 Goosewing Grey showed similar protection, if not better in corrosion performance as the reference samples. The second best was the chrome free system the AkzoNobel's primer IN7UD987 combined with the topcoat HPS200 White.

The model equations developed agree remarkably well with the realistic outdoor weathering data. The model is able to predict the levels of zinc runoff for a given time of exposure which agrees with the recorded data. The model equations can be used to extrapolate data to indicate rates for longer time. The extrapolated data may be interpreted with caution that only reflects the experimental period restricted behaviour.

A simple accelerated laboratory test was developed, the rain simulator, which attempts to mimic the runoff from outdoor weathering. Assessment of the zinc loss from the perforated coupons tested shows similar trends to those observed via the outdoor exposure of 18 months. This implies that rain simulator accelerated tests can provide valuable data for assessing organically coated galvanised steel that can be comparable to 18 months of outdoor exposure.

4.5 References

(1) Shohet, I. M.; Laufer, A. Journal of Construction Engineering and Management 1996, 122, 242-247.
(2) Veleva, L.; Acosta, M.; Meraz, E. Corrosion Science 2009, 51, 2055-2062.
(3) Belghazi, A.; Bohm, S.; Sullivan, J. H.; Worsley, D. A. Corrosion Science 2002, 44, 1639-1653.
(4) Penney, D. J.; Sullivan, J. H.; Worsley, D. A. Corrosion Science 2007, 49, 1321-1339.
(5) Elvins, J.; Spittle, J. A.; Worsley, D. A. Corrosion Science 2005, 47, 2740-2759.
(6) Marder, A. R. Progress in Materials Science 2000, 45, 191-271.
(7) Chung, S. C.; Lin, A. S.; Chang, J. R.; Shih, H. C. Corrosion Science 2000, 42, 1599-1610.
(8) Muster, T. H.; Neufeld, A. K.; Cole, I. S. Corrosion Science 2004, 46, 2337-2354.
(9) Muster, T. H.; Cole, I. S. Corrosion Science 2004, 46, 2319-2335.
(10) Chen, Z. Y.; Persson, D.; Leygraf, C. Corrosion Science 2008, 50, 111-123.
(11) Sastri, V. S. Corrosion inhibitors : principles and applications; Wiley: Chichester ; New York, 1998.
(12) Fujita, R.; Sakairi, M.; Kikuchi, T.; Nagata, S. Electrochimica Acta 2011, 56, 7180-7188.
(13) Revie, R. W.; Uhlig, H. H.; Uhlig, H. H. C. h. Uhlig's corrosion handbook; 2nd ed. ed.; John Wiley & Sons: New York ; Chichester, 2000.
(14) Filatov, G. V. Journal Name: Materials Science; Journal Volume: 29; Journal Issue: 6; Other Information: PBD: May 1994; TN: Translated from Fiziko-Khimicheskaya Mekhanika Materialov; 29: No. 6, 59-64(Nov-Dec 1993) 1994, Medium: X; Size: pp. 616-621.

Chapter 5

Investigation of corrosion using the Scanning Vibrating Electrode Technique (SVET)

5.0 Introduction

In chapter 4 the results from external exposure runoff and accelerated rain simulator exposure runoff were presented for a batch of organically coated steels to assess the performance of replacement chromate free systems. It was apparent that different paint systems displayed varying levels of Zn runoff. The aim of this section of work was to understand the cut-edge corrosion mechanisms present in a variety of organically coated steels and confirm the trends observed from the runoff experimental work via the scanning vibrating electrode technique (SVET). Correlation between the scanning vibrating electrode technique (SVET) data and runoff data from both external exposure and rain simulator was determined. A range of organically coated steel (OCS) samples were immersed in 0.1% $NaCl_{(aq)}$ and the corrosion mechanisms investigated using the SVET. The samples investigated in chapter 4 have been tested along with further production trials of chromate free organically coated steels.

5.1 Scanning Vibrating Electrode Technique applied to Organically Coated Galvanised Steels

The SVET has benefited from a wide acceptance as a powerful electrochemical technique for evaluation of corrosion inhibitor, detection and quantifying of corrosion defects and shown to be invaluable tool in the study of mechanistic investigations of corrosion in organic coated steels and specifically, cut edge corrosion [1-3]. The SVET is an electrochemical technique that relies upon the detection of the vertical component of the current flux in the electrolyte at known points above the corrosion features on a surface via a movable vibrating microtip. The use of organically coated galvanised steel (OCS) products is wide spread. Majority of failures for such products occur due to corrosion at the exposed metallic cutedge as outlined in previous chapters. SVET was used to investigate the cut-edge corrosion mechanisms and compare performance of a range of OCS samples. The samples were divided into two main groups:

- BASF's HPS200 (PVC top-coat)
- Becker's Prisma (PU top-coat)

The two groups were further divided to evaluate the impact of chrome free pretreatment on the corrosion inhibition by varying the use of industrial pretreatment inhibitor systems G1455 and TP10475. These were trialled with three assorted pre-treatment coating weights 6-7mg Ti/m^2, 8-10mg Ti/m^2 and 15-20mg Ti/m^2 and different cleaning agents Novamax 187U, Ridoline and S5117 prior to application of the pre-treatments. The current

production line chromate containing BASF and Becker systems were also tested using the SVET as references. The samples tested are shown in tables 5.1, 5.2, 5.3, 5.4, 5.5 and 5.6. In all tests the electrolyte solution used was 0.1% $NaCl_{(aq)}$ that was unstirred and open to air in ambient conditions during the experiment period giving a dissolved oxygen concentration of $2x10^{-4}$ mol dm^{-3}. Scans of the cut edges were recorded every hour for 24 hours.

Table 5.1 Batch 1 2007 chromate free trial samples (as runoff tested in chapter 4)

Sample Identification	TATA Identification	Metallic coating Galvalloy	Cleaner agent std=standard, f=fresh & (concentration %)	Pretreatment	Pretreatment weight (mg Ti or Cr/m^2)	Primer Code name	Primer Target DFT (µm)	Topcoat	Topcoat Target DFT (µm)	Gauge (mm)
KK-1	8ZM045	265 gm^{-2}	Novamax 187U (std)	NR6022 (Cr)	20-30	Coilprime HS	5	HPS200 Ultra - GWG	5	0.48
KK-2	8ZM073	265 gm^{-2}	Novamax 187U (std)	NR6022 (Cr)	20-30	Active B (Akzo)	5	HPS200 White - Active	5	0.58
KK-4	7ZM072	265 gm^{-2}	Novamax 187U (std)	G1455 (0Cr)	8-10	ANNP – IN7UD987	5	HPS200 Ultra	5	0.51
KK-5	7ZM080	265 gm^{-2}	Novamax 187U (std)	G1455 (0Cr)	8-10	BASF – CP71	5	HPS200 White	5	0.51
KK-6	7ZM082	265 gm^{-2}	Novamax 187U (std)	G1455 (0Cr)	8-10	ANNP – IN7UD987	5	HPS200 White	5	0.51
KK-7	7ZM083	265 gm^{-2}	Novamax 187U (std)	G1455 (0Cr)	8-10	BASF – CP71	5	HPS200 Ultra – GWG	5	0.49
KK-9*	9KR092	275 gm^{-2}	Novamax 187U (std)	NR6022 (Cr)	20-30	Coilprime HS	5	HPS200 Ultra	5	0.50

*Sample KK9 is MagiZinc metallic coating weight of 275g/m^2, remaining samples are Galvalloy metallic coating weight of 265g/m^2.

Novamax 187U is commercially available cleaner agent by Henkel, important constituents are sodium hydroxide and sodium xylenesulphonate.

Ridoline 1313 is commercially available cleaner agent by Henkel, important constituents are sodium hydroxide, magnesium nitrate and iron trinitrate nonahydrate.

S5117 is commercially available cleaner agent by Chemetakk, important constituents is sodium hydroxide.

NR6022 is commercially available pretreatment by Henkel, important constituents are dichromic tris(chromate) and chromium trioxide.

G1455 is commercially available pretreatment by Henkel, important constituents are dihydrogen hexafluorotitanate(2-) and phosphoric acid.

Coilprime HS is commercially available primer by BASF, important constituent is strontium chromate.

Active B is commercially available primer by Akzo Nobel, important constituent is strontium chromate.

BeckyPrim 246 is commercially available primer by Beckers, important constituent is hexavalent chromium inhibitor.

BeckyPrim 266 is commercially available primer by Beckers, important constituent is zinc phosphate.

ANNP-IN7UD987 is commercially available primer by Akzo Nobel, important constituents were unknown due to commercial sensitive reasoning.

BASF –CP71 is commercially available primer by BASF, important constituent are trizinc bis(orthophosphate) and a calcium ion exchange additive.

Table 5.2 Batch 2 Prisma System: cleaner and pretreatment (6-7 & 8-10 mg Ti/m^2) combinations

Sample Identification	TATA Identification	Metallic coating Galvalloy	Cleaner agent std=standard, f=fresh & (concentration %)	Pretreatment	Pretreatment weight (mg Ti or Cr/m^2)	Primer Code name	Primer Target DFT (µm)	Topcoat	Primer Target DFT (µm)	Gauge (mm)
KK-3	8ZM047	265 gm^{-2}	Novamax 187U (f)	NR6022(Cr)	20-30	BeckyPrim 246	25	Metallic silver (Prisma)	25	0.66
KK-8	7ZM079	265 gm^{-2}	Novamax 187U (f)	G1455 (0Cr)	8-10	BeckyPrim 266	25	Metallic silver (Prisma)	25	0.66
KK-11	2	255 gm^{-2}	Novamax 187U (f)	NR6022(Cr)	20-30	BeckyPrim 246	25	Metallic silver (Prisma)	25	~0.7
KK-12	3a	255 gm^{-2}	Novamax 187U (f)	G1455 (0Cr)	6-7	BeckyPrim 266	25	Metallic silver (Prisma)	25	~0.7
KK-13	3b	255 gm^{-2}	Novamax 187U (f)	G1455 (0Cr)	8-10	BeckyPrim 266	25	Metallic silver (Prisma)	25	~0.7
KK-14	5a	255 gm^{-2}	Ridoline 1313 (f)	G1455 (0Cr)	6-7	BeckyPrim 266	25	Metallic silver (Prisma)	25	~0.7
KK-15	5b	255 gm^{-2}	Ridoline 1313 (f)	G1455 (0Cr)	8-10	BeckyPrim 266	25	Metallic silver (Prisma)	25	~0.7

Table 5.3 Batch 3 BASF System: cleaner and pretreatment (6-7 & 8-10 mg Ti/m^2) combinations

Sample Identification	TATA Identification	Metallic coating Galvalloy	Cleaner agent std=standard, f=fresh & (concentration %)	Pretreatment	Pretreatment weight (mg Ti or Cr/m2)	Primer Code name	Primer Target DFT (µm)	Topcoat	Gauge (mm)
KK-16	7	255 gm^{-2}	Novamax 187U (f)	NR6022 (Cr)	20-30	Coilprime HS	5	HPS200 Ultra – GWG	~0.65
KK-17	8a	255 gm^{-2}	Novamax 187U (f)	G1455 (0Cr)	6-7	BASF – CP71	5	HPS200 Ultra – GWG	~0.65
KK-18	8b	255 gm^{-2}	Novamax 187U (f)	G1455 (0Cr)	8-10	BASF – CP71	5	HPS200 Ultra – GWG	~0.65
KK-19	9a	255 gm^{-2}	Novamax 187U (f)	G1455 (0Cr)	6-7	Modified – CP71	5	HPS200 Ultra – GWG	~0.65
KK-20	9b	255 gm^{-2}	Novamax 187U (f)	G1455 (0Cr)	8-10	Modified – CP71	5	HPS200 Ultra – GWG	~0.65
KK-21	11a	255 gm^{-2}	Ridoline 1313 (f)	G1455 (0Cr)	6-7	BASF – CP71	5	HPS200 Ultra – GWG	~0.65
KK-22	11b	255 gm^{-2}	Ridoline 1313 (f)	G1455 (0Cr)	8-10	BASF – CP71	5	HPS200 Ultra – GWG	~0.65
KK-23	12a	255 gm^{-2}	Ridoline 1313 (f)	G1455 (0Cr)	6-7	Modified – CP71	5	HPS200 Ultra – GWG	~0.65
KK-24	12b	255 gm^{-2}	Ridoline 1313 (f)	G1455 (0Cr)	8-10	Modified – CP71	5	HPS200 Ultra – GWG	~0.65

Table 5.4 Batch 4 Prisma System: cleaner and pretreatment (8-10 & 15-20 mg Ti/m^2) combinations

Sample Identification	TATA Identification	Metallic coating Galvalloy	Cleaner agent std=standard, f=fresh & (concentration %)	Pretreatment	Pretreatment weight (mg Ti or Cr/m^2)	Primer Code name	Primer Target DFT (µm)	Topcoat	Gauge (mm)
KK-27	Ref3	255 gm^{-2}	Novamax 187U (2%)	NR6022 (Cr)	20-30	BeckyPrim 266	25	Metallic silver (Prisma)	~0.64
KK-28	1	255 gm^{-2}	Novamax 187U (2%)	G1455 (0Cr)	8-10	BeckyPrim 266	25	Metallic silver (Prisma)	~0.53
KK-29	2	255 gm^{-2}	Novamax 187U (2%)	G1455 (0Cr)	15-20	BeckyPrim 266	25	Metallic silver (Prisma)	~.51
KK-30	3	255 gm^{-2}	S5117* (1.8-2.5%)	TP10475 (0Cr)	8-10	BeckyPrim 266	25	Metallic silver (Prisma)	~.51
KK-31	4	255 gm^{-2}	S5117* (1.8-2.5%)	TP10475 (0Cr)	15-20	BeckyPrim 266	25	Metallic silver (Prisma)	~.51

Table 5.5 Batch 5 BASF System: cleaner and pretreatment (8-10 & 15-20 mg Ti/m^2) combinations

Sample Identification	TATA Identification	Metallic coating Galvalloy	Cleaner agent std=standard, f=fresh & (concentration %)	Pretreatment	Pretreatment weight (mg Ti or Cr/m^2)	Primer Code name	Primer Target DFT (µm)	Topcoat	Gauge (mm)
KK-25	Ref1	255 gm^{-2}	Novamax 187U (2%)	NR6022 (Cr)	20-30	Coilprime HS	5	HPS200 Ultra – GWG	~0.64
KK-26	Ref2	255 gm^{-2}	Novamax 187U (2%)	NR6022 (Cr)	20-30	Coilprime HS	5	HPS200 Ultra – GWG	~0.64
KK-32	5	255 gm-2	Novamax 187U (2%)	G1455 (0Cr)	8-10	BASF – CP71	5	HPS200 Ultra – GWG	~.51
KK-33	6	255 gm-2	Novamax 187U (2%)	G1455 (0Cr)	15-20	BASF – CP71	5	HPS200 Ultra – GWG	~.51
KK-34	7	255 gm-2	S5117* (1.8-2.5%)	TP10475 (0Cr)	8-10	BASF – CP71	5	HPS200 Ultra – GWG	~.51
KK-35	8	255 gm-2	S5117* (1.8-2.5%)	TP10475 (0Cr)	15-20	BASF – CP71	5	HPS200 Ultra – GWG	~.51

The SVET software records each of the scans as grid files containing the SVET measured potential values in nV. All of scanned grid files containing the measured potentials were converted into values of Am^{-2} via the application of the calibration factor. Calibration factors were determined for each experiment and used for the conversion of the corresponding scan grid files. The calibrated data was imported into Golden Software Surfer 10 allowing each of the calibrated grid files to be displayed as false colour SVET iso-current contour maps. These maps clearly identify areas of anodic (red) and cathodic (blue) activities. Anodic regions where metal is oxidised recorded as areas of positive current density whereas cathodic sites registered negative current densities by the use of correctly configured and calibrated SVET. Representative iso-contour maps for scans of a chrome free system sample comprise of maps after every 4hours of immersion in $0.1\%NaCl_{(aq)}$ over a period of 24hours experiment are shown in figure 5.1.1.

The zinc – aluminium organically coated steel coupons tested all exhibited localised zinc dissolution. In these cases of cut edge SVET experiments it was clearly evident that the iron accommodated the cathodic regions where oxygen reduction occurs and the anodic areas were confined to the alloying layer. The anodic activity was seen from typical SVET iso-current maps (figure 5.1) to be situated at the immediate edges of the cathodic activity signifying the alloying layer providing the sacrificial protection of the steel substrate at the cut-edge. The alloy layer consists of primary phase zinc in form of zinc rich dendrites surrounded by zinc-aluminium lamellar. Microscopy work and literature [4-6] confirmed the anodic activity occurred in the primary zinc rich phase, figure 5.1.2 illustrates the area of localised anodic events in the alloy layer.

The SVET calibrated data was further exploited to gain an understanding of anodic events that occurred during the period of the experiment via the hourly logged grid files. Anodes possessing an intensity greater than 1 A m^{-2} were considered and tracked for intensity over the duration of the 24 hour scan. The data was also processed to provide a semi-quantitative assessment of metal loss for the specimens following the method outlined in chapter 2.

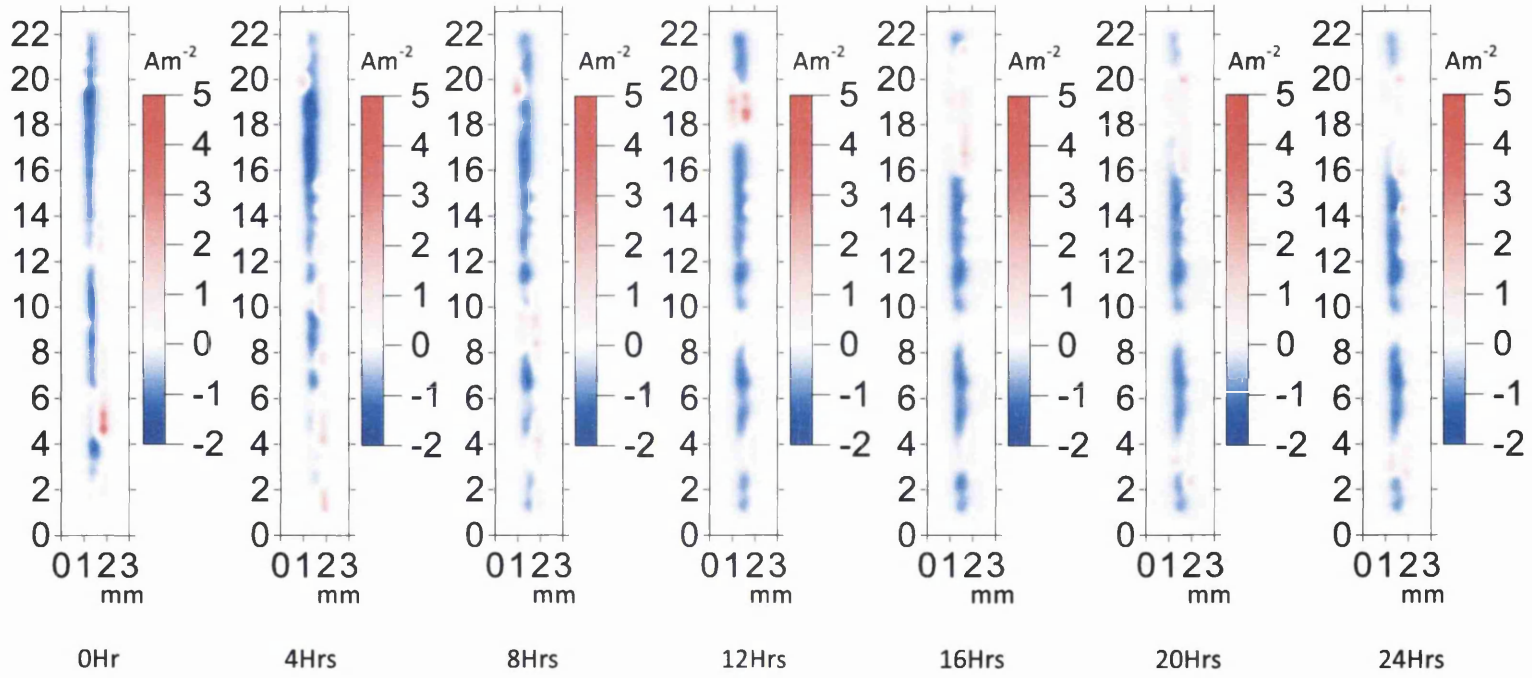

Figure 5.1.1 SVET iso-current contour maps of a cut edge specimen tested for 24 hours in 0.1%$NaCl_{(aq)}$ showing cathodic activity on the steel substrate (blue) with anodic activity (red) localised to the Zinc alloy coating

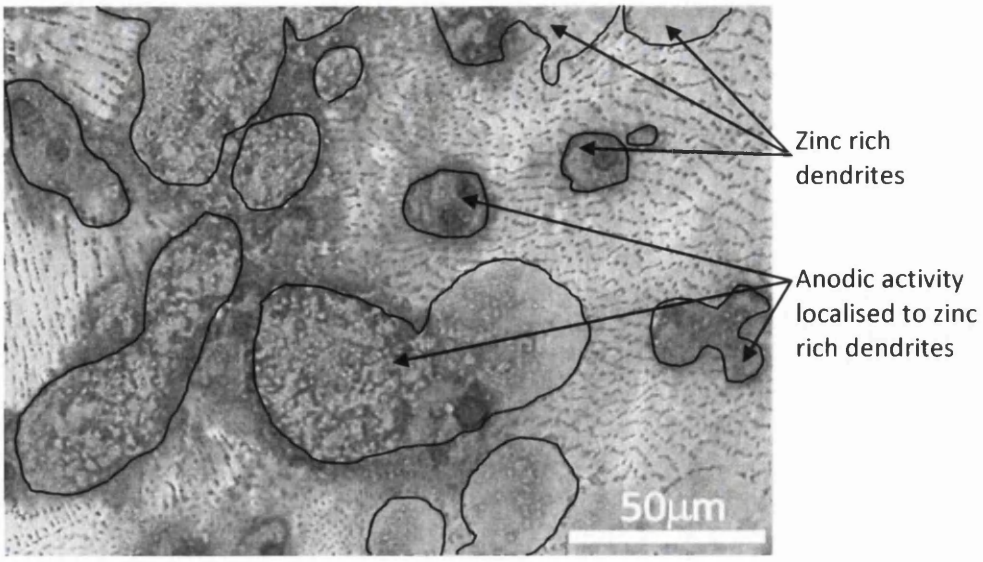

Figure 5.1.2 Localised anodic events on the zinc rich dendrites within the alloy coating.

5.2 SVET - Anodic activity analysis and Semi-quantitative mass loss assessment

5.2.1 Batch 1 2007 chromate free trial samples (as runoff tested in chapter 4)

Batch 1 materials (shown in table 5.1) comprised of chromated reference samples and chromate free OCS systems from a 2007 production trial. The SVET scanned a defined grid above the cut edges hourly over a 24 hour period. The anode activity for the duration of the experiment was examined for each of the samples is summarised in figure 5.2.1. A distinct trend was observed in the anode activity time, most anodes were predominantly active for 0-6 hours, fewer were active between 6-12 hours and a smaller number again for 12-18 hours. This anodic behaviour was evident in all the samples however the critical difference is the number of anodes that were active for the duration of experiment i.e. 18-24 hours. It is not desirable to have anodes that are active for the duration of the experiment due to the pitting or crevice like corrosion effect at the continuously active anodic sites. These long lived anodes also tend to have the highest intensities in terms of current density over their lifetime making them even more damaging to the material.

The chromate containing reference samples, KK-1 and KK-2, showed 13% and 19% respectively of the anodes being active for 18-24 hours. The chromate containing MagiZinc sample KK-9 had the desired minimum anodic activity after 18 hours. All the samples exhibited a large number of short lived anodes which can be acceptable if their current density intensities are low as corrosion products are formed which result in anodic site being neutralised or cause hindrances to further corrosion activity at that site. All of the chromate free systems had lower long lived anodic activity than the reference sample of

which the particular systems that performed the best were KK-6 and KK-7 having 8% and 5% of long lived anodic events. Overall, the chromate free samples seem to have higher peak intensities over the reference samples which may indicate a reason for the higher Zn loss measured for these systems compared with reference KK1.

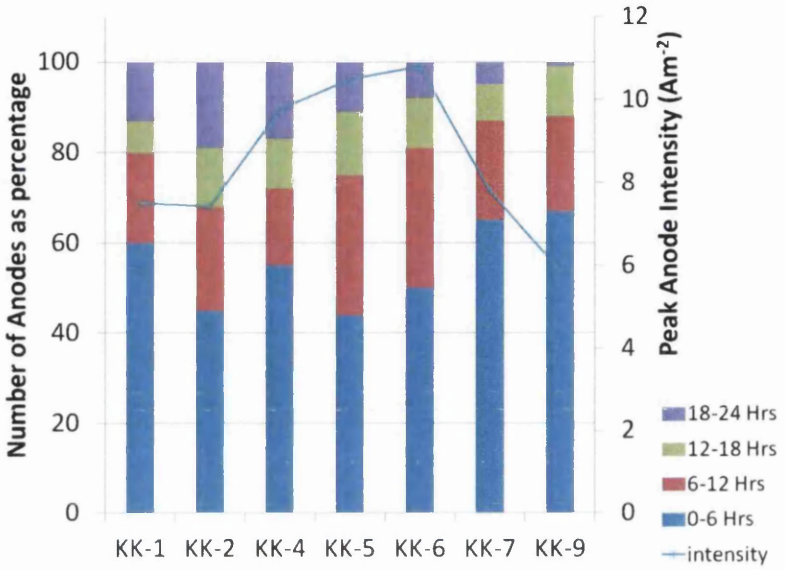

Figure 5.2.1 Percentage of anode life time plot and average anode peak intensity for sample in table 5.1.

The average total zinc loss measured over the scan area of 3mm x ~20mm using the SVET microtip and converted to units of mg m^{-1} of cutedge for each of the material listed in table 5.1 is displayed in figure 5.2.2. The performance of these materials can easily be assessed and ranked with respect to metal loss. Current production line samples (KK1 and KK2) were used as references setting the standard for chrome free systems to be compared against. Samples listed in table 5.1 were obtained from Corus Colors UK trials in 2007 (now Tata Steel Europe Colors. The SVET measured Zn metal loss data displayed in figure 5.2 showed that the chromate containing reference sample KK-1 being 4.9 mg m^{-1} and KK-2 having 8.1 mg m^{-1}. The chromate free systems KK-4 having Zn loss of 9.7 mg m^{-1} and KK-5 having 12 mg m^{-1} were significantly higher than the reference samples. However Systems KK-6 and KK-7 had an estimated total zinc loss of 6.14 mg m^{-1} and 6.05 mg m^{-1} respectively. These chromate free systems showed comparable performance to the reference chromate samples. Sample KK-9 tested was a new Zinc-aluminium-Magesium alloy (Magizinc) with chromate based coating also showing a comparable performance to the reference samples, where observed Zn loss was 5.8 mg m^{-1}.

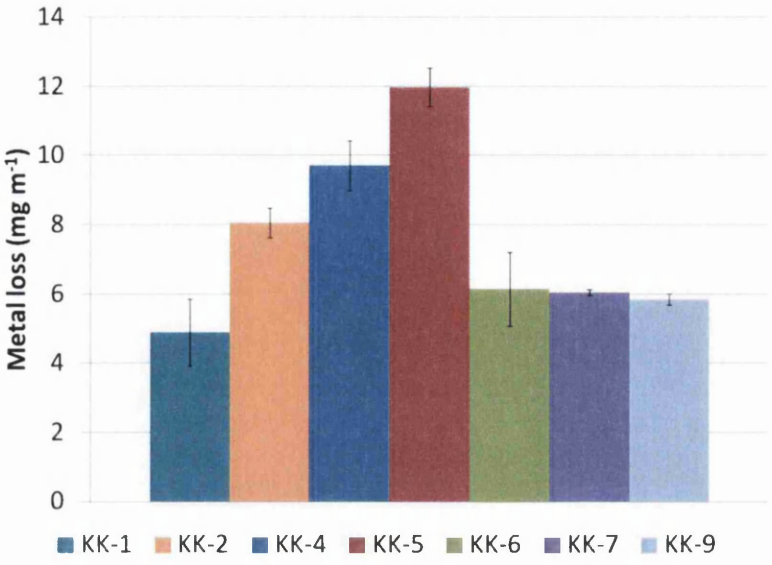

Figure 5.2.2 SVET calculated metal loss for Batch 1 samples in table 5.1.

It is interesting as to why the chromate free samples KK-6 and KK-7 outperform the other two Cr free samples KK-4 and KK-5. The reason may be due to the combinations of primer and top-coat used for these systems (pre-treatment and cleaner was the same for all four samples). KK-4 and KK-5 have primers and top-coats matched from different paint suppliers i.e. an Akzo Nobel primer with a BASF top-coat and vice versa whereas KK-6 and KK-7 have matching primers and top-coats i.e. Akzo Nobel primer and top-coat and BASF primer and top-coat. These data therefore suggest that mismatching primers and top-coats in these chromate free systems may have an effect on the cut-edge corrosion resistance and that a synergy exists when the primer and top-coat are sourced from the same manufacturer. These differences could be due to adhesion effects causing electrolyte ingress into the OCS layers or allowing small crevices to form that may then accelerate the cut-edge corrosion.

5.2.2 Batch 2 Prisma System: cleaner and pretreatment (6-7 & 8-10 mg Ti/m^2) combinations

Assessment of SVET data for samples tested in table 5.2 Becker's Prisma system. The main differences between the samples within this batch were the cleaner agents used, Novamax 187U and Ridoline 1313, and chromate free pretreatment weights 6-7 mg Ti/m^2 and 8-10 mg Ti/m^2. Distinct trends were observed for anode activity where most anodes were predominantly active for 0-6 hours, fewer were active between 6-12 hours and a lower count was recorded between 12-18 hours. This anodic behaviour was evident for all samples in this batch however the critical difference was the number of anodes that were active for the duration of the experiment i.e. 18-24 hours, see figure 5.2.3.

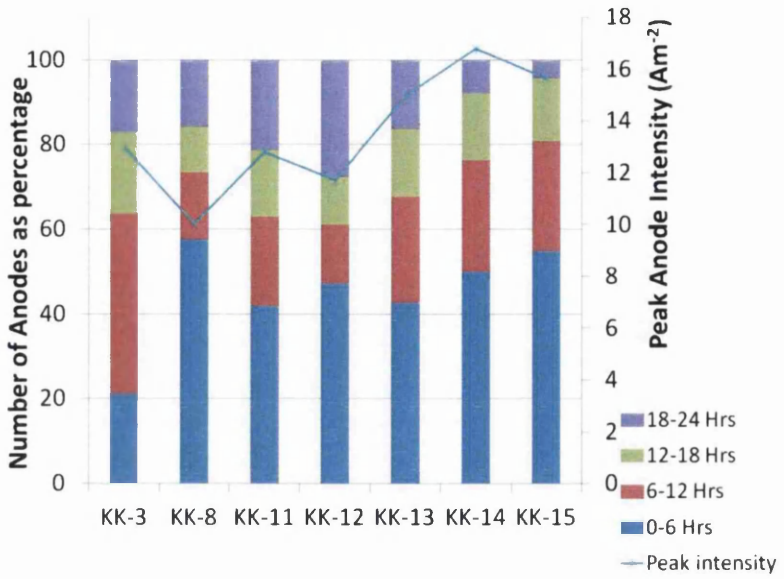

Figure 5.2.3 Percentage of Anode life time plot and average anode peak intensity for Prisma systems 6-10mg Ti/m^2.

The sample KK-8 displayed the desired anodic activity, where a larger percentage of anodes were observed initially between 0-6 hours and subsequently much reduced anode numbers were apparent. The respective peak intensity value was relatively low 10 Am^{-2}. The reference sample, KK-3, from 2007 production line displayed a relatively larger percentage of active anodes between 6-12 hours. Samples KK-3 and KK-8 both exhibited similar number of long lived anodes for the duration of the experiment, 17% and 16% respectively. The observed peak intensity for KK-3 was recorded to be 13 Am^{-2}. The Tata Steel lab prepared reference sample KK-11 displayed a marginally increased anodic activity for the 18-24 hours duration, 21%. The remaining samples all showed reduced count of long lived anodes with the exception of sample KK-12. Industrial cleaning agent Novamax 187U had been used in preparing samples KK-12 and KK-13; whereas samples KK-14 and KK-15 had been treated with cleaning agent Ridoline 1313. A marked reduction in the long lived anodic activity was observed for samples that had been treated with cleaning agent Ridoline 1313. However with the observed reduction of the percentage of anodic activity in the 18-24 hours resulted in higher values recorded for the average peak intensity. In addition the pretreatment weight does influence the anodic activity detected. Samples KK-12 and KK-14 were both applied with pretreatment containing titanium dioxide (TiO_2) having a target coating weight of 6-7 mg m^{-2}; whereas sample KK-13 and KK-15 were applied with TiO_2 pretreatment target coating weight of 8-10 mg m^{-2}. Samples comprised of a higher pretreatment coating weight KK-13 and KK-15 exhibited a lower percentage of

anodes that were active for 18-24 hours. The observed reduction in the number of anodes active for 18-24 hours was half of that realised by equivalent samples but with a lower pretreatment coating weight 6-7 mg m^{-2}.

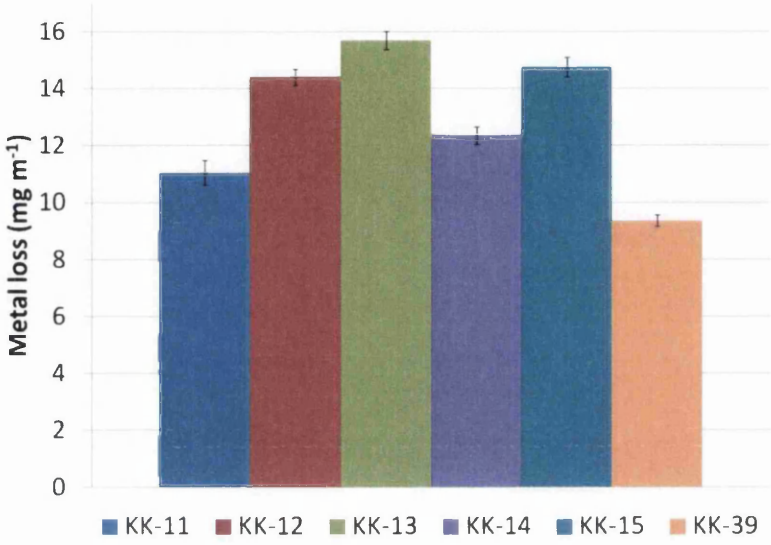

Figure 5.2.4 SVET calculated metal loss for samples in table 5.2.

The SVET derived total zinc loss for samples in table 5.2 are shown in figure 5.2.4, where KK-11 is the reference sample lab prepared by Tata Steel Europe and KK-39 is current production line material (2011), both samples were chromate containing. The total zinc loss figures for KK-11 and KK-39 were 11.0 and 9.4 mg m^{-1} respectively. The remaining samples all showed a greater total zinc loss figure implying a relatively inferior corrosion inhibiting characteristics. A trend was apparent from the total zinc loss data, which was systems that contained a lower pretreatment coating weight of 6-7 mg Ti/m^2 performed marginally better than systems with pretreatment weight of 8-10 mg Ti/m^2. In addition samples KK-14 and KK-15 treated with cleaning agent Ridoline 1313 had comparatively lower total zinc loss figures than the samples KK-12 and KK-13 which had been treated cleaning agent Novamax 187U implying a synergy that may exist between the cleaning agent Ridoline 1313, pretreatment G1455, BeckyPrim 266 primer and Prisma metallic silver topcoat. In the application of organic coating layers to steels adhesion is critical in maintaining the lifetime of the product and thus the cleaning prior to coating application is critical. These data suggest that the Ridoline 1313 cleaner prepared the surface more efficiently for suitable adhesion of the subsequent Becker's coating layers. Loss of adhesion of the coatings can cause electrolyte ingress and focussed crevice corrosion of metallic coatings where adhesion has been lost.

5.2.3 Batch 3 BASF System: cleaner and pretreatment (6-7 & 8-10 mg Ti/m^2) combinations

Anodic behaviour was observed for samples listed in table 5.3. These samples were prepared by Tata Steel Europe laboratories however the final topcoat was applied at Swansea University laboratories. The topcoat was applied as guided by BASF consultant but proved to be a challenging task resulting in topcoat delamination poor uniformity in coating thickness. This is reflected in the SVET anode analysis were the results were inconclusive, figure 5.2.5. There was no real trend observed other than they all exhibited relatively larger percentage of anodic activity during the initial 0-6 hours.

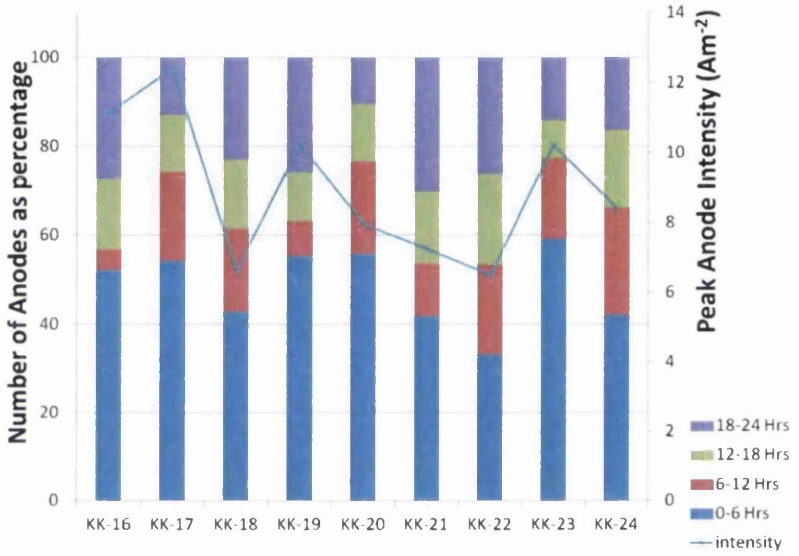

Figure 5.2.5 Percentage of Anode life time plot and average anode peak intensity for BASF systems 6-10mg Ti/m^2.

The total zinc loss data for samples in table 5.3 are shown in figure 5.2.6. The poor adhesion of topcoat resulted in incoherent data. However from the samples tested majority of the samples that had been treated with Riodline 1313 did show marginally higher metal loss suggesting inferior corrosion inhibition by the coating system. This may be due to inadequate synergistic effects between the Ridoline 1313 and remaining constituents of the BASF coating system.

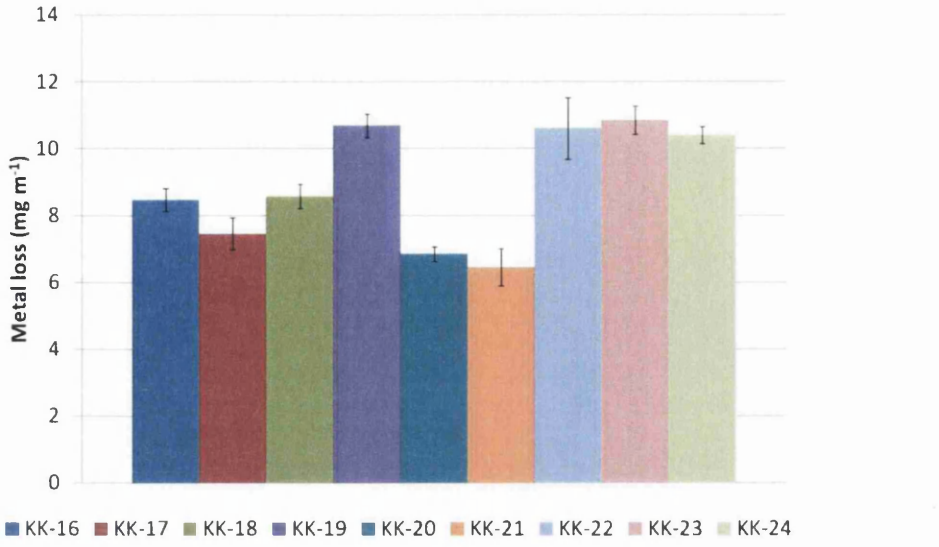

Figure 5.2.6 SVET calculated metal loss for samples in table 5.3.

5.2.4 Batch 4 Prisma System: cleaner and pretreatment (8-10 & 15-20 mg Ti/m^2) combinations

The batch of Becker's Prisma coating systems listed samples in table 5.4 were subjected to SVET testing. The anodic behaviour was observed and anode life time measured, figure 5.2.7. Reference sample KK-27, exhibited the highest level of short lived anodes 47% which is favoured over large number of long lived anodes. Samples KK-28 and KK-29 were treated with cleaning agent Novamax 187U and applied with low levels of pretreatment (G1455) weight followed by the Becker's primer and topcoat. KK-28 displayed the highest levels of long lived anodic activity. KK-29 had been applied with greater pretreatment weight 15-20 mg Ti/m^2 than 8-10 mg Ti/m^2 pretreatment applied to KK-28, the effects of which were apparent in the levels of long lived anodic activity. KK-28 demonstrated 33% of anodic activity in the 18-24hours period where as KK-29 showed levels of 18%. Samples KK-30 and KK-31 were treated with Chemetall's cleaning agent S5118 and applied with two levels of pretreatment (G1455) 8-10 mg Ti/m^2 and 15-20 mg Ti/m^2 weight respectively followed by the Becker's primer and topcoat. The 18-24 hours of anodic activity for KK-30 was recorded to be 21% and 5% for KK-31. The higher pretreatment weights seem to have the desired effect of retarding the number of long lived anodes. Similarly the application of cleaning agent S5118 when used in conjunction with the G1455 pretreatment and the Becker's Prisma primer and topcoat resulted in the improvement of reduced anodic activity in the 18-24hours period.

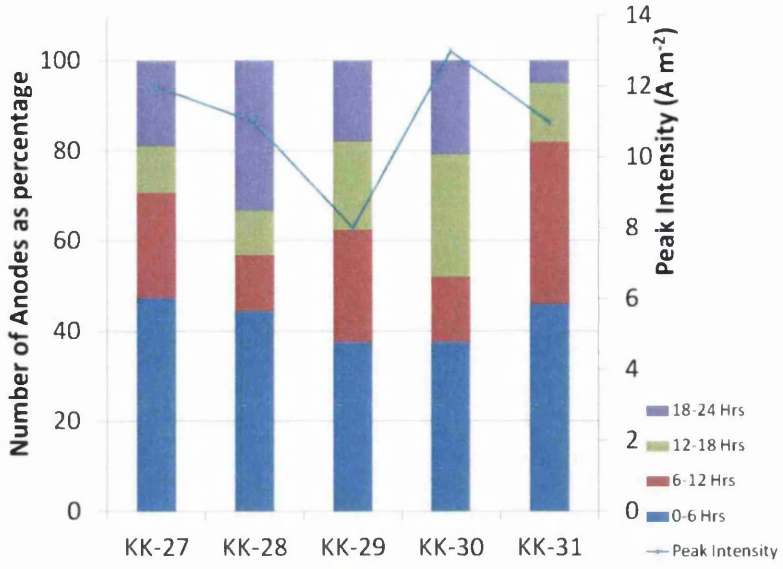

Figure 5.2.7 Percentage of Anode life time plot and average anode peak intensity for Prisma systems 8-20mg Ti/m^2.

The average total zinc loss for samples in table 5.4 is shown in figure 5.2.8. Reference sample KK-27 showed metal loss of 8.44 mg m^{-1}. For samples that had a higher 15-20 mg Ti/m^2 pretreatment coating weight demonstrated lower metal loss figure than their counterpart specimens within this batch. Implying improved corrosion inhibition provided by the zinc phosphates contained within the pretreatment. Zinc phosphates tend to be sparingly soluble in an aqueous environment and yield improved bonding to the applied substrate. Subsequently the primer and topcoat applied benefit from improved adherence to the substrate. However there were two different combinations of cleaner agent and pretreatments compared samples KK-28 and KK-29 had been applied with Novamax 187U and G1455 whereas samples KK-30 and KK-31 applied with S5118 and the TP10475. The metal loss figures recorded for samples KK-28 and KK-29 were lower than those measured for KK-30 and KK-31 implying that the combination of Novamax 187U and G1455 with the Becker's Prisma coating system has enhanced corrosion inhibition than that of S5118 and TP10475. The Henkel's cleaner agent Novamax 187U, the chemical constituents are sodium hydroxide and sodium xylenesulphonate. This cleaner solution is commercially used in dilute form typical concentration of ~2.5% (volume). Novamax 187U is particularly good in degreasing of the substrate. The application of the cleaning agent is via jets which lends itself to mechanical removal of some of the loose oxides on the surface, thus providing a relatively clean surface for pretreatment application. The pretreatment Henkel's G1455 bonds extremely well to the treated substrate surface. The Becker's Prisma system when

used in combination with Chemetall's cleaner agent S5118 and pretreatment TP10475 is lacking the synergistic inhibition effects seen with the Henkel's Novamax 187U and G1455.

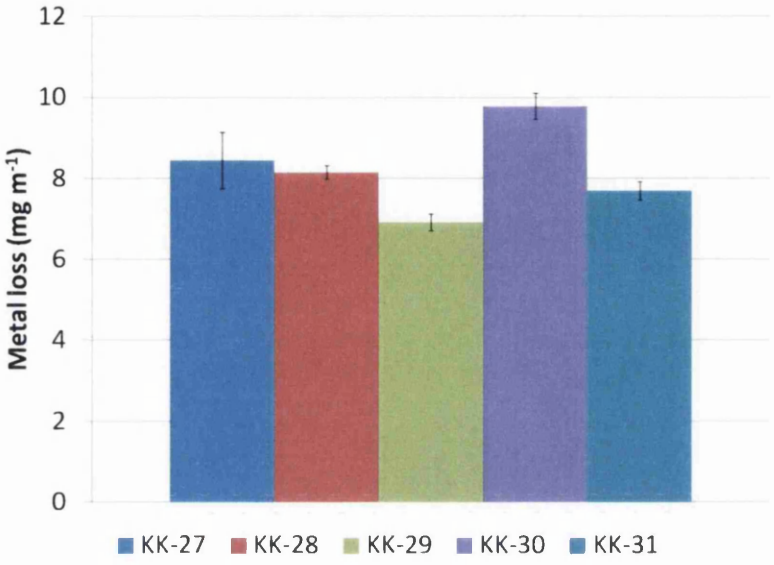

Figure 5.2.8 SVET calculated metal loss for samples in table 5.4.

5.2.5 Batch 5 BASF System: cleaner and pretreatment (8-10 & 15-20 mg Ti/m^2) combinations

Anode activity plots for samples listed in table 5.5 are shown in figure 5.2.9. The reference sample KK-25 is production line material and KK-26 is reference sample prepared at Tata Steel Europe laboratories. Both the reference samples exhibited similar anodic behaviours with a noticeable difference of measured peak anodic intensity, KK-25 exhibited an anodic peak intensity of 13A m^{-2} whereby KK-26 showed a lower anodic peak intensity of 8A m^{-2}. Samples KK-25 and KK-26 showed values of 16% and 12% of anodic activity for the duration of 18-24hours. All the chrome free systems tested within this batch showed greater percentage of anodic activity for the duration of 18-24 hours than the reference samples with the exception of KK-32 that had 14% active anodes for the duration of the experiment.

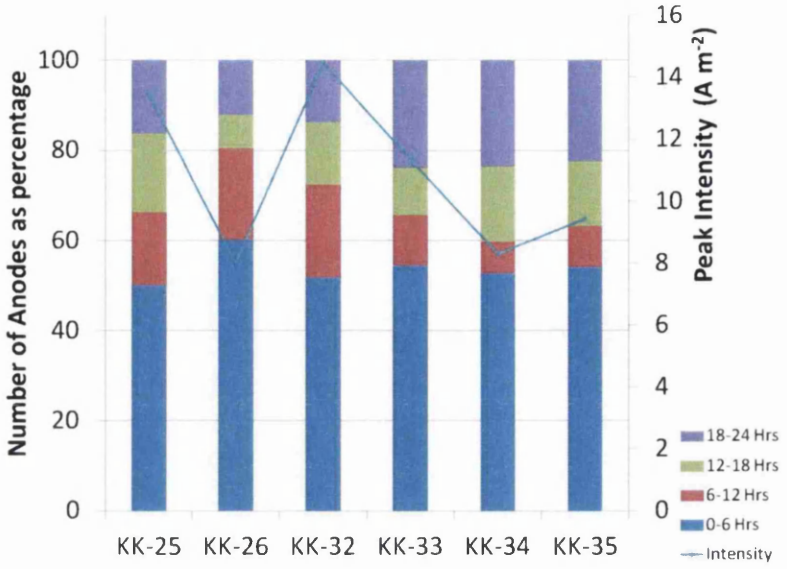

Figure 5.2.9 Percentage of Anode life time plot and average anode peak intensity for BASF systems 8-20mg Ti/m^2.

The SVET derived metal loss for the samples in table 5.5 are shown in figure 5.3.0. The reference samples KK-25 and KK-26 both showed the lowest metal loss 6.0mg m^{-1} and 6.8mg m^{-1} respectively. The chromate free samples all exhibited greater metal loss than the reference samples. Considering the pretreatment weight and metal loss figures it was clear that BASF coating system had enhanced corrosion inhibition with a lower 8-10mg Ti/m^2 pretreatment weight than the 15-20 mg Ti/m^2. The higher pretreatment weight resulted in greater metal loss than the lower pretreatment by a factor of 1.2. Samples KK-34 and KK-35 treated with Chemetall's cleaner agent S5118 followed by the application of Chemetall's pretreatment TP10457 exhibited lower metal loss figures than Henkel's system. The BASF's coating system when used in combination with Henkel's Novamax 187U and G1455 is lacking the synergistic inhibition effects seen with the Chemetall's cleaner agent S5118 and pretreatment TP10475.

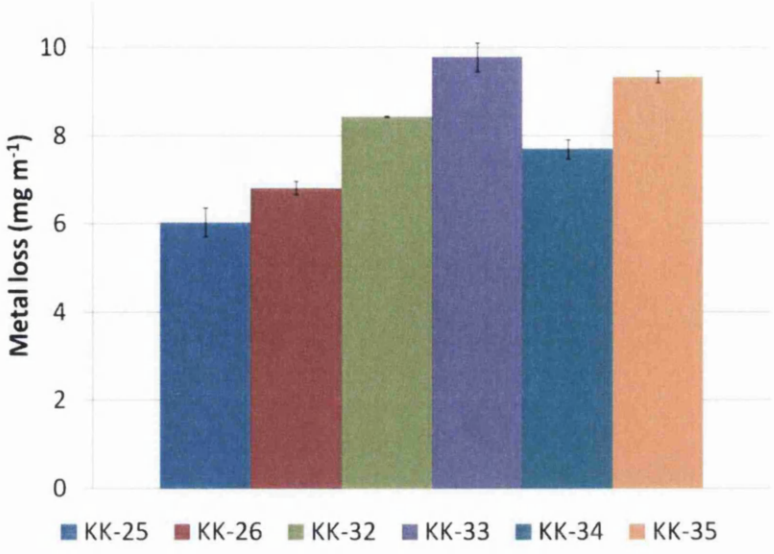

Figure 5.3.0 SVET calculated metal loss for samples in table 5.5

5.3 Comparison of SVET zinc loss data with zinc runoff data.

Seven organically coated galvanised steel samples plus a blank to assess the background levels of metallic ions in the environment have been exposed at the Swansea University roof top as described in section 2.2 and discussed in chapter 4. This site can be classified as marine due to the proximity to the Swansea bay. The summary of materials open to the elements of natural weathering are listed in table 5.1. Rain water runoff has been collected on a monthly basis from each sample in vessels over a period of 18 months, analysed for metal ions using ICP-MS and runoff data as has been compared to the predicted metal loss from 24 hour SVET experiments.

Outdoor exposure is extremely important in characterising materials corrosion performance, more rapid testing combined with mechanistic and kinetic determination is desirable. The SVET employed in this investigation has been shown to give relatively reproducible and semi-quantitative assessments of corrosion in 24 hours. The outdoor zinc runoff data for the samples described in table 5.1 has been compared with the zinc loss predicted by the SVET for such materials in 0.1% $NaCl_{(aq)}$ after 24 hours immersion. The cumulative outdoor runoff data after 2,7 and 18 months and the SVET derived Zn loss is compared in figure 5.3.1. Establishing a relationship between the SVET derived zinc loss data and outdoor runoff data is difficult, however some similarities in the overall systems performance can be seen to agree. The 24 hour SVET test provides an indication of runoff obtained after 7 months external weathering. The differences observed are mostly due to the electrolyte used. In the SVET experiments 0.1% $NaCl_{(aq)}$ solution is utilised which is

significantly different to external rainfall. The outdoor samples experience wet and dry periods and the formation of passivation films which is more limited in the saline solution. However the use of a very simple electrolyte 0.1% $NaCl_{(aq)}$ and any association between SVET derived zinc loss and outdoor runoff data is promising and provides a scope for development of this rapid test for evaluating longer-term material performance.

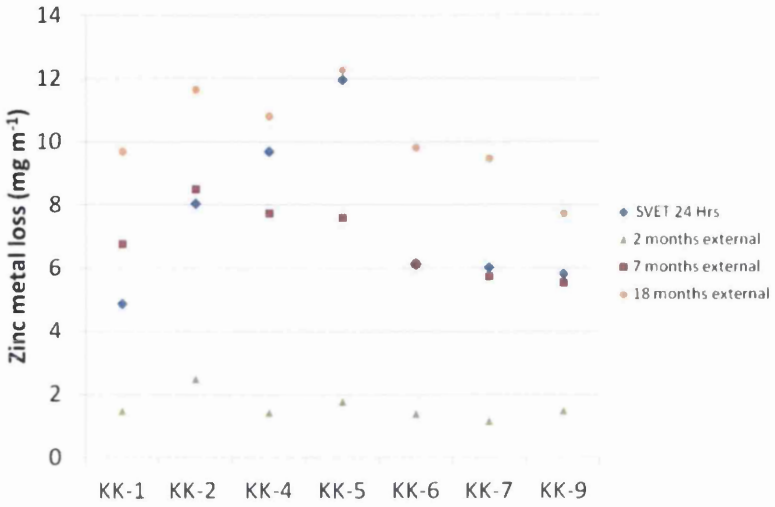

Figure 5.3.1 Comparison of SVET derived Zn loss and outdoor runoff data

5.4 Conclusions

The SVET has been used to assess the corrosion mechanisms and comparative performance of organically coated galvanised steels in 0.1% $NaCl_{(aq)}$ electrolyte with hourly scans over a period of 24Hrs.

The SVET generated data was used to produce isocurrent maps over the exposure period of 24 hours for each of the materials. Such maps highlight areas of anodic and cathodic activity over the cutedge surface allowing mechanism of corrosion to be assessed over time.

The OCS materials all show localised corrosion behaviour and the trends observed with respect to their corrosion performance were similar to those seen by both the accelerated runoff experiment and outdoor weathering. The anode analysis and a semi-quantitative analysis of zinc loss combined provided a valuable means of assessing the corrosion performance of the test samples. Anode analysis confirms that majority of the anodic activity during the SVET experiment approximately occurs in the initial 6 hours after which a combination of the corrosion products and inhibitor interaction hinders further corrosion. Also the number of anodes that remain active for the duration of experiment affect the

peak anodic current intensity; simply more anodes reduces the peak anodic current intensity and vice versa. SVET work has highlighted the synergistic effect between the primer and topcoat in corrosion prevention by either or both inhibitor release and straightforward barrier protection.

It has also become apparent from SVET study that Becker's Prisma paint system performs better with regards to corrosion inhibition when applied to substrates that have been treated with Henkel's Ridoline 1313 and Henkel's pretreatment Henkel's Bondrite G1455 coating weight of 8-10mg m^{-2}. Becker's Prisma systems that had been treated with Henkel's Novamax 187U performed relatively better than those treated with Chemetal's S5118 cleaning agent. When considering the pretreatment weight effects for Beckers system with regards corrosion performance the higher pretreatment coating weight 15-20mg m^{-2} than 8-10mg m^{-2} proved to be marginally more effective in corrosion inhibition.

The SVET data for samples prepared with BASF's paint system revealed that samples that had been treated with Henkel's Novamax 187U cleaning agent showed improved corrosion performance than samples treated with Chemetall's S5118 cleaning agent. Also, samples that had Chemetall's pretreatment TP10475 performed marginally better in corrosion inhibition than the Henkel's Bondrite G1455. The pretreatment weight effects upon corrosion inhibition were also examined via the SVET and revealed slight improvement in corrosion performance with higher pretreatment weight 15-20 mg m^{-2} than 8-10 mg m^{-2} pretreatment coating weight. Comparative study of Ridoline 1313 and Novamax as well as two levels of pretreatment weights 6-7 and 8-10mg m^{-2} results were inconclusive.

Considering chromate and chrome free systems i.e. 2007 trial, the chrome free systems did show comparable levels of corrosion protection to the chromate systems, with the correct match of organic coatings. However from other trials it seems that the chrome free systems are considerably more sensitive to other coatings present within the system; whereas chromate systems appear to perform well and are more tolerant to other coatings within the systems. These findings suggest that perhaps chrome free systems have a narrower set of chemical conditions in which the inhibition is active whereas chromate systems are more versatile.

5.4 References

(1) Worsley, D. A.; MucMurray, H. N. Research in Chemical Kinetics 1997, 4, 149-202.
(2) Worsley, D. A.; Williams, D.; Ling, J. S. G. Corrosion Science 2001, 43, 2335-2348.
(3) McMurray, H. N.; Powell, S. M.; Worsley, D. A. Br. Corros. J. 2001, 36, 42-48.
(4) Elvins, J.; Spittle, J. A.; Worsley, D. A. Corrosion Science 2005, 47, 2740-2759.
(5) Elvins, J.; Sullivan, J. H.; Spittle, J. A.; Worsley, D. A. Corrosion Engineering, Science and Technology 2005, 40, 43-50.
(6) Challis, M.; Worsley, D. A. Br. Corros. J. 2001; 36, 297-303.

Chapter 6

Corrosion of pure Zinc in aqueous saline solutions

6.0 Introduction

Currently the widespread use of zinc and its alloys for protection of steel is due to the ability of Zn to galvanically protect steel. Zinc in galvanised hot dip steel is common with applications as roofs, fences, tubes, facades for buildings. As a consequence there is a need to better understand the principles of Zn corrosion allowing effective design and development of future corrosion resistant alloys, inhibitors and protective coatings. In addition, an improved knowledge of Zn self corrosion is critical to improve the efficiency of the sacrificial anodes for cathodic protection. A substantial body of literature concerning the corrosion of Zn materials exists [1-5]. Zinc dissolves in aqueous solution by means of an electrochemical reaction with water most likely producing zinc hydroxide. The zinc hydroxide is believed to form nearly over the whole exposed surface providing a protective film. At certain points the metal seems to remain uncovered and local attack continues, resulting in pitting [1]. It is widely accepted that the presence of aggressive aqueous species, such as chloride ions, causes rapid breakdown of the partially protective surface. In this work, scanning vibrating electrode technique (SVET) has been used to map changes in local electrochemical activity over commercial-purity zinc samples (99.99% purity) freely corroding in $NaCl_{(aq)}$ electrolyte. The aim of this section is to characterise any observed localised corrosion phenomena and to determine a correlation between the corrosion rate and morphology for zinc in different $NaCl_{(aq)}$ electrolyte concentrations.

6.1 SVET resolved Zinc surface corrosion

SVET analysis, the corrosion events occurring on the surface of Zn are defined as two specific regions, anodic where zinc dissolution occurs and cathodic where oxygen reduction transpires. The circuit in this electrochemical reaction between the anodic events is completed by electronic conduction through the bulk metal. Zn possesses sufficiently high electronic conductivity that any charge generated will dissipate over the entire metal surface, making it effectively a plane of constant potential. Conversely the conductivity of the electrolyte $NaCl_{(aq)}$ solution is several orders of magnitude lower than that of the metal. Consequently the passage of ionic current through the electrolyte generates potential gradients, with lines of iso-potential laying normal to the lines of current flux in solution. The SVET functions by registering the vertical component of current flux to the corroding surface. A positive potential depicts area of anodic occupancy and hence a negative potential represents cathodic activity.

Repetitive SVET scanning of the Zn surface helped resolve and visualise the time dependent changes in local corrosion current density patterns. Surface current maps/plots of current density derived from the SVET are shown in figures 6.1, 6.2, 6.3 & 6.4. In these plots the red colour represents areas of anodic activity and blue representing the areas of cathodic activity. It is believed that upon immersion in $NaCl_{(aq)}$ solution electrolyte, an imperfect film of zinc (hydr)oxide is formed on the exposed Zn surface, where Zn^{2+} ions formed by the anodic dissolution of zinc via reaction 6.1. A second region covers the remaining area that is considered to correspond to the cathodic area where reduction of dissolved oxygen occurs via reaction 6.2.

$$Zn_{(s)} \rightarrow Zn^{2+}_{(aq)} + 2e^{-} \quad (6.1)$$

$$2H_2O_{(l)} + O_{2(g)} + 4e^{-} \rightarrow 4OH^{-}_{(aq)} \quad (6.2)$$

In solution of high concentrations of 1.0% (wt) $NaCl_{(aq)}$ saline electrolyte it is evident that the localised corrosion plays a role in the growth of a surface hydroxide film where a distributed anode appears to be galvanically coupled with large areas of cathodic activity, figure 6.1. At time t=0 upon immersion the recorded peak current density of the anodic regions was $22.5Am^{-2}$ and the peak cathodic current density $-1.1Am^{-2}$. In contrast to the magnitude of the measured anodic peak current density the cathodic peak current density is considerably lower this can be explained by larger region on the Zn surface that supports the cathodic reaction and fewer anodic regions exist. The SVET may also fail to detect dispersed cathodic activity due to low intensity and therefore current loops will not pass through the plane of scan. The proximity of the cathodic and anodic events are relatively vast and the anodes that do exist are relatively widespread resulting in shallower pitting. With passage of time the small cluster of anodes show an incremental increase to maximum of $63Am^{-2}$ and the overall cathodic current density peaked at $-62\ Am^{-2}$. The contour maps illustrate that the majority of the Zn surface is supporting a cathodic reaction and the active anodes dissipate with time and only very small number continue to grow in strength resulting in shallow wide pits. In electrolyte solution of 0.1% (wt) $NaCl_{(aq)}$, at time t=0 the peak current density for the anodic activity measured was $16Am^{-2}$ and the peak current density for the cathodically active regions was $-2.8Am^{-2}$. At scans immediately after immersion revealed that there was more anodic sites active than in saline solution of higher concentration but the peak anodic current densities measured were considerably lower. With the progress of time similarly to the higher $NaCl_{(aq)}$ concentration anodes became passivated and or in most cases the anodic events grew in area and reduced their

respected current density and consequently losing their magnitude of pitting potential. The same phenomenon was observed in higher $NaCl_{(aq)}$ concentration but the effect was less pronounced. Figure 6.2, illustrates the contour maps associated with SVET scans of Zn in 0.1%(wt) $NaCl_{(aq)}$ solution.

In the instance of Zn exposed to 0.01% (wt) $NaCl_{(aq)}$, SVET surface corrosion contour maps are illustrated in figure 6.3. Upon immersion there was a marked increase in the number of anodes observed and a decrease in the spacing between the anodic and cathodic regions, which is indicative that there is more localised pitting action than seen in the higher concentrations of $NaCl_{(aq)}$ solutions. This does not imply that active pits in this case are more aggressive, infact higher concentrations of $NaCl_{(aq)}$ will result in pits that are more aggressive as seen by the corresponding peak intensities. The lower conductivity of the 0.01% $NaCL_{(aq)}$ electrolyte limits the distance between anode and cathode due to the increased resistivity of the solution thus hindering the ionic transport through solution restricting the anode and cathode separation. At time t=0 the measured peak anodic current density was $0.58Am^{-2}$ and the cathodic peak current density $-0.58Am^{-2}$. These values are relatively lower than those recorded in higher concentrations of $NaCl_{(aq)}$, however a point to note is the close proximity of the anodic and cathodic regions, these conditions favour pitting establishing narrower pits than those encountered in higher $NaCl_{(aq)}$ solutions. The peak current densities measured remained constant through the period of the experiment again suggesting a continued electrochemical reaction at a constant rate.

SVET scans of corroding Zn in 0.001%(wt) $NaCl_{(aq)}$ saline electrolyte solution are shown in figure 6.4. At time t=0 upon immersion the measured peak current density for the anodic activity was $0.46Am^{-2}$ and the counter cathodic peak current density was $-0.46Am^{-2}$. There is measured difference of $0.12Am^{-2}$ less peak current density in 0.001%(wt) $NaCl_{(aq)}$ than in the case of 0.01%(wt) $NaCl_{(aq)}$ solution. However, a point of interest similar to that mentioned before was a further increase in the number of anodic sites and the close proximity of cathodic and anodic events resulting in pitting. The active anodes were noted to maintain the peak current density implying continued aggressive pitting with increasing severity as more anodes become apparent.

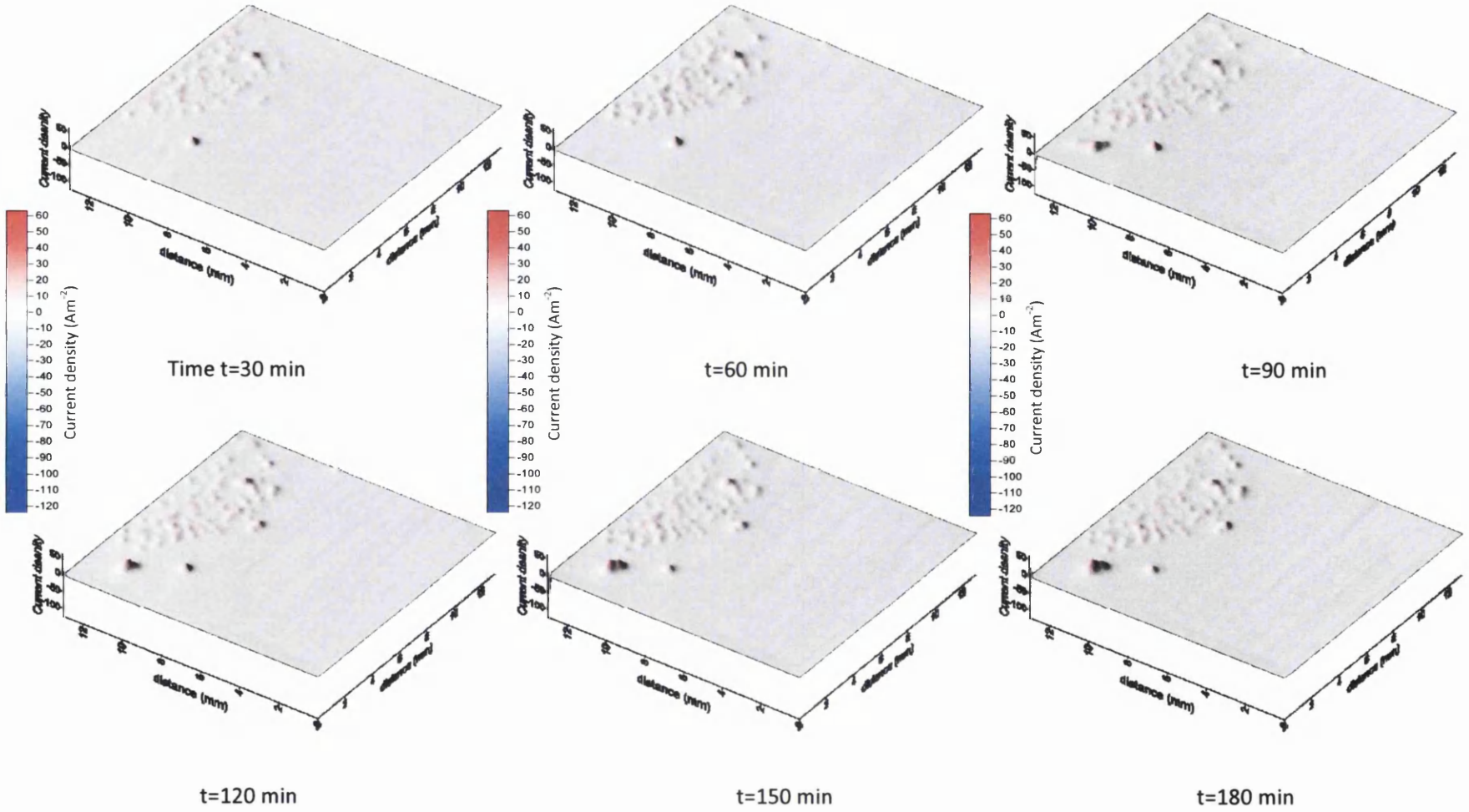

Figure 6.1 Surface plot showing the distribution of normal current density, above zinc sample in aerated 1.0%(wt) $NaCl_{(aq)}$ solution at time 0min→180min.

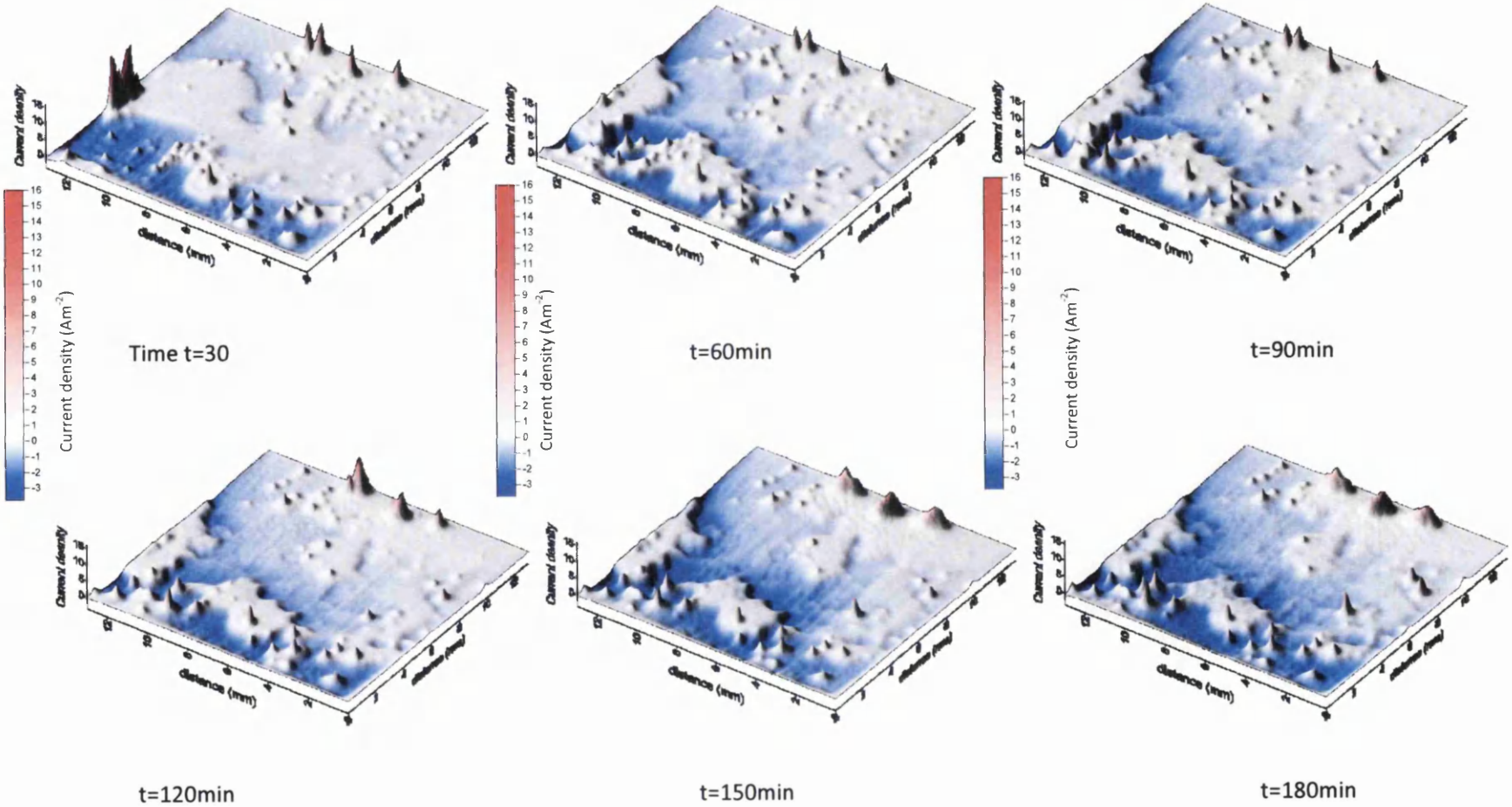

Figure 6.2 Surface plot showing the distribution of normal current density, above zinc sample in aerated 0.1%(wt) $NaCl_{(aq)}$ solution at time 0min→180min.

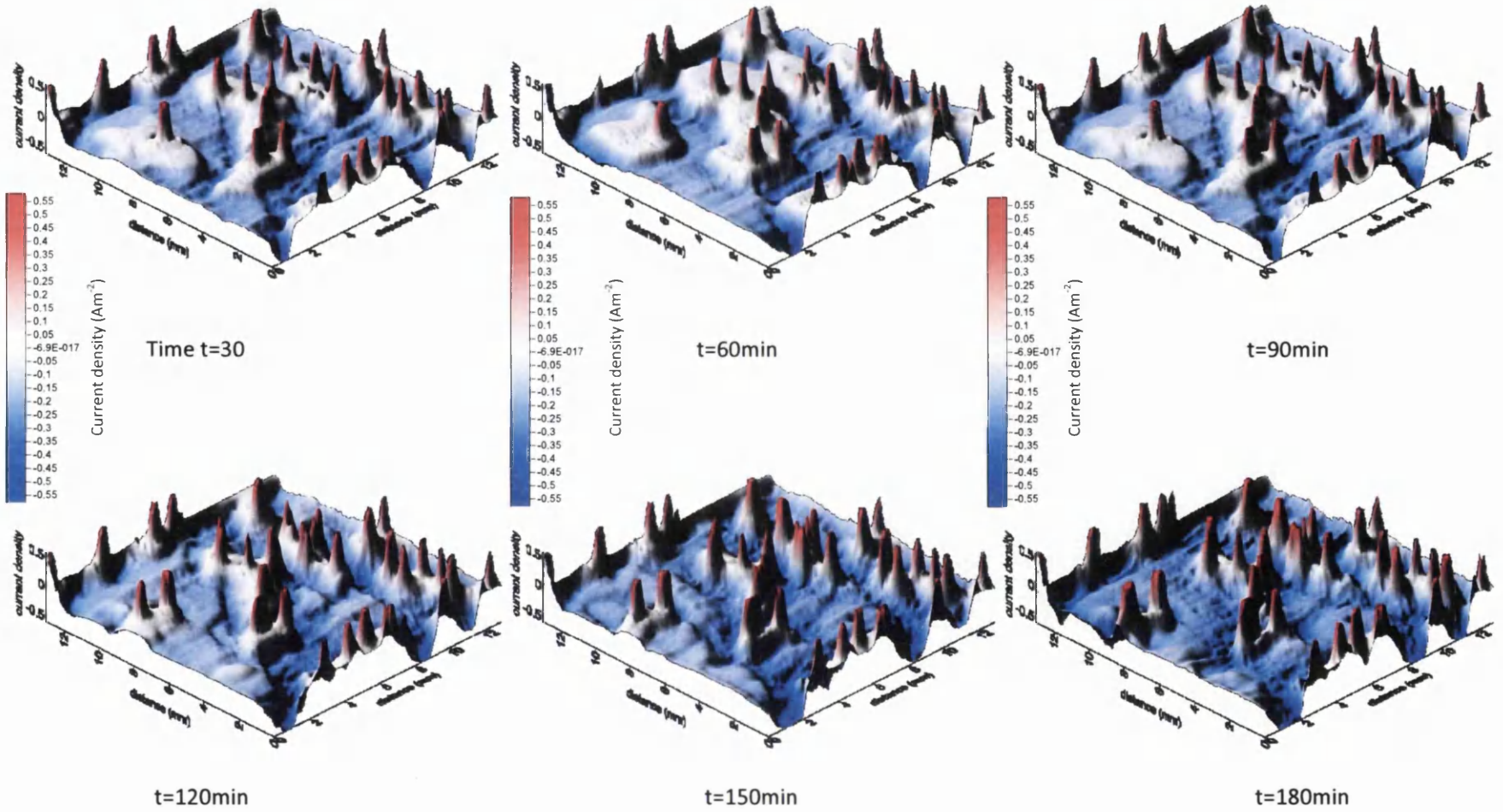

Figure 6.3 Surface plot showing the distribution of normal current density, above zinc sample in aerated 0.01%(wt) $NaCl_{(aq)}$ solution at time 0min→180min.

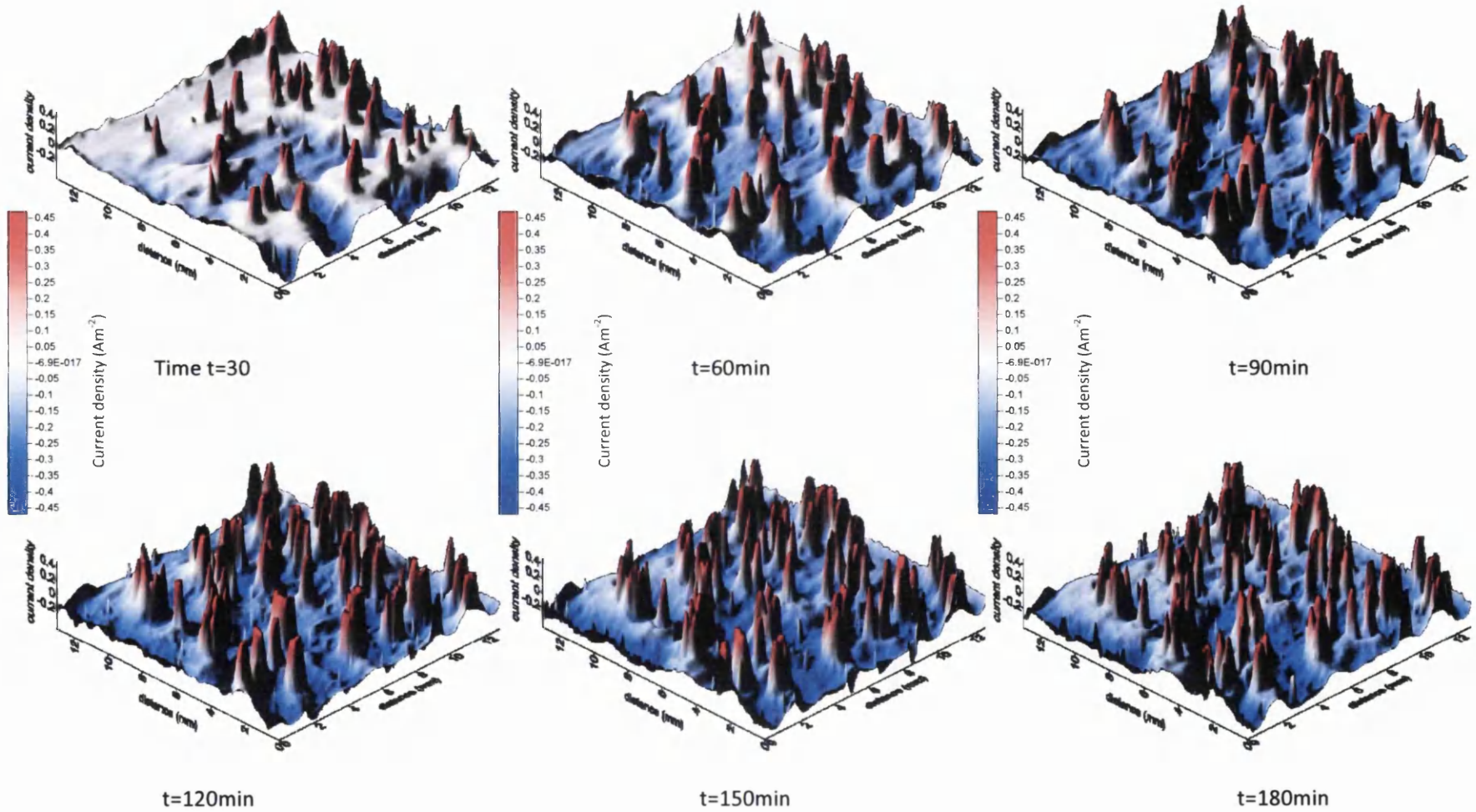

Figure 6.4 Surface plot showing the distribution of normal current density, above zinc sample in aerated 0.001%(wt) $NaCl_{(aq)}$ solution at time 0min→180min.

6.2 Relationships and corrosion pit population model derivation

The detailed processes in pitting corrosion are complex. The pitting mechanism on zinc involves a number of factors, typically, physical imperfections on the metal surface which establishes the initial point of attack and secondly the solution or electrolyte. The chemical nature and the pH of the electrolyte will determine whether corrosion attack will occur and the nature of subsequent corrosion phenomenon for example passivation or repassivation after the initial corrosion, remain localised and develop into a pit or spread out and lead to general corrosion. When corrosion starts at the imperfections, the dissolution of zinc results in a weak acidification inside the pits due to the hydrolysis of zinc ions. Zinc is thought not to pit in the classical sense in that hydrolysis of Zn^{2+} ions produces weakly acidic conditions. However when ionic flow is restricted the conditions may be sufficiently aggressive to maintain a stable pit like anode. When ionic transport is efficient, such as in high concentrations of saline solutions, the anodes and cathodes can be physically separated, and ionic transport allows the acid at the anodes to spread dissolving the pre-existing oxide film hence leading to a general from of corrosion. In electrolytes of weak saline solutions, the ionic conductivity is poor, resulting in anodes and cathodes becoming closely spaced. In this case, the acid at the anodes is neutralised by the base generated at the cathodes and hinder the acidic spread. While the corroding sites keep active, the surrounding areas remain unattacked until pits are developed [6,7]. Due to the complexities surrounding the establishment and sustainability of corrosion pits, the associated pH factor has been excluded to simplify the model derivation below.

An estimated total equivalent Zn loss after each scan was calculated by applying Faraday's law to the SVET data. These have been displayed in figure 6.5 as plots of estimated Zn loss against time, the gradient of which provides the corrosion rate, table 6.1. Figure 6.5 shows that the corrosion rate of pure Zn was linear and the extent of corrosion was highly dependent on solution conductivity as expected with more Zn loss observed in the higher concentration saline solutions.

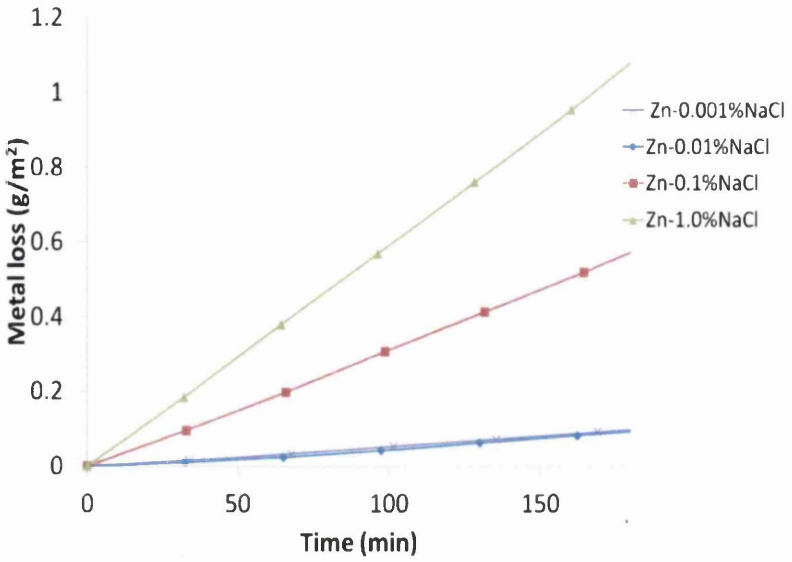

Figure 6.5 Plots of estimated metal (Zn) loss vs immersion time derived from SVET data.

Table 6.1 $NaCl_{(aq)}$ concentration and SVET derived corrosion rates.

$NaCl_{(aq)}$ solution concentration %(wt)	SVET derived Corrosion Rate (g mm^{-2} sec^{-1})
5.0	0.0087
1.0	0.0059
0.1	0.0031
0.05	0.0031
0.01	0.0004
0.005	0.0004
0.001	0.0005
0.0005	0.0002

Further SVET tests were also performed using 5.0%wt, 0.05%wt, 0.005%wt and 0.0005%wt NaCl(aq) solution concentrations to provide further insight into the relationship between solution conductivity and corrosion of pure Zn. The trends stated previously were observed and respective corrosion rates derived and stated in table 6.1. These concentrations were considered to provide further data in order to establish a good correlation. The derived corrosion rates for their respected $NaCl_{(aq)}$ concentrations were plotted on log_{10} scale, figure 6.6 versus the concentration of $NaCl_{(aq)}$. A mathematical correlation was observed, equation 6.3. Where R_{cor} is the Corrosion rate (g m^{-2} s^{-1}) and c is the saline solution $NaCl_{(aq)}$ concentration (%wt).

$$R_{cor} = 0.0055 \times c^{0.3927} \quad (6.3)$$

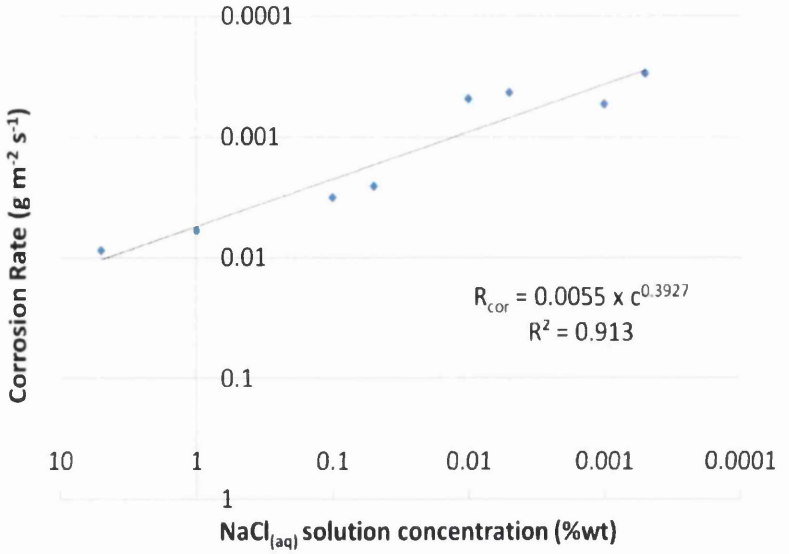

Figure 6.6 Log_{10} plot of corrosion rate vs $NaCl_{(aq)}$ solution concentration from SVET data.

The corrosion rates illustrated above have been derived from SVET data, SVET actually records the local potentials (nV). The measured voltage can be integrated over the total scan area and multiplied with the experiment's calibration factor resulting in local current. Hence a relationship can be shown between the conductivity and SVET derived current, I. Figure 6.7 shows graph depicting relationship between the concentration of $NaCl_{(aq)}$ solution and SVET derived total anodic current.

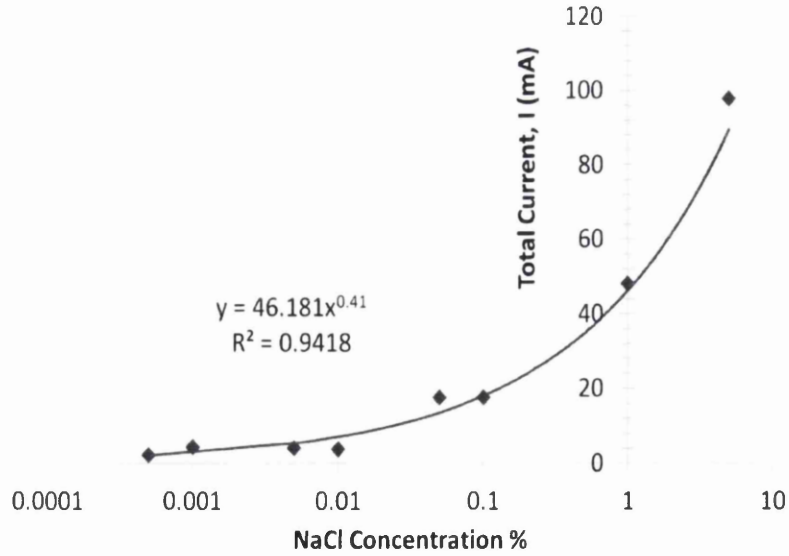

Figure 6.7 Graph of $NaCl_{(aq)}$ solution concentration vs SVET derived total anodic current.

By using this experimentally determined relationship observed between the SVET derived total current and $NaCl_{(aq)}$ solution concentration equation 6.4, another correlation can be

derived that can assist in prediction of number of potential pits with respect to the solution concentration.

$$I = 46 \times c^{0.41} \tag{6.4}$$

Where I is the total SVET derived current (μA) and c is the $NaCl_{(aq)}$ solution concentration (%wt). Based on the experimentally derived relationship in equation 6.4 it can be stated that a power law relationship exists between the total SVET derived current (I) and $NaCl_{(aq}$ $solution_{)}$ concentration (%wt) and hence the solution conductivity (K) which is determined by NaCl concentration, described by equation 6.5. where K is empirically observed. From the experimental data it can therefore be stated that approximately,

$$I \propto K^{0.5} \tag{6.5}$$

An assumption can be made that the individual pit current (i) is dependent upon the number of pits (n), equation 6.6.

$$i = {}^{I}/_{n} \tag{6.6}$$

Consider two active anodes on the substrate the spacing between the anodic centres is governed by the conductivity of the electrolyte, figure 6.8. An assumption was made that a pit cannot establish itself within another active pits maximum ionic transfer zone where L is a length parameter characteristic of the effective anode to cathode distance associated with an individual pit.

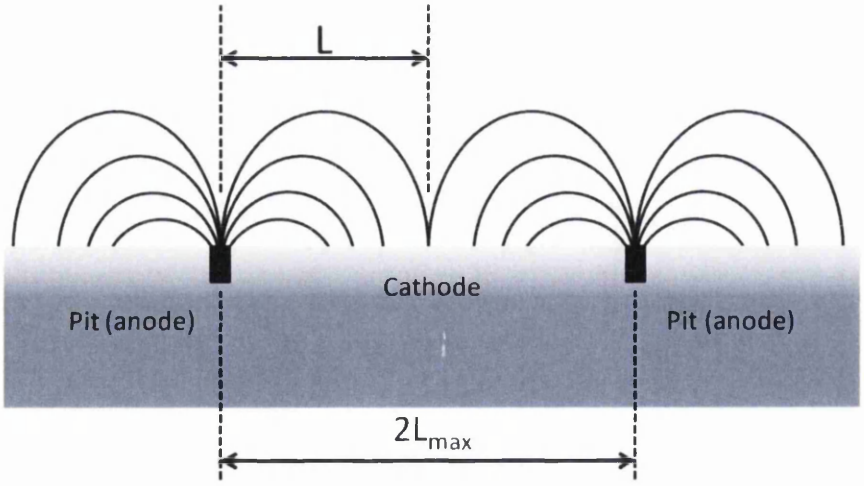

Figure 6.8 Model anode localisation diagram.

Ohms law states that voltage is a product of current and resistance, hence the individual pit voltage (ΔV) can be shown to be, see equation 6.7.

$$\Delta V = \frac{i}{K} \times L^g \tag{6.7}$$

Where ΔV is the ohmic contribution to the individual pit cell potential, i is the individual pit current, K is the electrolyte conductivity, L is a length parameter associated with the electron transfer distance via the electrolyte and g is a geometric factor associated with the shape of the current distribution emanating from the pit. A pit will remain active only when $\Delta V \leq \Delta V_{max}$, where ΔV_{max} is the maximum permissible ohmic drop.

Combining equations 6.5 and 6.6;

$$I \propto K^{-0.5} \times n^{-1} \tag{6.8}$$

and combine equations 6.8 and 6.7;

$$\Delta V \propto K^{-1} \times n^{-1} \times L^g \tag{6.9}$$

For a given ΔV_{max} above equation 6.9 can be rearranged to,

$$L^g_{max} \propto K^{0.5} \times n \tag{6.10}$$

Thus for a sample area A the number of pits possible per unit area can be defined by equation 6.11, figure 6.9.

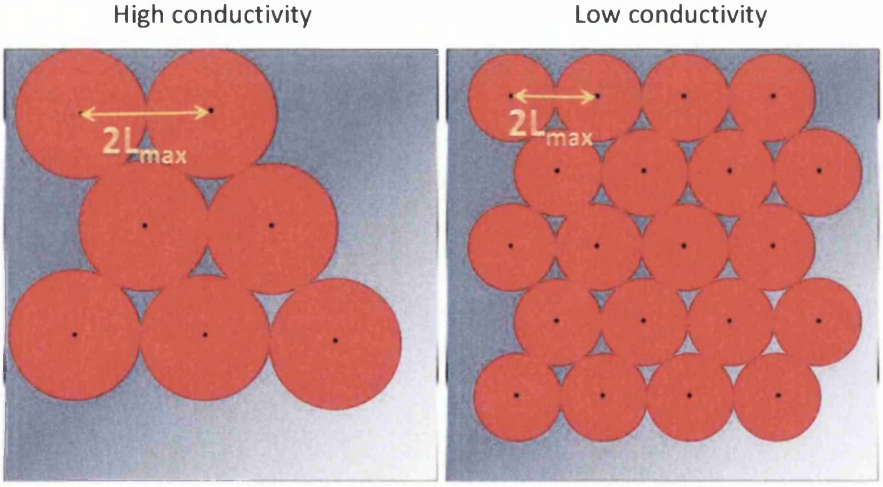

Figure 6.9 Showing anodes and their corresponding ohmic drop zone.

Number of possible pits n,

$$n = \frac{A}{\pi L^g_{max}} \tag{6.11}$$

Anode and cathode spacing can be related to conductivity, K, via combining equations 6.10 and 6.11,

$$L_{max}^{g} \propto K^{0.5} \times L_{max}^{-2}$$

$$L_{max}^{2g} \propto K^{0.5}$$

$$L_{max} \propto K^{0.25\,g} \tag{6.12}$$

A relationship between number of pits and conductivity of electrolyte can be derived by combining equations 6.11 and 6.12,

$$n \propto K^{0.5\,g} \tag{6.13}$$

Experimental results revealed Zn in lower concentrations of $NaCl_{(aq)}$ solution exhibited a higher number of more closely distributed localised anodes than in higher $NaCl_{(aq)}$ concentrations. Anodes detected in the higher $NaCl_{(aq)}$ concentrations have higher peak current density values than those found in lower $NaCl_{(aq)}$ concentrations. The model agrees well with the results from the study.

6.3 Conclusions

Commercially pure zinc 99.99% was subjected to SVET corrosion study in order to understand the corrosion behaviour of Zn. Zn is the majority element in the Zn-Al alloy that is often applied to sheet steel for protection against corrosion.

Several SVET experiments were performed with varying concentrations of $NaCl_{(aq)}$ electrolyte concentrations. A clear and concise trend became apparent that a 99.99% purity zinc foil surface exposed to lower concentrations of saline solution resulted in densely populated localised anodic events in contrast to Zn in higher concentration of saline solution. Anodes detected in higher $NaCl_{(aq)}$ concentration possessed higher peak current density than those found in lower $NaCl_{(aq)}$ concentrations.

A model was derived that related pit or anode site population with solution conductivity that agrees well with the SVET results.

6.4 References

(1) Shreir, L. L. E. Corrosion Vol. 1. - 2; 2nd edition. ed.; Butterworths: [S.l.], 1976.
(2) Chen, Z. Y.; Persson, D.; Leygraf, C. Corrosion Science 2008, 50, 111-123.
(3) Veleva, L.; Acosta, M.; Meraz, E. Corrosion Science 2009, 51, 2055-2062.
(4) Elvins, J.; Spittle, J. A.; Worsley, D. A. Corrosion Science 2005, 47, 2740-2759.
(5) Edavan, R. P.; Kopinski, R. Corrosion Science 2009, 51, 2429-2442.
(6) Izquierdo, J.; Nagy, L.; Varga, Á.; Santana, J. J.; Nagy, G.; Souto, R. M. Electrochimica Acta 2011, 56, 8846-8850.
(7) Zhang, X. G. Corrosion and electrochemistry of zinc; Plenum: New York ; London, 1996.

Chapter 7

Effect of ultrasonic irradiation on the microstructure and corrosion rate of Zn/Al alloys

7.1 Introduction

Ultrasonic irradiation of solidifying alloy melts has been shown to have significant effects on the microstructure and mechanical properties of a range of important engineering alloys as shown previously [1,2,3,4,5,6,7,8,9,10,11,12,13] and in section 1.7. In this chapter ultrasound has been used to irradiate castings of Zn-4.8wt% Al alloys. These galvanising alloys predominantly evaluated in the organically coated steels in chapters 3, 4 and 5 to assess the microstructural changes induced and their influence on the corrosion resistance of the alloy. The aim of this section of work was twofold, one to determine the affect of ultrasound on the microstructure of the solidifying Zn-4.8% Al alloy melt. Secondly to assess the corrosion behaviour of the modified microstructure in comparison to the non-ultrasound manipulated microstructure.

7.2 Solidification of Zn - 4.8wt% Al alloys as predicted by the phase diagram

The Zn - 4.8wt% Al alloy under investigation is hypereutectic lying just to the right of the eutectic point of 5 wt% Al in the Zn/Al equilibrium phase diagram as shown in the schematic in figure 7.1. On cooling from the liquid phase through the liquidus line nucleation of β crystals of primary Zn occurs at some undercooling below the liquidus temperature and the remaining liquid ahead of the solidification front becomes enriched in Al. As cooling proceeds the β crystals start to grow into a dendritic structure under practical cooling rates and when the remaining liquid reaches 5 wt% Al it solidifies into a lamellar eutectic of alternating sheets of Zn and Al. A rod eutectic can form but generally at very high cooling rates, around the primary dendrites due to orientation effects or with small additions of ternary elements such as Mg. The final microstructure is therefore composed of primary zinc dendrites in a matrix of lamellar Zn/Al eutectic.

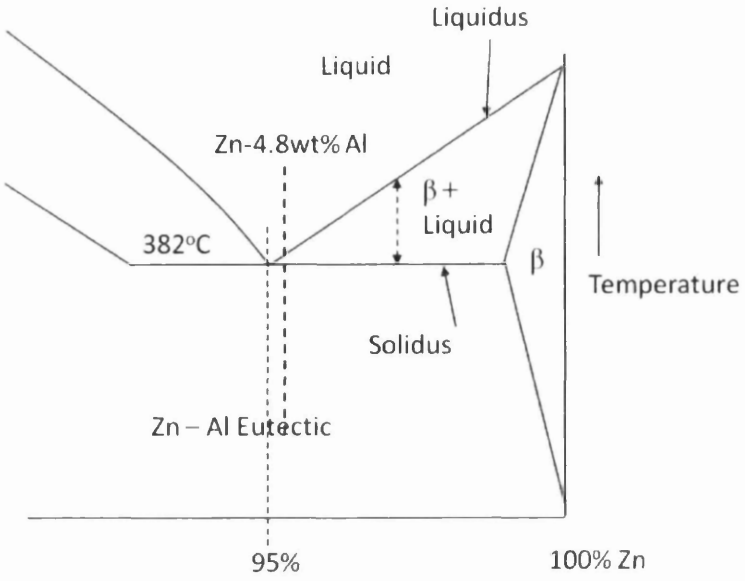

Figure 7.1 Schematic portion of Zn – Al equilibrium phase diagram

7.3 Microstructure morphology of cast Zn – 4.8wt% Al alloys with no ultrasonic irradiation and with ultrasonic irradiation

Figure 7.2 shows macro digital camera images of sectioned casts of Zn – 4.8 wt% Al alloy having had no ultrasound during solidification, figure 7.2A and having ultrasonic irradiation during solidification, figure 7.2B. Figure 7.2 shows that the sample that had experienced irradiation had a much finer grain structure below the position of the ultrasound horn and this structure extended throughout the casting vertically and laterally to the chill zone. The casting that had no ultrasound had a much larger grain structure throughout the suggesting that the ultrasound had a significant impact on the solidification of the alloy.

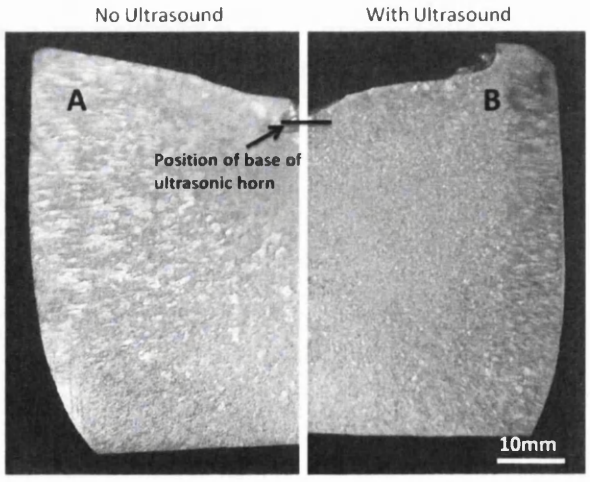

Figure 7.2 macro digital camera images of sectioned casts of Zn – 4.8 wt% Al alloy A) no ultrasound during solidification B) ultrasonic irradiation during solidification.

An optical microscope image of the Zn – 4.8wt% Al alloy without ultrasonic irradiation is shown in figure 7.3A. The microstructure was composed of primary Zn rich β dendrites surrounded by a eutectic of Zn / Al as described in section 7.2. The eutectic structure was primarily of lamellar morphology with alternating lamellae of Zn and Al with some pockets of rod eutectic observed next to primary and secondary dendrite arms of the Zn rich β phase. The formation of rod eutectic next to the dendrite arms was most likely as a result of lamellae becoming forced to growth at orientations away from the preferred growth direction as shown by previous research [14, 15]. Figure 7.3B shows an optical microscope image of the typical microstructure of the cast Zn – 4.8wt Al alloy that was ultrasonically irradiated. Once again the structure was characterised by the Zn rich β phase and a Zn / Al eutectic but there were significant morphology changes compared with the casting produced without ultrasonic irradiation. The primary Zn rich β phase had changed from dendritic to globular and although the majority of the eutectic was still lamellar, there were significant areas where the eutectic growth has become disrupted forming almost spherical colonies of anomalous eutectic growth. These regions of anomalous eutectic were often characterised by numerous primary β globules at their periphery as highlighted in figure 7.3.

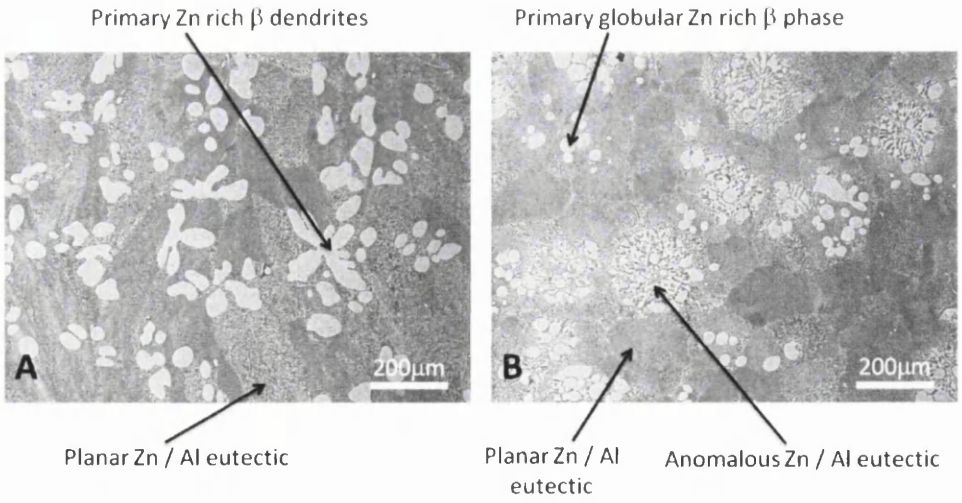

Figure 7.3 Optical micrographs of Zn – 4.8wt% Al Alloy solidified A) without ultrasound B) with ultrasound

Figures 7.4A-D illustrate the microstructures of the alloys with no ultrasound (A and B) and with ultrasound (C and D) at two distances away from the ultrasound horn in order to evaluate the effect of the irradiation with distance. The distances are 20 mm (A and C) and 40 mm (B and D). The change from dendritic primary β phase to globular is evident when

comparing the non-irradiated and irradiated sample images at 20 mm away from the horn (A and C). There is also a significant increase in the number of primary β phase crystals in the ultrasound sample indicating a higher nucleation rate and also the primary phase and eutectic cell size also appear to be considerably smaller. This influence on the microstructure persists to 40 mm below the ultrasound horn as evidenced by figure 7.4D.

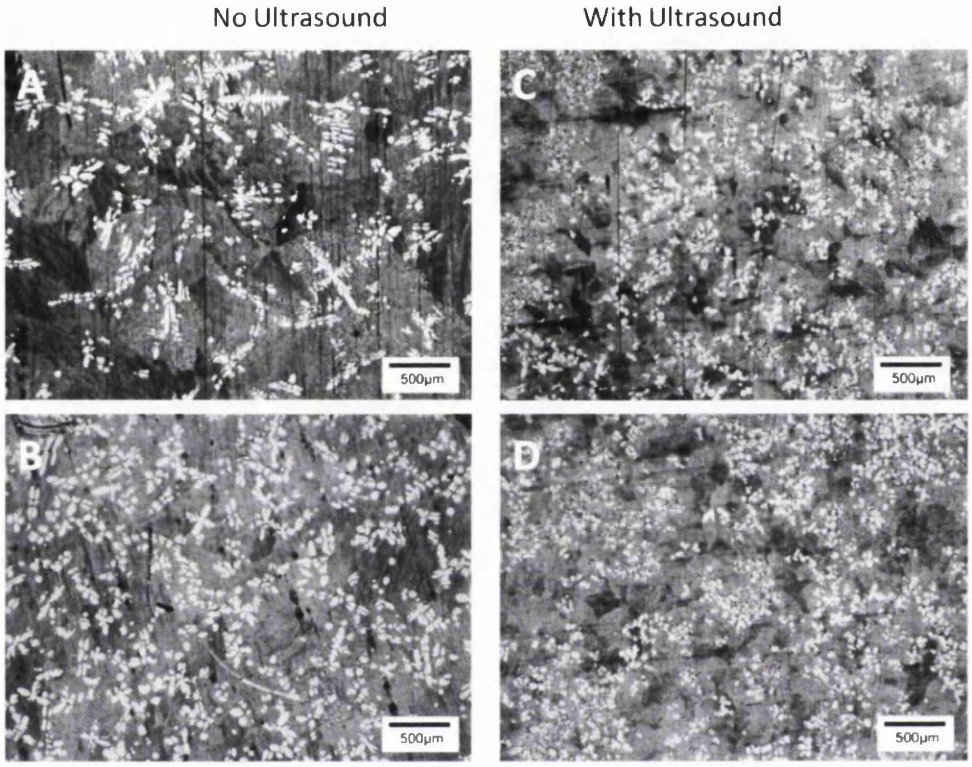

Figure 7.4 Optical micrographs of Zn – 4.8wt% Al Alloy solidified with no ultrasound (A and B) and with ultrasound (C and D) at two distances away from the ultrasound horn in order to evaluate the effect of the irradiation with distance. The distances are 20 mm (A and C) and 40 mm (B and D).

The number of dendrites or primary phase crystals per mm^2 was evaluated for each alloy condition and as a function of distance away from the ultrasound horn. The data is presented in figure 7.5. It can be clearly seen that there is a significant increase in the numbers of dendrites per mm^2 when ultrasound is applied during solidification at all distances considered and this is especially prominent over the first 20 mm away from the horn. At 5 mm from the horn there were almost 60 dendrites mm^{-2} for the ultrasound sample compared with 1 dendrite mm^{-2} for the sample with no ultrasound. In the sample with no ultrasound this low dendrite number at the centre of the casting close to the top represents the last liquid to solidify and this will be of eutectic composition so there will be

relatively few if any primary crystals. The conditions imparted by the ultrasound thus seem to allow enhanced nucleation of primary phase throughout the solidification. At distances greater than 20 mm there is a marked increase in dendrite numbers in the no ultrasound sample rising from < 20 dendrites mm^{-2} at 1.5 mm to a fairly stable 60 dendrites mm^{-2} at distances > 20 mm.

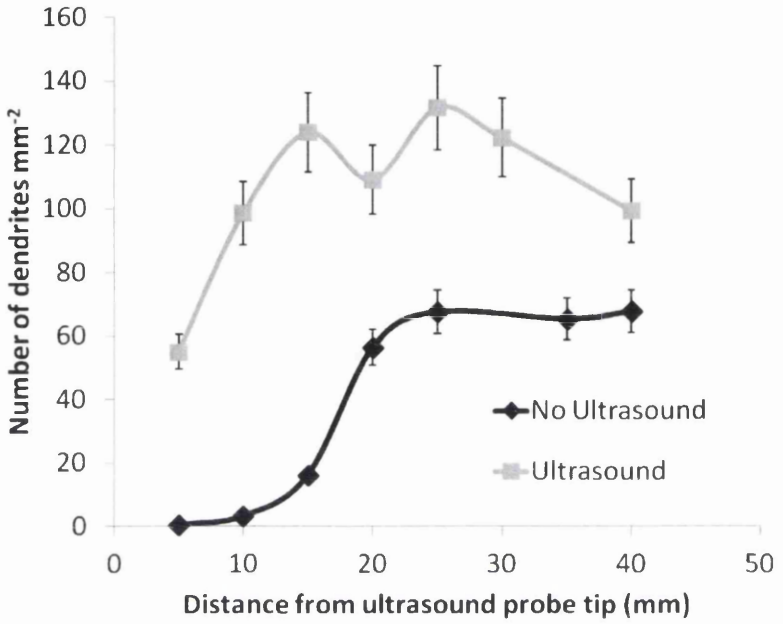

Figure 7.5 The number of primary phase crystals per mm^2 evaluated for each alloy condition and as a function of distance away from the ultrasound horn.

The number of dendrites or primary phase crystals present is indicative of the nucleation rate and thus the increase in nucleation rate of the sample solidified with ultrasound as a function of distance from the horn was plotted in figure 7.6. Examination of figure 7.6 shows that close to the horn, at 5 mm, there is a massive increase in the nucleation rate of primary phase of approximately 55 times in the ultrasound samples. This increase in nucleation rate falls with distance from the ultrasound horn but even at 40mm there is twice the nucleation rate of primary phase in samples exposed to ultrasound during solidification as shown by the magnified portion of the graph in figure 7.6. The increased nucleation rate (N) with vertical distance from the horn (x)(mm) can be approximated fairly well using a power law relationship as shown in figure 7.9 and equation 7.1 and thus.

$$N = 1500.x^{-2} \qquad (7.1)$$

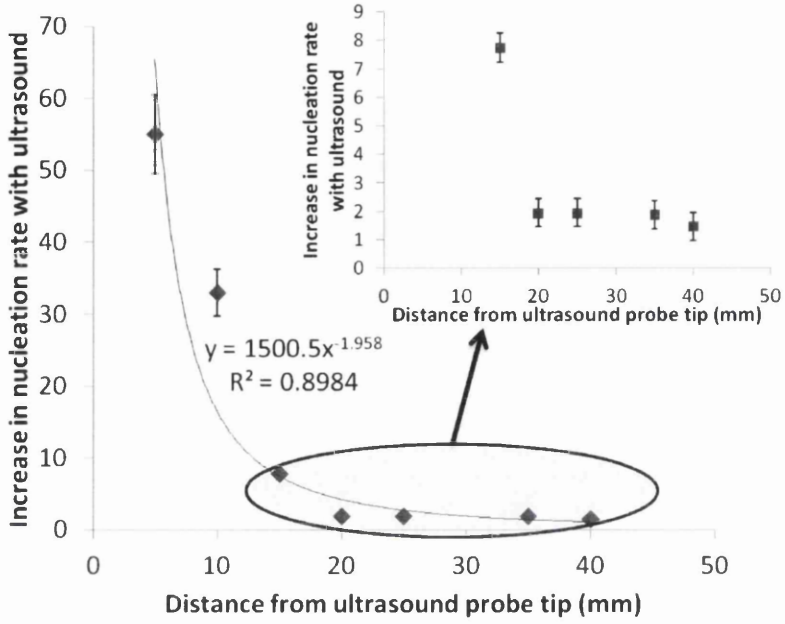

Figure 7.6 Increase in nucleation rate of the sample solidified with ultrasound as a function of distance from the ultrasound probe tip.

The instantaneous volume fraction of primary β phase for each image was also evaluated as a function of distance from the horn for samples with no ultrasound and with ultrasound. The results are shown in figure 7.7.

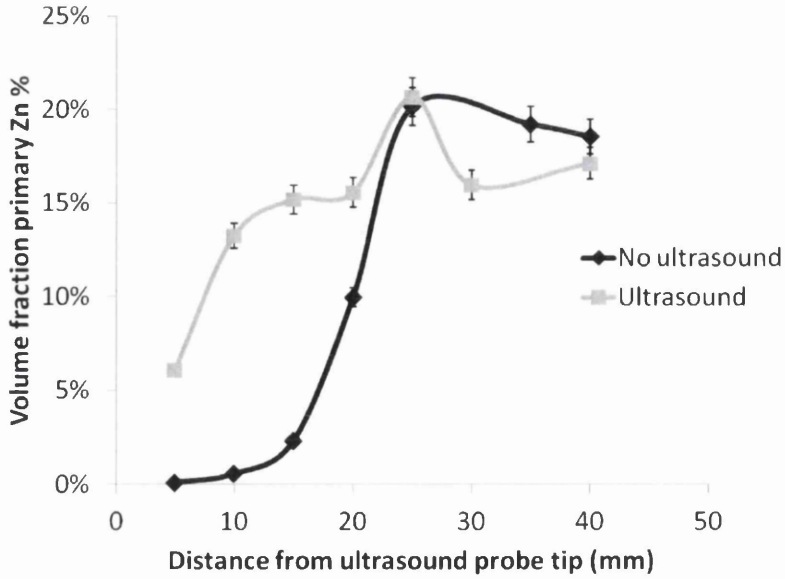

Figure 7.7 Instantaneous volume fraction of primary β phase as a function of distance from the ultrasound probe tip for samples solidified with and without ultrasound.

Once again the major differences were observed over the first 20 mm from the ultrasound horn with a significant increase in volume fraction of primary β phase in this area of the casting when ultrasound was applied. This again indicates that nucleation was facilitated by the application of ultrasound. The volume fractions of primary phase at distance > 20 mm from the horn were fairly similar with a typical value of around 17% primary β phase for both casting conditions. The application of the ultrasound produced a more even distribution of primary β phase throughout the casting whereas there is significant non-uniformity of primary β volume fraction with distance from the horn when no ultrasound was applied. These instantaneous volume fraction data and the number of dendrites per mm^{-2} were then used to calculate an average dendrite size (mm^2) as a function of distance from the horn for both castings and is presented in figure 7.8.

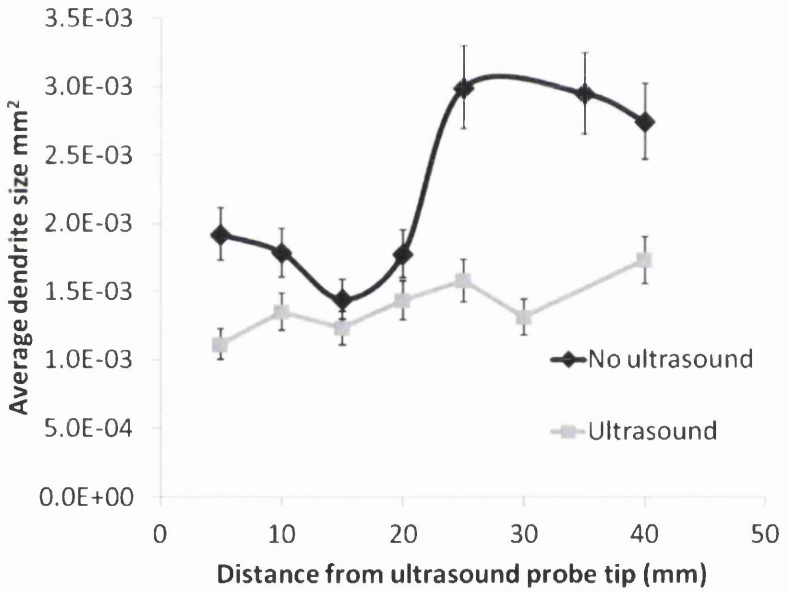

Figure 7.8 Average dendrite size (mm^2) as a function of distance from the ultrasound probe tip for samples solidified with and without ultrasound.

These data show that the average dendrite or primary crystal size in castings exposed to ultrasound varied between a minimum of 1.1×10^{-3} mm^2 at 5 mm and a maximum of 1.7×10^{-3} mm^2 at 40 mm from the horn. For the sample with no ultrasound the average dendrite size varied between a minimum of 1.4×10^{-3} mm^2 at 15 mm and a maximum of 2.99×10^{-3} mm^2 at 25 mm from the horn. Thus, considering figure 7.8, the primary phase crystals were

consistently smaller when ultrasound was applied during solidification and maintained a much more uniform size throughout the casting.

Figures 7.2 – 7.8 thus demonstrate that the application of ultrasound to the solidifying Zn – 4.8wt% Al alloy has a significant influence on the final microstructure of the alloy. The ultrasound samples are generally characterised by globular primary β phase morphology with a large increase in nucleation of this phase. The eutectic structure is also altered with areas of disruption of stable planar eutectic growth forming colony like structures of anomalous eutectic. Ultrasound creates a unique environment within the melt on irradiation. The Ultrasound waves create areas of compression and rarefaction within the melt that leads to the formation of cavitation where the melt is literally torn apart by the vibration creating a cavity. These cavities are generally unstable and collapse in on themselves which causes large local temperature and pressure increases. In fact locally temperatures may reach 5000°K and several hundred atmospheres of pressure [11]. The ultrasound waves also move through the melt in a phenomenon known as acoustic streaming that can cause rapid agitation and mixing and can influence convective heat flow. The cavitation phenomenon can also aid degassing of melts and removal of gas from the surfaces of intermetallic /oxide inclusions thus potentially providing suitable surfaces for nucleation events [1].

The transition of the primary Zn rich β phase from dendritic to globular on application of ultrasound may be due to a number or combination of factors. Dendritic growth is caused by compositional variations along a solidifying interface that cause protrusions to grow from a planar interface. As the protrusions solidify solute is rejected into the surrounding liquid and thus the local liquidus temperature is depressed. The protrusion will continue to grow if the thermal gradient ahead of the interface is below a critical gradient determined by the change in local liquidus temperature i.e. the liquid ahead of the interface is supercooled. This is known as constitutional supercooling as composition changes ahead of the interface determine the supercooling. As the protrusion grows, liquid lateral to the growing protrusion becomes enriched in solute and thus will freeze at some lower temperature. This encourages further growth of a protrusion outwards into the melt and thus the breakdown of a planar interface. The interface of the protrusion itself may also experience compositional variations along its length and cause further protrusions to form from the parent structure. These are known as secondary dendrite arms with the initial protrusion being the primary dendrite arm. This partioning of solute ahead of interfaces

coupled with temperature gradients ahead of the interface lead to the formation of dendrites.

In terms of ultrasonic irradiation the mixing and flow of liquid induced by acoustic streaming and local cavitation events may offer sufficient stirring to rapidly remove solute build up ahead of growing interfaces. This homogenising of the liquid ahead of the solidification front would therefore promote stability of the planar interface by removing constitutional supercooling effects and thus prevent the formation of stable dendrite arms producing globular primary crystals of β. The fluid dynamics induced by the ultrasound may also have the effect of fragmenting dendrites that form in the melt by breaking off any secondary arms that form due to forces induced by acoustic streaming and cavitation [16]. This would then produce a final microstructure of globular primary β as the dendrite arms are removed. It would also contribute to the observed increase in primary β crystals attributed to an increase in nucleation as each arm removed would form a "stand alone" crystal in its own right. Acoustic streaming induced fluid flow may also disrupt dendrite formation through the bending of secondary dendrite arms that would induces stresses at the root of the arms. This stress would cause localised heating of the root and if close to the liquidus temperature could cause re-melting of the root and subsequent detachment of the arm [17]. It is extremely difficult to prove which of these effects has a dominant role in the breakdown of dendritic growth due to the difficulty of monitoring microscopic solidification in such an extreme environment. However, Figure 7.7 demonstrates that there was much improved mixing when ultrasound was applied to the melt as the volume fraction of primary β is much more even throughout the casting with a only small eutectic rich area just below the ultrasonic horn extending to 5mm whereas a stable volume fraction was not achieved until a depth of 25mm in the sample cast without ultrasound. This implies that the liquid was mixed more thoroughly achieving a more homogenous mix and that local compositional differences during solidification were rapidly removed.

Figures 7.5 and 7.6 show that the number of primary β crystals was much greater in the ultrasound sample with a particular increase in number observed close to the probe. This could be due to the improved mixing as highlighted previously but is also indicative of an enhanced nucleation rate and this is evidenced by the fact that the number of primary phase crystals is twice as high in the ultrasound samples even at depths of 40mm from the ultrasound probe. The apparent increased nucleation may be an artefact of dendrite arm

fragmentation as describe earlier but may also be an actual physical increase in nucleation events initiated by the conditions that the irradiation creates. The cavitation of the liquid leads to collapse of the cavities as described earlier creating extremes of temperature and pressure on a very localised scale. Prior to collapse the cavities that form increase in size with the expansion half period of the ultrasonic cycle. This expansion encourages liquid evaporation into the cavity and this process tends to reduce the cavity temperature. If this temperature change is sufficient to drop the temperature of the cavity below the equilibrium freezing temperature then the melt at the cavity interface will become undercooled and encourage nucleation at the periphery of the cavity [8,9,10,11,12,13]. Therefore, the number of nuclei would be substantially increased as cavitation occurs especially near to the probe surface where the intensity of ultrasound will be greatest. These cavitations events may therefore encourage nucleation due to undercooling effects induced by local temperature changes and also as increased pressure associated with cavitation collapse favours an increase in undercooling of the alloy and thus solidification can occur with a smaller critical nuclei radius. Therefore the nucleation rate is increased and more primary phase crystals will be formed. Whether or not the local temperature increase associated with cavitation would allow the nuclei formed to persist or re-melt is unclear but if the pressure was imparted on the surrounding liquid radially to the implosion increased nucleation may be sustained. Degassing of particles within the melt may also provide further surfaces for nucleation and the alloy melt used here will certainly contain a number of intermetallic dross phases that could potentially act as nucleants [1,2,3].

The eutectic structure in the non-ultrasound samples is primarily lamellar with alternating sheets of Zn and Al. Some rod eutectic is formed around the secondary dendrite arms where preferred orientation growth is disrupted by the dendrite arms [14,15]. These eutectics are shown in figure 7.9.

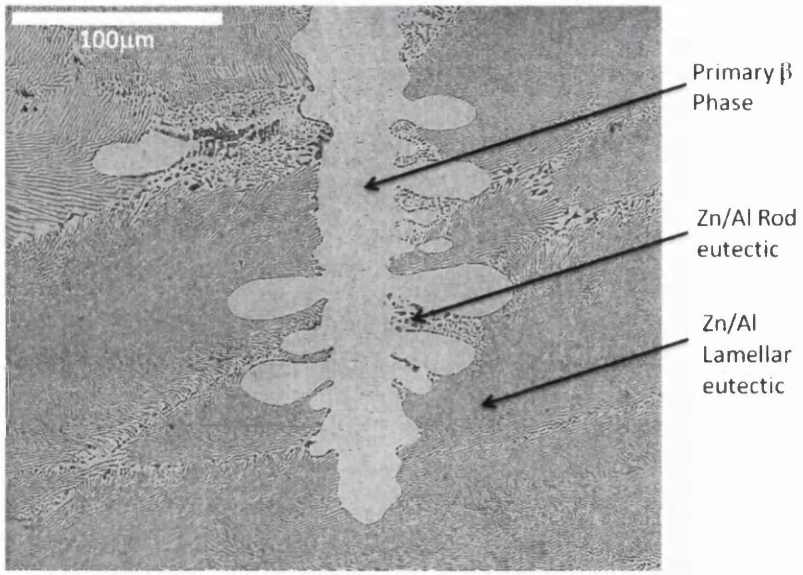

Figure 7.9 Phases present in Zn – 4.8wt% Al alloy solidified without ultrasound.

Lamellar eutectic formation as demonstrated in figure 7.9 is associated with lateral diffusion of Al from growing phases of Zn and vice versa in a process known as coupled growth that allows lamellae of each phase to grow concurrently and adjacent to each other. Examination of figure 7.10 for the Zn – 4.8wt% Al alloy solidified with ultrasound shows that although the regular lamellar Zn/Al is still present there are also numerous almost spherical colonies of anomalous eutectic growth.

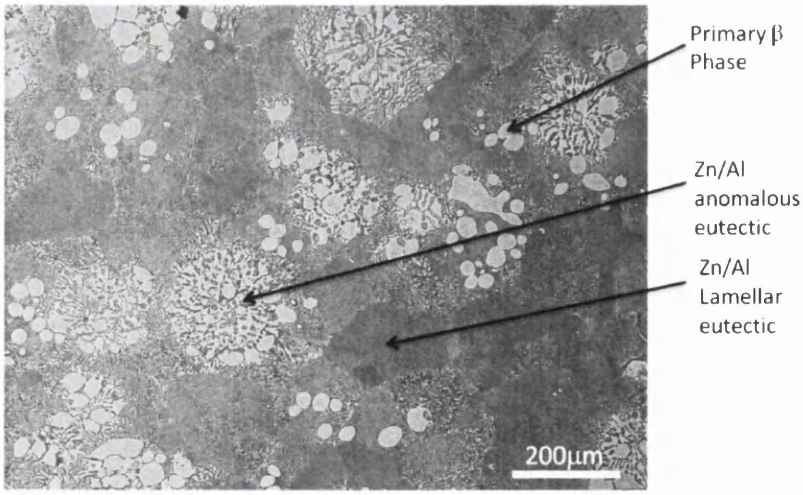

Figure 7.10 Phases present in Zn – 4.8wt% Al alloy solidified with ultrasound.

The regions of anomalous eutectic are intriguing and demonstrate a region where solidification conditions have changed locally to breakdown the stable lamellar growth. These areas within the structure seem to have a similar shape throughout all the micrographs examined and it can be postulated that these regions may be associated with

cavitation events. Stable planar growth resulting in a lamellar structure is promoted by a low growth rate, a steep temperature gradient ahead of the growth front and the absence of mixing due to the need for short range diffusion. Thus, at a site of cavitation, implosion of the cavity will cause a massive disruption to the liquid locally and as the melt cools and solidification starts the turbulence and mixing created by cavitation will destroy the conditions for stable lamellar growth and hence areas of anomalous eutectic solidify. The localisation of these areas within the microstructure may support the argument that they are associated with cavitation events occurring at the point of eutectic solidification. These areas in the microstructure often have primary β crystals at their periphery or interior suggesting that these were sites where either the β had nucleated at the interface of the cavity or eutectic phases were nucleating from the prior β crystals. The fact that the majority of the eutectic within the structure is regular lamellar supports the argument that localised disruption to solidification has occurred in these regions. However, it also suggests that mixing due to acoustic streaming has less effect on the short range diffusion layers adjacent to solidifying interfaces and thus in terms of primary β phase solidification it maybe more likely that dendrite arm fragmentation is the cause of the breakdown in dendritic structure rather than disruption of constitutional supercooling effects.

7.4 Corrosion behaviour of Zn – 4.8wt% Al alloys solidified with and without ultrasound as determined by the SVET

Both castings of Zn – 4.8wt% Al alloys with and without ultrasonic irradiation during their solidification have been prepared as described in section 2.5.2 for SVET testing. The samples were prepared to give false cut edges to mimic service conditions and three areas on the castings were scanned to assess the effect of distance from the ultrasonic horn on the change in microstructures effect on corrosion resistance. Figure 7.11 shows typical 3D current density maps for samples A) without ultrasound B) with ultrasound. The maps were plotted in Surfer 10 (Golden Software).

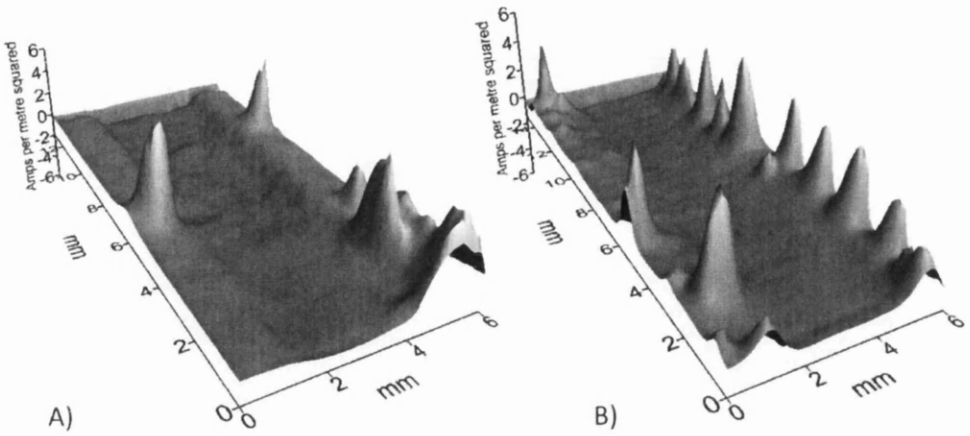

Figure 7.11 Typical current density maps for Zn - 4.8wt% alloys solidified A) without ultrasound B) with ultrasound, as detected with SVET in 0.1% NaCl

The current density maps show that anodic activity was focussed towards the edges of the scan area where the Zn – 4.8wt% Al alloy was exposed. The centre portion of the scan was persistently cathodic over the steel insert thus confirming that the alloy was sacrificially protecting the steel as per an in service cut-edge of production material. There were generally a greater number of anodic peaks observed on samples tested that were solidified with ultrasonic irradiation. This persisted from scan to scan at the scan areas top and middle (5mm and 25mm from the horn) interrogated on each casting with a false cut edge. A similar number of anodes were observed for both materials at the bottom scan position (45mm from the horn).

SVET measured Zn loss data is presented in figure 7.12 for both alloys at the three distances from the ultrasonic horn.

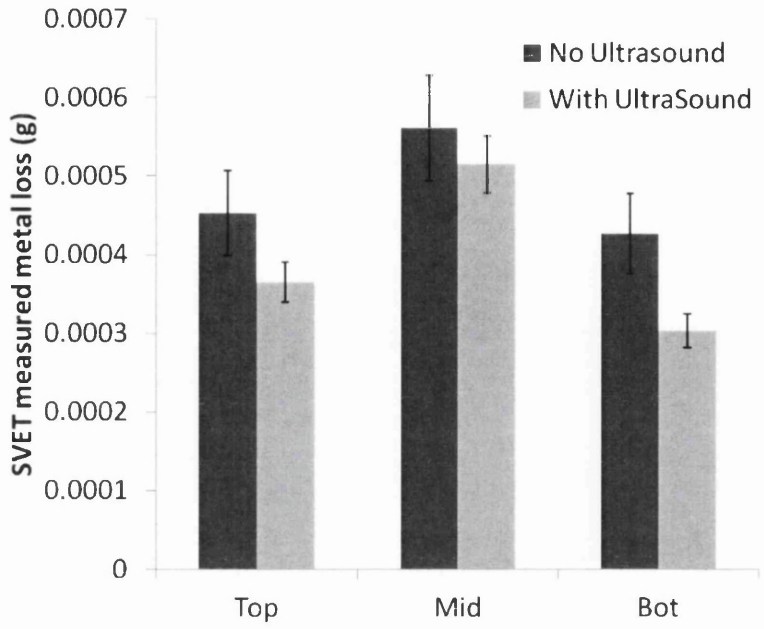

Figure 7.12 SVET determined Zn loss for both castings of Zn – 4.8wt% Al alloy with a false cut edge for areas at various distances from the ultrasonic probe: Top – 5mm, middle (Mid) – 25mm, bottom (Bot) – 45mm.

The data presented in figure 7.12 represents an average of two tests for each experimental condition and the error bars reflect the limits of these data observed. It can be seen from figure 7.12 that the samples that experienced ultrasonic irradiation during solidification generally outperformed the non ultrasound samples at all positions through the casting in terms of SVET measured Zn loss. This may therefore be of potential interest for the steel manufacturer. It is interesting to look at the lifetime of anodes that develop over the course of 24 hours as longer lived anodes will be more damaging than short lived anodes especially if they maintain a relatively high intensity. Figure 7.13 shows the percentage of anodes that are active for defined time frames, 0-6 hours, 6-12 hours, 12-18 hours and 18-24 hours for both alloy preparation conditions. The graph shows that for both the top and middle scan positions, 5mm and 25mm from the ultrasonic horn, the sample irradiated with ultrasound showed a reduction in anodes that had the longest lifetimes i.e. those having an intensity of greater than 1 Am^{-2} for 18 – 24 hours of the experiment time.

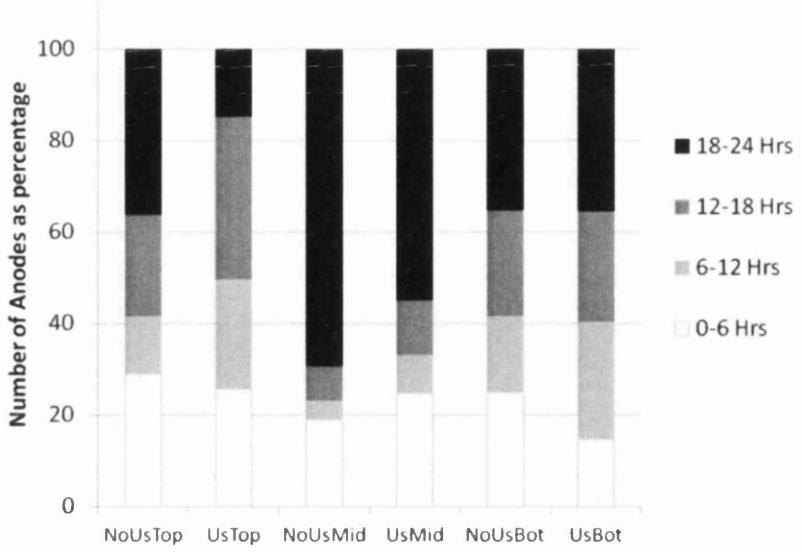

Figure 7.13 Percentage of anodes that are active for defined time frames, 0-6 hours, 7-12 hours, 13-18 hours and 19-24 hours for Zn-4.8wt% Al alloys with and without ultrasonic irradiation during solidification.

These data suggest that the change in microstructure induced by ultrasound imparts an improved corrosion performance on the Zn – 4.8wt% Al alloy at cut-edges. Previous work has shown that the size of the primary Zn rich β dendritic phase is critical in determining corrosion behaviour of this alloy and modifications of the dendrite size through cooling rate, coating thickness or steel substrate thickness can significantly influence the corrosion performance of the alloy [14,15,22]. When cut edge corrosion occurs and the Zn alloy acts to protect the steel anodic activity becomes focussed on the Zn rich β dendrites preferentially. This is shown in figure 7.14 where localised corrosion of the β phase was observed on examination of the corroded alloy after immersion in 0.1% NaCl in the SVET experiments.

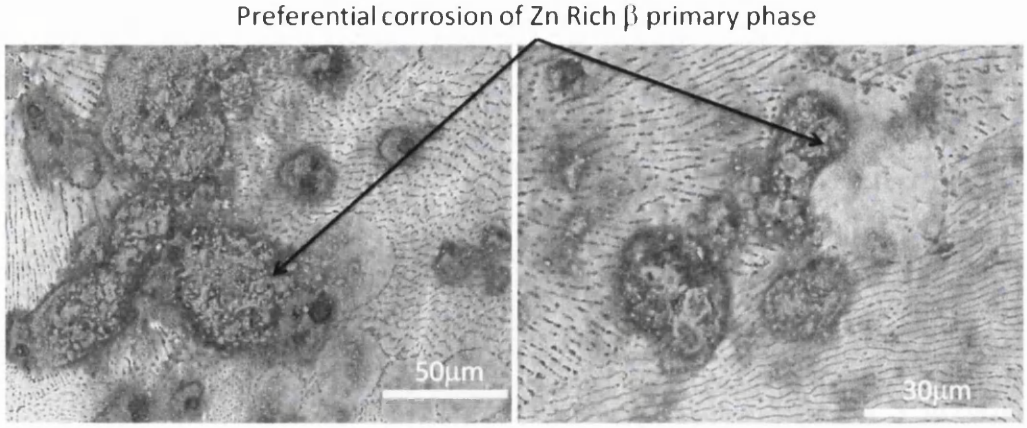

Figure 7.14 Electron microscope images showing preferential corrosion of Zn rich β phase after immersion of Zn – 4.8wt% Al alloy in 0.1% NaCl for 24 hours.

Attack at the eutectic phases is delayed until the local chemical environment around the corroding dendrite becomes suitably aggressive with regards to pH or local Cl^- concentration. The eutectic phase is less easily corroded due to the presence of the Al rich lamellar that promote the formation of an Al_2O_3 film offering a degree of initial protection in the electrolyte. The Al_2O_3 is an insulator and thus electron transfer processes are slowed dramatically thus affecting the anode and cathode redox couple. Figure 7.15 shows that for the alloy sample irradiated with ultrasound during solidification there is a general trend between the number of dendrites per mm^2, the volume fraction of primary Zn rich β phase, the average dendrite size with the SVET measured Zn loss suggesting that indeed dendrite morphology was a controlling factor on anodic dissolution rate. Figure 7.15 also shows that for the non ultrasound sample the trend holds for the middle and bottom areas considered during the SVET testing but the top portion of the casting is predominantly eutectic in this sample and thus the relationship breaks down. Here the corrosion may involve de-alloying of the Zn rich lamellar from the eutectic phase driven ultimately by the cathodic activation of the steel insert. Thus, it would seem that the application of ultrasound on solidification reduces the corrosion rate of the alloy through morphological changes to the primary β phase. As this phase is the focussed point for anodic attack the modification to smaller, more numerous dendrites reduces the corrosion rate as the small primary crystals provide sites for anodes with shorter lifetimes and are less likely to develop into deeper crevice like features that may be seen with larger dendrites. Larger dendrites may support longer lived anodes and as metal is excavated through the anodic process localised aggressive chemical conditions may occur that could expedite the corrosion processes in the region local to the dendrite hence increasing the corrosion rate.

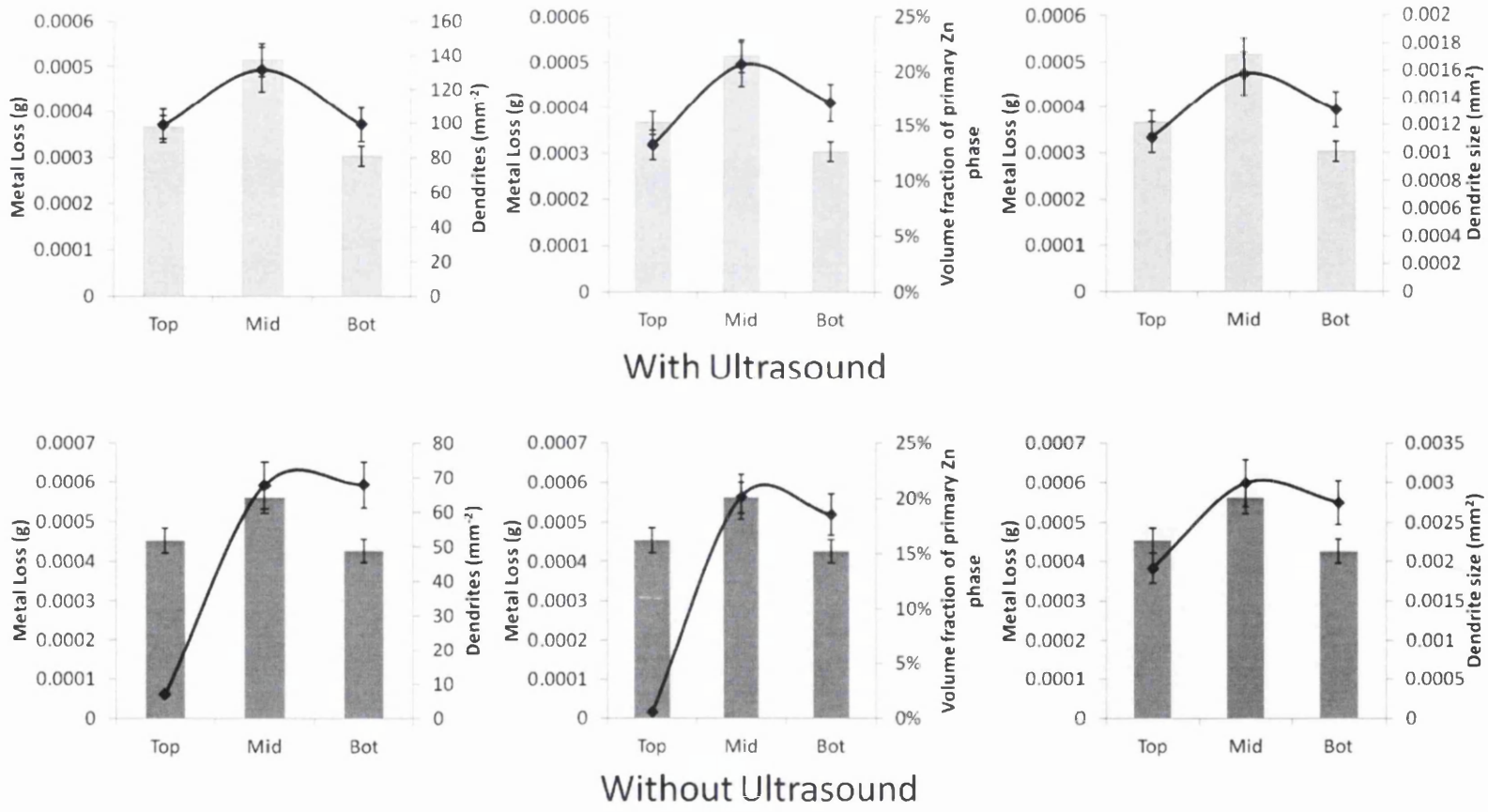

Figure 7.15 Graphs show effects of dendrite morphology on the SVET measured Zn loss of Zn – 4.8wt% Al alloys with a false cut edge solidified with and without ultrasound

7.5 Conclusions

The application of ultrasound to the solidifying melt of Zn – 4.8wt % Al alloys significantly altered the morphology of the final microstructure and also influenced the corrosion behaviour as evidenced through SVET. Samples irradiated with ultrasound had smaller primary β phase crystals but with an apparent enhanced nucleation rate. The ultrasound sample also demonstrated a much more uniform distribution of primary phase with a stable volume fraction of β observed throughout the casting in comparison to the non ultrasound sample. The morphology of the phases within the microstructure were altered with the application of ultrasound from dendritic to globular primary β and in localised areas from lamellar to anomalous eutectic. These changes were attributed to the physical action of the ultrasound disrupting compositional effects, the fragmentation of dendrites and cavitation events causing disruptive mixing leading to the breakdown of coupled eutectic growth.

The change in microstructure morphology induced by ultrasound had a generally positive effect on the corrosion behaviour of the alloy in 0.1% NaCl when investigated in the SVET. A steel insert was incorporated into the samples to create a false cut-edge thus mimicking in service conditions. The primary β crystals were the focussed sites for anodic dissolution and the smaller primary β crystals induced by the ultrasound reduced the corrosion rate by preventing the establishment of crevice like phenomena that may be associated with larger dendritic features. This was demonstrated by a reduction in lifetimes of anodic features on the ultrasound samples. It was also shown that changes in volume fraction, dendrite number and dendrite size generally influenced the corrosion rate with reductions in these factors subsequently reducing the corrosion rate of the alloy.

7.6 References

(1) Eskin, G.I. Ultrasonic Sonochemistry 2001, 8, 319-325.
(2) Eskin, G.I. Ultrasonic Sonochemistry 1995, 2, 137-141.
(3) Eskin, G.I.; Makarov, G.S.; Pimenov, YU.P. Advanced Performance Materials 1995, 2, 43-50.
(4) Abramov, V.; Abramov, O.; Bilgakov, V.; Sommer, F. Materials Letters 1998, 37, 27-34.
(5) Yanfen, H; Ke, L.; Jun, W.; Da, S.; Baode, S. Materials Science and Engineering 2005, 405, 306-312.
(6) Zhongtao, Z.; Tingju, L.; Honyun, Y.; Jian, Z.; Jie, L.; Materials and Design 2009;30:851-856.
(7) Feng, H.K.; Yu, S.R.; Li, Y.L.; Gong, L.Y.; Materials Processing Technology 2008;208:330-335.
(8) Soare, A.; Dijkink, R.; Pascual, M.R.; Sun, C.; Cains, P.W.; Lohse, D.; Stankiewicz, A.I.; Kramer, H.J.M. Crystal Growth and Design 2011;11:2311-2316.
(9) Gao, D.; Li, Z.; Han, Q.; Zhai, Q. Materials Science and Engineering 2009;502:2-5.
(10) Li, J.; Chen, W.; Liu, Q.; Wang, X.; PROCESS MET 2008;79:358
(11) Ramirez A, Qian M, Davis B, Wilks T, StJohn DH. Scripta Materialia 2008;59:19-22.
(12) Qian, M.; Ramirez, A.; Das, A. Crystal Growth and Design 2009;311:3708-3715.
(13) Jian, X.; Xu, H.; Meek, T.T.; Han, Q. Materials Letters 2005;59:190-193.
(14) Jackson, K.A.; Hunt J.D. Transactions of the Metallurgical Society 1966;236:1129-1142.
(15) Mollard, F.R.; Flemings, M.C. Transactions of the Metallurgical Society 1967;239:1534-1546.
(16) Hellawel, A.; Liu, S.; Lu, S.Z. Minerals Metals Materials Society 1997;49:18-20.
(17) Tiller, W.A.; O'Hara, S. The Solidification of Metals, London: The Iron and Steel Institute; 1968

Chapter 8

Future Work

8.0 Proposal for future work

Areas for potential future work include:

Continue the investigation into the zinc runoff from outdoor weathering of existing samples for a longer period than 18 months. This will enable a more robust mathematical model to be derived that can prove useful in forecasting the longevity of the organically coated galvanised steel. The model and data can also assist in development of new organic coating systems. Characterisation of corrosion products formed on the coated steels from outdoor exposure may also be useful undertaking. A variety of techniques can be employed to obtain information of composition of the formed corrosion products. These include x-ray photon spectroscopy (XPS) for qualitative/quantitative analysis of thin films, Ion chromatography for analysis of soluble anions, SEM/EDX for studies of product morphology and compositional analysis and x-ray powder diffraction (XRD) for identifying crystalline phases. Analysis of corrosion products from weathered materials may aid the development of novel electrolytes for accelerated tests in order to improve the correlation of such tests with natural exposure as well as assessing the effect of environment on the corrosion behaviour of the materials.

Improvements of the accelerated tests developed in chapter 4. Novel electrolytes can be developed using a variety of ionic addition to distilled water to mimic actual rain more closely. Care must be taken to ensure that such electrolytes are not too aggressive such that the corrosion mechanism of the coated steels does not alter. Analysis of blank samples from rainwater collected from the outdoor location can be used to develop ionic additions pH level for the electrolytes. Development of electrolytes may lead to improved correlations of the accelerated tests with the outdoor weathering data. Use of variety of wet and dry cycles may also improve the accelerated tests further imitating real weather conditions.

Further SVET experimental work to examine the corrosion inhibition effects of the individual active inhibitor species contained within the different components of the paint system. This will assist in identifying the components and the magnitude of their impact upon corrosion inhibition. Such data may prove useful in development of new paint systems.

Further work on Ultrasonic irradiation of melts is also envisaged. This could encompass an investigation into the time and power of irradiation and also irradiation of new Zinc-Aluminium-Magnesium alloys for Galvanising to assess the effects on microstructures and

corrosion rates. Some thought will also be required as to how such irradiation could be achieved on a production line and this may involve pulsed lasers or vibration of rolls or baffles to induce ultrasound into the solidifying Zn after the air knife section of the galvanising process.